

**Université de Reims
Champagne Ardenne**

France - Chine

**Dalian University
of Technology**

Thèse de DOCTORAT

Présentée à l'Université de Reims Champagne-Ardenne

Pour l'obtention du grade de

DOCTEUR en Génie Civil et Mécanique

par

Monsieur Yangjun LUO

ETUDE NUMERIQUE ET OPTIMISATION DE CONCEPTION DES POUTRES MIXTES ACIER-BETON ASSEMBLEES PAR COLLAGE

Soutenue publiquement le 08 Juin 2009

Devant la commission d'examen

Prof. DELMAS Yves	Université de Reims Champagne-Ardenne	Président
Prof. BATOZ Jean-Louis	Université de Technologie de Compiègne	Rapporteur
Prof. ZHENG Changliang	Dalian Maritime University	Rapporteur
Prof. GUO Ying-Qiao	Université de Reims Champagne-Ardenne	Examineur
Prof. LI Gang	Dalian University of Technology	Examineur
Prof. ZHANG Hongwu	Dalian University of Technology	Examineur
Prof. KANG Zhan	Dalian University of Technology	Co-directeur
Prof. LI Alex	Université de Reims Champagne-Ardenne	Co-directeur

NUMERICAL STUDY AND DESIGN OPTIMIZATION OF BONDED STEEL-CONCRETE COMPOSITE BEAMS

Yangjun LUO

Laboratoire de Génie Civil, GRESPI EA n°4301
Université de Reims Champagne-Ardenne, France
State key Laboratory of Structural Analysis for Industrial Equipment
Dalian University of Technology, China

To my family

Acknowledgements

First and foremost, I would like to express my deepest gratitude to my two advisors, Prof. Alex LI and Prof. Zhan KANG, for all their support and guidance. I have greatly benefited from frequent and inspiring discussions with them. It is extremely fortunate for me to have had an excellent co-supervision from them during the three years of this research.

Prof. Yves DELMAS deserves a special appreciation for his willingness to be the jury president of my doctoral dissertation. Moreover, I would like to thank Prof. Jean-Louis BATOZ from Université de Technologie de Compiègne (France) and Prof. Changliang ZHENG from Dalian Maritime University (China) for their critical review and valuable suggestions for improving this dissertation.

I would also like to thank teachers and schoolmates in the GRESPI, UFR Sciences, Université de Reims Champagne-Ardenne. The relaxed and genuine academic atmosphere in there has helped my studies and research intensely. I would especially like to thank Prof. Ying-Qiao GUO, Dr. Yuming LI, Alexandre GACON, Ismaïl YURTDAS, Jie SHEN and Ming DONG for their never-tiring help in my living and study in France.

My thanks go to all teachers and my friends in the State Key Laboratory of Structural Analysis for Industrial Equipment, Dalian University of Technology (China), for all their suggestions and support during the course of this work. I am especially grateful to Prof. Hongwu ZHANG, Prof. Gang LI and Prof. Yuefang WANG as the thesis jury members. Dr. Guozhong ZHAO is also acknowledged for his help in this cooperative project.

Financial support from the Science and Technology Service, Embassy of France in China, is also gratefully acknowledged.

Last but not least, I would like to thank my family for all their support and especially my beautiful wife Lili QU for her show of unequalled patience, understanding and love during the long wait for the conclusion of this dissertation.

Mai 2009, Reims, France

Abstract

In this thesis, numerical study and design optimization problems for the bonded steel-concrete beam are addressed. The steel-concrete composite beam bonded by adhesive has its particular advantages over the traditional composite beam and is attracting increasing attentions. The aim of the present study is to provide a fundamental understanding as well as the computational framework of numerical simulation and design optimization of bonded composite beams.

Firstly, as a prerequisite, an experimental push-out test is carried out to investigate the debonding failure mode and to determine the bonding shear strength between the concrete and the steel. The debonding failure takes place within the first 2-5 mm of the concrete from the adhesive/concrete interface and the epoxy adhesive bonding connection can provide a bonding shear strength of 6.36MPa. Then, a validated three-dimensional nonlinear finite element model was proposed to predict the parametric effects of bonded steel-concrete composite beams. From the simulating results, it is shown that the response of the bonded composites is influenced significantly by elastic modulus of adhesive, the bonding strength and the bonding area, rather than the adhesive layer thickness.

Secondly, for determining a more reasonable initial topology configuration, a three-dimensional topology optimization methodology of the bonded composite beam is presented. Following Solid Isotropic Material with Penalization (SIMP) approach, an artificial material model with penalization for elastic constants is assumed and elemental density variables are used for describing the structural layout. The considered problem is thus formulated as to find the optimal material density distribution that minimizes the material volume under specified displacement constraints. By using the adjoint variable method for the sensitivity analysis, the optimization problem is efficiently solved by the gradient-based optimization algorithm. The proposed topology approach presented a new structural topology of bonded steel-concrete composite beam.

Further, by using a probability and convex set mixed model, a reliability assessment strategy is presented for structures exhibiting both stochastic and bounded uncertainties in material properties, geometrical dimensions and loading conditions. The safety measure of a

structure is quantified by a reliability index defined by a nested minimization problem. An iterative procedure is developed for seeking the worst-case point and the most probable failure point in the standard uncertainty space. Numerical examples demonstrated illustrated the validity and effectiveness of the proposed method. The proposed reliability index is then employed to assess the reliability of a bonded steel and concrete composite beam.

Finally, the method for the reliability-based optimization design of the bonded composite beam is developed. The optimization problem incorporating constraints of mixed reliability indices is mathematically formulated. By using the performance measure approach, the optimization problem is converted into more tractable one. Moreover, the double-loop optimization problem is transformed into an approximate single-loop minimization problem using the linearization-based technique, which further facilitates efficient solution of the design problem. Two examples regarding design optimization of a mathematical function and a truss structure demonstrated the validity of the proposed formulation as well as the efficiency of the presented numerical techniques. As a consequence, the comparisons of optimization results for the bonded composite beam showed the significant meaning of accounting for the uncertainties in the composite beam optimization design by a reliability-based approach.

Résumé

La présente thèse consiste à effectuer une étude numérique et optimisation de conception des poutres mixtes acier-béton assemblées par collage. Ce type de poutre mixte dispose d'avantages particuliers par apport à la poutre mixte traditionnelle au niveau du transfert des efforts entre le béton et l'acier et la liaison béton-acier. Elle est devenue de plus en plus attractive dans le secteur industriel. L'objectif de ce travail est de fournir une compréhension fondamentale, de proposer un modèle numérique et de donner une optimisation de conception des poutres mixtes acier-béton assemblées par collage.

Tout d'abord, comme une condition préalable, des essais de push out ont été effectués afin de connaître le mode de rupture et de déterminer la résistance au cisaillement de l'adhérence acier-béton. Les résultats montrent que la rupture de l'éprouvette acier-béton collée se trouve dans le béton, située à la position de 2-5mm par rapport à l'interface acier-béton. La connexion assurée par adhésive peut alors fournir une contrainte d'adhésion de 6.36MPa. Un modèle numérique non linéaire de trois dimensions a été également proposé et validé dans ce travail. Ce modèle permet de prédire les effets paramétriques sur le comportement mécanique de la poutre mixte acier-béton. A partir des résultats obtenus par simulation numérique, on trouve que le comportement mécanique de la poutre mixte collée est principalement influencé par le module élastique de l'adhésive, la résistance et la surface d'adhésion, et légèrement influencé par l'épaisseur du joint d'adhésive.

Ensuite, pour déterminer une configuration topologique initiale plus raisonnable, une méthodologie d'optimisation de topologie de trois dimensions de poutre mixte collée est présentée. Suivant l'approche "Solid Isotropic Material with Penalization" (SIMP), un modèle de matériau artificiel avec pénalisation pour les constantes élastiques est adopté. Les variables de la densité élémentaire sont utilisées pour décrire le planning de structure. Le problème considéré est donc formulé afin de trouver la distribution de densité de matériau qui minimise le volume de matériau sous des conditions aux limites des déplacements spécifiques. En utilisant la méthode de variable adjoint pour l'analyse de sensibilité, le problème d'optimisation est résolu efficacement par l'algorithme d'optimisation fondé sur le gradient. L'approche de topologie a présenté une nouvelle topologie de poutre mixte acier-béton collée.

De plus, en utilisant un modèle mixte de la probabilité et d'ensembles convexes, une stratégie d'estimation de la fiabilité pour les structures est présentée pour montrer les incertitudes stochastique et non-stochastique dans les propriétés de matériau, les dimensions géométriques et les conditions de charges. Une mesure de sécurité de la structure est quantifiée par un index de fiabilité défini par un problème d'optimisation emboîtée. Une procédure itérative est également développée pour relocaliser le point le plus défavorable et le point de rupture le plus probable dans l'espace d'incertitude standard. Les exemples de calcul par la simulation numériques ont montré la validité et l'efficacité de la méthode proposée. L'index de fiabilité proposé a été employé pour estimer la fiabilité de poutre mixte acier-béton.

Enfin, la méthode pour la conception des poutres mixtes collées fondée sur l'optimisation de fiabilité a été développée. Le problème d'optimisation comprenant les contraintes des indices mixtes de fiabilité est mathématiquement formulé. En utilisant l'approche de mesure de la performance, le problème d'optimisation est converti en un problème plus tractable. De plus, le problème d'optimisation de double-boucles est transformé en un problème d'optimisation d'une seule boucle approximative en utilisant la technique de linéarisation qui facilite alors la solution efficace du problème de conception et de dimension. Deux exemples concernant l'optimisation de conception et de dimension d'une fonction mathématique et une structure en treillis ont démontré la validité du modèle proposé ainsi que l'efficacité de la méthode numérique présentée. Les comparaisons des résultats d'optimisation sur les poutres mixtes ont montré les sens significatifs en prenant en compte des incertitudes dans la conception des poutres mixtes par une approche fondée sur la fiabilité.

CONTENTS

Acknowledgements.....	I
Abstract.....	II
Résumé	IV
List of figures	IX
List of tables.....	XI
CHAPTER 1: INTRODUCTION.....	1
1.1 BACKGROUND AND MOTIVATION	2
1.2 STRUCTURE OF THE DISSERTATION	4
1.3 REVIEW OF PREVIOUS WORK ON COMPOSITE BEAMS	5
1.3.1 <i>The metal shear connector</i>	5
1.3.2 <i>Traditional steel and concrete composite beams</i>	9
1.3.3 <i>Bonded steel and concrete composite beams</i>	14
1.4 REVIEW OF STRUCTURAL OPTIMIZATION DESIGN.....	17
1.4.1 <i>Structural optimization</i>	17
1.4.2 <i>Structural topology optimization</i>	19
1.4.3 <i>Structural optimization design under uncertainty</i>	24
CHAPTER 2: NONLINEAR FINITE ELEMENT SIMULATION OF BONDED COMPOSITE BEAMS	29
2.1 INTRODUCTION.....	30
2.2 PUSH-OUT TEST.....	30
2.2.1 <i>Push-out specimen</i>	31
2.2.2 <i>Materials</i>	32
2.2.3 <i>Test preparation</i>	33
2.2.4 <i>Push-out results</i>	35
2.3 FINITE ELEMENT MODEL OF BONDED COMPOSITE BEAMS	37
2.3.1 <i>Concrete/adhesive interface modeling</i>	38
2.3.2 <i>Concrete modeling</i>	39
2.3.3 <i>Adhesive and steel modeling</i>	41
2.4 VALIDATION OF THE FINITE ELEMENT MODEL.....	42

2.5 EFFECTS OF PARAMETERS.....	44
2.5.1 Effects of the elastic modulus of adhesive	44
2.5.2 Effects of the adhesive layer thickness	46
2.5.3 Effects of the bonding strength.....	48
2.5.4 Effects of the bonding area.....	49
2.6 SUMMARY	51
CHAPTER 3: TOPOLOGY DESIGN OF THE BONDED COMPOSITE BEAM.....	52
3.1 INTRODUCTION.....	53
3.2 TOPOLOGY DESIGN OF THE BONDED COMPOSITE BEAM.....	53
3.3 SOLUTION STRATEGY	56
3.3.1 SIMP approach	56
3.3.2 Solving algorithm of optimization problem.....	58
3.3.3 Sensitivity analysis	61
3.4 OPTIMAL STRUCTURAL LAYOUT	63
3.5 SUMMARY	66
CHAPTER 4: STRUCTURAL RELIABILITY ASSESSMENT BASED ON	
PROBABILITY AND CONVEX SET MIXED MODEL	67
4.1 INTRODUCTION.....	68
4.2 GENERAL CONCEPTS OF PROBABILISTIC MODEL AND CONVEX MODEL	
.....	69
4.2.1 Probabilistic model	69
4.2.2 Non-probabilistic convex model.....	71
4.3 RELIABILITY ANALYSIS UNDER PROBABILITY AND CONVEX SET	
MIXED MODEL.....	76
4.4 SOLUTION STRATEGY FOR STRUCTURAL RELIABILITY INDEX.....	79
4.4.1 Mathematical programming method.....	79
4.4.2 Direct iterative approach	80
4.5 NUMERICAL EXAMPLES	82
4.5.1 Example with explicit performance function.....	82
4.5.2 Reliability analysis of a cantilever beam	84

4.6 RELIABILITY ASSESSMENT OF THE BONDED COMPOSITE BEAM.....	86
4.7 SUMMARY	89
CHAPTER 5: RELIABILITY-BASED DESIGN OPTIMIZATION OF THE BONDED COMPOSITE BEAM	90
5.1 INTRODUCTION.....	91
5.2 RELIABILITY-BASED STRUCTURAL OPTIMIZATION WITH PROBABILITY AND CONVEX SET MIXED MODEL	92
5.2.1 Optimization problem and performance measure approach	92
5.2.2 Design sensitivity analysis of the target performance	95
5.2.3 Solution strategy.....	97
5.2.4 Validation by numerical examples	102
5.3 OPTIMIZATION OF THE BONDED COMPOSITE BEAM	107
5.3.1 Optimization modeling	109
5.3.2 Solutions and comparisons.....	112
5.4 SUMMARY	115
CHAPTER 6: CONCLUSIONS.....	117
6.1 SUMMARY	118
6.2 OUTLOOK.....	120
BIBLIOGRAPHY	121
Curriculum Vitae	133

List of figures

Fig. 1.1	Classification of the connectors and comparison of mechanical property [6].....	6
Fig. 1.2	Forces applied to the connector in a composite beam	8
Fig. 1.3	Push-out test	8
Fig. 1.4	Push-in test	8
Fig. 1.5	Double push-out test.....	8
Fig. 1.6	The effective width definition of a composite beam	13
Fig. 1.7	Sizing optimization.....	19
Fig. 1.8	Shape optimization	19
Fig. 1.9	Topology optimization	19
Fig. 1.10	Ground structure.....	20
Fig. 1.11	Schematic representation of material microstructure [79]	21
Fig. 1.12	Comparison of cell configurations for topology optimization	22
Fig. 2.1	Dimensions of push-out specimen (unit: mm)	31
Fig. 2.2	The surface treatment before bonding.....	33
Fig. 2.3	Location of instrumentations (unit: mm).....	34
Fig. 2.4	Push-out loading equipment.....	35
Fig. 2.5	Failure mode of push-out specimen	35
Fig. 2.6	Load versus strain in the web of steel girder.....	36
Fig. 2.7	Average shear stress versus slip curve	36
Fig. 2.8	Finite element mesh for a quarter of the composite beam.....	37
Fig. 2.9	Schematic illustration of concrete/adhesive interface modeling	38
Fig. 2.10	Concrete stress-strain curve for uniaxial loading	40
Fig. 2.11	Sketch of the composite beams	43
Fig. 2.12	Load-deflection curves from finite element model and test results.....	43
Fig. 2.13	Load-deflection curves of composite beams for various elastic modulus of adhesive	44
Fig. 2.14	Relationship between the initial stiffness and elastic modulus of adhesive	45
Fig. 2.15	Load-deflection curves of composite beams for various adhesive thicknesses.....	46
Fig. 2.16	Relationship between relative ultimate load and adhesive layer thickness	47
Fig. 2.17	Load-deflection curves of composite beams for various bonding strengths	48
Fig. 2.18	Relationship between ultimate load and bonding strength.....	49

Fig. 2.19	Distribution of the bonded region	49
Fig. 2.20	Relationship curves between ultimate load and relative bonding area.....	50
Fig. 3.1	Schematic illustration of material topology optimization	54
Fig. 3.2	Design domain of the bonded composite beam (Unit: mm).....	55
Fig. 3.3	The penalty effect with different penalization factors in SIMP model	57
Fig. 3.4	Iteration history of the topology optimization.....	64
Fig. 3.5	Plan views of the optimal structural layout.....	64
Fig. 3.6	3-D optimal layout of the bonded composite beam.....	65
Fig. 4.1	Joint probability density function.....	70
Fig. 4.2	Specific cases of convex models for three uncertain variables	72
Fig. 4.3	Three specific normalized multi-ellipsoid convex model	74
Fig. 4.4	Schematic illustration of the non-probabilistic reliability index in the normalized space	74
Fig. 4.5	Schematic representation of the reliability index under mixed model in the u -space.....	77
Fig. 4.6	Flowchart of the iteration process	82
Fig. 4.7	Three assumed probabilistic distributions for uncertain variable y	83
Fig. 4.8	A cantilever beam.....	85
Fig. 4.9	Iteration histories of reliability evaluation for the cantilever beam.....	86
Fig. 4.10	The composite beam P1	87
Fig. 4.11	Iteration histories of reliability evaluation for the composite beam P1	88
Fig. 5.1	Schematic representation of the performance measure approach	94
Fig. 5.2	Flow chart of the traditional nested double-loop approach	98
Fig. 5.3	Flowchart of the optimization process using the linearization-based approach	101
Fig. 5.4	Iteration histories of the optimization with different initial design points	104
Fig. 5.5	The ten-bar truss structure.....	105
Fig. 5.6	Iteration histories of the optimization.....	107
Fig. 5.7	Optimization parameter model of the bonded composite beam	108
Fig. 5.8	Iteration histories of the optimization.....	113
Fig. 5.9	Load-deflection curves at nominal values of uncertain inputs for three different designs	114
Fig. 5.10	A comparison of the middle cross-section	114
Fig. 5.11	A comparison of the steel girder	115

List of tables

Table 2.1	Composition proportion in one cubic meter concrete.....	32
Table 2.2	Mechanical properties of epoxy adhesive.....	33
Table 2.3	Material properties of the composite beams	42
Table 4.1	Comparison of reliability results under mixed model and assumed distribution of y	84
Table 4.2	Uncertainty characteristics of the cantilever beam.....	85
Table 4.3	Summary of results for the cantilever beam example.....	86
Table 4.4	Mean values of the material properties for the composite beam P1	87
Table 5.1	Solutions for the mathematical example.....	103
Table 5.2	Uncertainty properties for the ten-bar truss structure	105
Table 5.3	Optimal solutions using different approaches	106
Table 5.4	Uncertainty properties for the bonded composite beam	108
Table 5.5	Optimal solutions for the bonded composite beam	112

CHAPTER 1: INTRODUCTION

1.1 BACKGROUND AND MOTIVATION

Steel and concrete composite beams have been widely used in multi-storey buildings and bridges all over the world. Market investigation on bridges built in France [1] showed that the steel-concrete composite constructions have been growing steadily over the last two decades and the competitive span range is from 30m to 110m. This kind of structures has drawn intense attentions in both academic and practical communities because of their significant economic and structural advantages in comparison to conventional reinforced concrete structures [2]. Those advantages include: reduction in construction depth, increase in span length, savings in structural weight and the rapid construction procedure.

The steel and concrete composite beams combine the high tensile strength of steel with the high stiffness and the compressive strength of concrete, and thus create a more effective integrated configuration. In general practice, a steel girder is used to support the reinforced concrete slab. When the top flange of the girder is effectively connected to the concrete slab by means of shear connectors, the composite or integral action will be achieved by preventing the relative slip. Therefore, a fundamental point for the structural behavior and design of composite beams is the level of connection and interaction between the steel beam and the concrete slab. Traditionally, the concrete slab and the steel beam were connected by means of a mechanical fasten method. In this method, metal connectors such as headed studs and hoops, usually welded to the upper flange of the steel girder, are placed in fresh concrete initially, and then acted as vertical or horizontal stops after the concrete hardens. The main advantages of the traditional method are its mature technique and simple procedure.

However, the traditional mechanical fasten method has also its weaknesses, which may substantially reduce the durability of the steel-concrete composite structures. First, the metal shear connectors may induce the origin of cracking in concrete because of the stress concentration. Second, the traditional connection technique will reduce the fatigue life of the structure due to the welding between the connectors and the steel girder. For these reasons, adhesive bonding method has been developed as a new method in steel-concrete composite structures since the beginning of the 1960s and has been proved to be very efficient. In this

new technique, the concrete slab and the steel girder are connected by an adhesive joint. This adhesive joint can tightly combine the concrete slab and the steel girder together and ensure the continuity of the stress distribution over the composite beam sections. Therefore, the stress concentration caused by metal connectors is not a concern any more and the welding is also avoided. Furthermore, the adhesive bonding method makes it possible to directly use a prefabricated concrete slab, which will considerably simplify the manufacture procedure and reduce the construction cost.

In fact, adhesive bonding method has already become one of the most accepted techniques for strengthening reinforced concrete structures with a steel plate or fiber-reinforced polymer (FRP) on the tensile side. However, the studies on extending the adhesive bonding method to the steel and concrete composite beams are still limited. The application of this alternative technique can introduce some particular issues such as the debonding mode and the adhesive failures. Although some investigations on this topic have been conducted, the fundamental debonding failure mechanism is yet not fully understood, and the effects of some relevant parameters still need to be explored. In addition, owing to the difference in mechanical behavior between the adhesive joint and the metal connector, and also the dissimilarity in structure design between the composite beams and the FRP strengthen beam, there is no much available guidance for the design of the bonded steel and concrete composite beam. Therefore, further studies on the mechanical behavior as well as the design optimization techniques, including topology optimization, sizing optimization and reliability-based optimization, of this new type of structures are necessary. It can be anticipated that the adhesive bonded steel and concrete composite beam may share an increasing market in the future when these crucial problems are solved.

The first purpose of this dissertation is to propose an effective nonlinear finite element model for analyzing the bonded composite beam. It is well known that laboratory tests require a great amount of time, are very expensive and, in some cases, even impractical. On the other hand, the finite element method has become a powerful tool for the analysis of a wide range of engineering problems. Hence, numerical simulation is considered as a pre-requisite work in this treatise.

Secondly, this dissertation studies the topology optimization problem of the bonded steel and concrete composite beam. Structural topology optimization is used to find optimal topology layout characterized by lower cost while satisfying structural performance requirements and it has been successfully employed in a wide range of practical design problems. However, topology optimization work is lacking on the bonded composite beam.

Further, by using a new probabilistic and convex set mixed model to describe inherently uncertainties, this dissertation presents a reliability-based design optimization problem of adhesive bonded composite beams. In a practical steel and concrete composite structure, the uncertain scatter of structural parameters, such as geometrical dimensions and material properties, about their nominal values is unavoidable. The reliability evaluation and optimization design of the bonded composite beam with uncertainty have not been addressed in the literature.

1.2 STRUCTURE OF THE DISSERTATION

This dissertation is organized as follows:

In chapter 1, the research background and motivation of this work are briefly presented. Previous works on composite beams and optimization design is then reviewed.

In chapter 2, based on the experimental results by push-out tests, a three-dimensional nonlinear finite element model to simulate the mechanical behavior of bonded steel and concrete beams is proposed. The comparisons of results by numerical simulation with experimental results of simply supported composite beams illustrate the applicability and the validity of the proposed numerical methods. Then the verified finite element model is employed to investigate the effects of some important parameters on the composite beam behavior.

Chapter 3 presents a three-dimensional topology optimization of composite beams by using the Solid Isotropic Material with Penalization (SIMP) approach. The adjoint variable scheme for design sensitivity analysis is discussed. The structural optimization problem is then solved by a gradient-based algorithm using the obtained sensitivity.

Chapter 4 investigates the reliability assessment of bonded composite beams exhibiting both stochastic and bounded uncertainties by using a proposed probability and convex set mixed model. Numerical examples are given to demonstrate the applicability and effectiveness of the proposed mixed model.

In chapter 5, based on the probability and convex set mixed model in chapter 4 and optimal topology layout in chapter 3, a reliability-based design optimization of the bonded steel and concrete composite beam incorporating reliability constraints is mathematically formulated. A linearization technique is developed to further facilitate efficient solution of the optimization problem. The methodology is applied to design the simply supported bonded composite beams with a concentrated load.

In chapter 6, important conclusions are drawn and some future work in this area is suggested.

1.3 REVIEW OF PREVIOUS WORK ON COMPOSITE BEAMS

The objective of this section is to present a review of the previous work on the steel and concrete composite beams. Herein, studies on the traditional metal shear connector as well as the composite beam are first summarized. Then, the adhesive bonding method used in the steel and concrete composite beam is reviewed.

1.3.1 The metal shear connector

In a traditional steel and concrete composite beam, metal shear connectors are welded on the top flange of the steel beam before the concrete slab is cast. The role of metal shear connectors is of primary importance. Without them, there is no collaboration between the steel girder and the concrete slab. The function of the metal connector is to prevent, or at least to restrict the slip which can occur along the steel-concrete interface, and thus ensured the two different materials acting as a single unit. Since Newmark et al. [3] first used the studs with or without head into composite beams in 1950s, a variety of shapes and devices, such as bolt, channel, external bolt, friction grip bolt, have been developed as shear connectors [4]. Up to

now, economic considerations continue to motivate the development of new products in USA, Italy, Germany, Japan and France. However, among them the headed stud is the most largely used one in composite beams.

1.3.1.1 Classification of the connectors

According to the mechanical characterization (Fig.1.1), the metal connectors can be classed into three types, namely the rigid connector, the ductile connector and the semi-ductile connector [5, 6]. In general, the mechanical characterization of the connectors was obtained by carrying out a standardized test called push-out test.

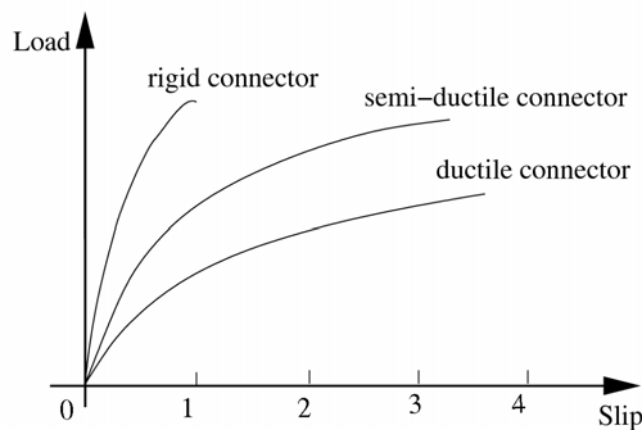


Fig. 1.1 Classification of the connectors and comparison of mechanical property [6]

(1) Rigid connector

A connector is rigid if it presents an ideally elastic behavior up to destroy. In the practical engineering, we rarely used the completely rigid connector because it is difficult to manufacture and can introduce brittle fractures.

(2) Ductile connector

A connector is considered as ductile when it has the ability of presenting sufficient plastic deformation under shearing. As prescribed in the section 10.2 of Eurocode 4 [5], a slip

of 6mm to the ultimate load in the standardized push-out test is competent to characterize a connector as ductile.

(3) Semi-ductile connector

As proposed by Rabih [6], a connector is referred to as “semi-ductile” or “semi-rigid” if it can exhibit an ideally elastic-plastic behavior. This means that an ideally elastic behavior is firstly exhibited and then a perfectly plastic behavior follows at a certain load point.

In addition, according to the number of connectors, a connection can also be classed as full shear connection or partial shear connection. We can consider a composite beam to be full shear connection when an increase in the number of connectors does not involve any more increase of the flexural strength of the beam. The failure of the beam with a full shear connection is characterized by the plasticization (or the instability) of the steel girder or by the ruin of the concrete. Correspondingly, connection is partial shear connection when the number of connectors in a shearing zone is lower than the number necessary for obtaining a full shear connection. In this case, there is a slip in the steel-concrete interface. The failure of the composite beam with a partial connection will occur with the exhaustion of its flexural strength.

1.3.1.2 Tests for the connectors

In a composite beam, the metal connector is subjected to a bending moment M , a shear force V and a normal tension force F (Fig.1.2). Generally speaking, the connector mostly risks of destroying by shearing while the tensioning is relative small. Consequently, several testing approaches were developed to characterize the mechanical behavior of the connectors under shear loads.

- ① Push-out test: A schematic representation of the push-out test is given in Fig.1.3. It is the standardized test proposed by Eurocode and makes possible to determine the ultimate load, the failure mode and the load-slip curve.
- ② Push-in test: Compares to the push-out test, push-in test posits the concrete slab in the middle, and each face of the slab is connected to a steel girder. [7] (Fig.1.4).

③ Double push-out test: As shown in Fig.1.5, double push-out test is more complicated because it is a double symmetric shear test which consists of two steel girders and four groups of shear connectors [8].

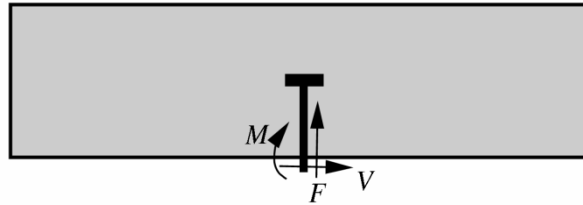


Fig. 1.2 Forces applied to the connector in a composite beam

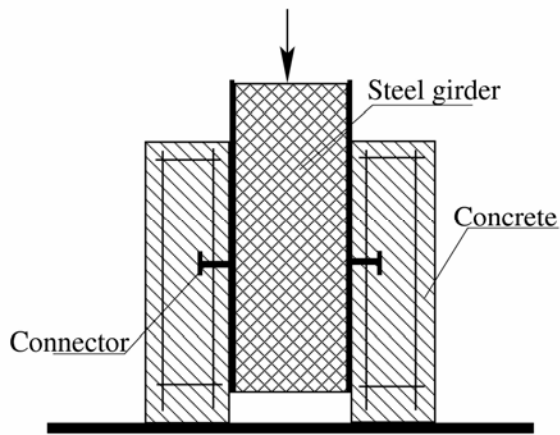


Fig. 1.3 Push-out test

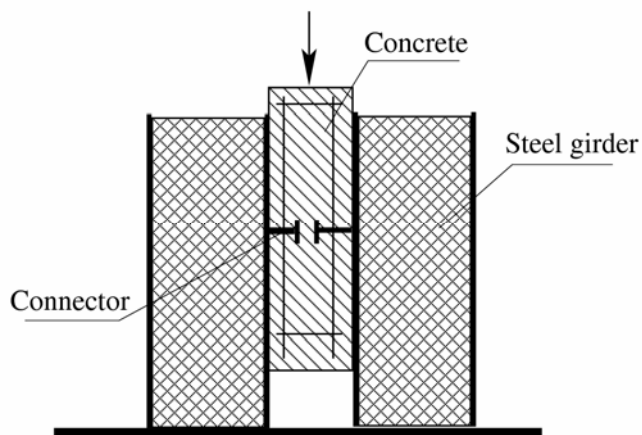


Fig. 1.4 Push-in test

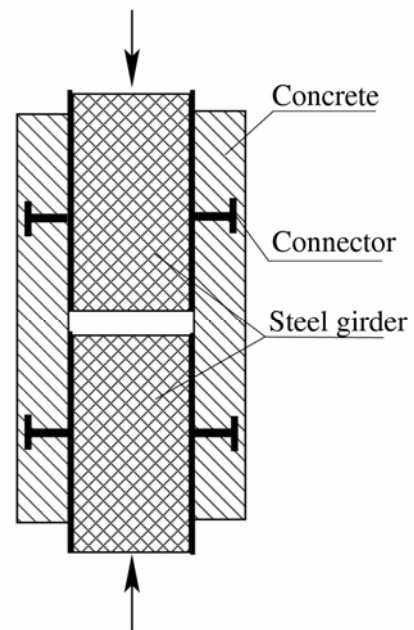


Fig. 1.5 Double push-out test

Obviously, the basic principles of these different tests are in common. However, the comparison tests [9] have shown that the push-out test is the most representative and easily-implemented operation of characterizing the connectors in a composite beam. On the other hand, it should be noted that there are some crucial problems in the push-out test:

- ① The size of the concrete slab and the quantity of the reinforcement may be different between the push-out test and the reality.
- ② The numbers of connectors are usually different, only one or two in the case of the push-out test while more in the reality. This may raise the question of the group effect.
- ③ The transverse inflection is not well represented in the push-out test.

1.3.2 Traditional steel and concrete composite beams

A traditional steel and concrete composite beam consists of a steel girder and a reinforced concrete slab, which are connected by metal shear connectors. It is common sense that concrete is strong in compression but weak under tension, while steel is strong in tension but susceptible to buckling under compressive forces. The fact that each material is used to take advantage of its positive attributes makes the composite construction very efficient and economical.

1.3.2.1 Experimental research

Experiments on traditional steel and concrete composite beams were first studied by Chapman and Balakrishnan [10] in 1960s. Since then, a significant amount of experimental research focusing on the behavior of the traditional composite beams has been reported in the literature.

Under static loads, the ruin of the composite beam may occur because of the local dislocation in the concrete, the fracture of the shear connectors or the excessive plastic deformation of steel girder. The early research mainly studied the mechanical behavior of the traditional composite beams such as the flexural strength [11] and the ultimate strength [12]. Later, Johnson and Willmington [13] conducted experiments on continuous composite beams

in combined negative bending and vertical shearing. Their test results indicated that the longitudinal steel reinforcement in the concrete slab can also increase the strength and stiffness in vertical shearing. Roberts and Al-Amery [14] carried out a series of experimental tests of short-span composite plate girders, and the results showed that adequate connectors can significantly enhance the shear strength of the composite structure. Nie et al. [15] suggested an empirical equation for calculating the shear strength of steel-concrete composite beams by sixteen simply supported specimens. They indicated that the concrete flange itself can bear 33%-56% of the total ultimate shear in the composite beams. Allison et al. [16] tested five composite plate girders and one steel plate girder with slender vertically stiffened webs to study the action of the shear connection on tension field.

Moreover, to investigate the impairment of the structural strength due to web openings, Clawson and Darwin [17] tested six composite beams with rectangular web openings, which were uniform in opening size while different in location of openings. Lebet and Ducret [18] explored the causes of transverse cracking in the concrete slab by in-situ measurements and laboratory tests, and they also studied the effect of concrete hydration in the steel and concrete composite bridges. Jurkiewicz and Braymand [19] investigated the influence of the initial transverse cracks by testing a pre-cracked steel-concrete composite beam. Measured data showed a strong discontinuity existing in the longitudinal distribution of the slip, which led to a noticeable deflection of studs.

Recently, some experimental studies focus on the new strengthening methods for composite beam design. Chen [20] proposed a steel-concrete composite beam prestressed with external tendons in negative moment regions, which can effectively prevent the concrete cracking forming. Jurkiewicz and Hottier [21] presented an innovative horizontal connection equipped in steel-concrete composite beams to avoid welding. The push-out tests as well as the bending tests validated that the innovative connection did not fail during the test and allowed for efficient transmitting of shear forces from the slab to the girder. Al-Saidy et al. [22] suggested a strengthened steel-concrete composite beam by attaching Carbon Fiber Reinforced Polymers (CFRP) plates to the bottom flange and the web of the steel girder. The experimental results showed that using lightweight CFRP plates could enhance the strength and stiffness of steel-concrete composite girders by up to 45% of the original strength.

1.3.2.2 Numerical method research

Because laboratory tests require a great amount of time and cost, many research efforts have also been devoted into the development of various analytical methods as well as the finite element method. It is well known that the finite element method is a very powerful numerical method for simulating complicated engineering problems. Since 1950s, the finite element method has been developed to solve a variety of structural and multi-physical problems [23-25].

In 1977, Wegmuller et al. [26] firstly applied the nonlinear finite element method into composite steel-concrete bridges. A layered model together with an incremental iterative procedure is employed to determine the response of the bridge in the post-elastic range. Then, by establishing the element shear stiffness properties with empirical force-shear deformation relationship, Razaqpur and Nofal [27] developed a three-dimensional bar element to model the nonlinear behavior of the shear connectors in composite concrete-steel structures. Salari et al. [28] developed a new composite beam element based on the governing equations of the composite beam with deformable shear connectors under small displacements. Therein, a distributed spring model is used to account for the shear deformation at the interface. Fabbrocino et al. [29] proposed a numerical procedure based on well-known kinematic models to analyze the behavior of composite beams under short term loads. An original moment-curvature generalized relationship for the cross section was introduced for analyzing the structural behavior easily. Faella et al. [30] used a displacement-based finite element model to solve steel-concrete composite beams with flexible shear connection. The stiffness matrix and the fixed-end nodal force vector are directly derived from the “exact” solution of Newmark’s differential equation. Sebastian and McConnel [31] developed a nonlinear finite element program for modeling composite beams. Concrete is represented as a nonlinear elastic isotropic material before cracking and nonlinear orthotropic thereafter, while steel is assumed to be initially elastic but with strain-hardening capabilities after yielding. A specialized stub element with empirical nonlinear shear force-slip relationships was used at the concrete slab-steel beam interface to model shear connector. Sapountzakis and Katsikadelis [32] presented a new model to analyze the reinforced concrete slabs stiffened by steel beams with deformable connection including creep and shrinkage effect. Moreover, this

model was used to solve the dynamic problem of the same composite structures [33]. In addition, Dall'Asta and Zona [34] introduced a new three-field mixed beam element and two displacement-based beam elements for the non-linear analysis of composite beams with deformable shear connection.

The above works have implemented the proposed finite element models for particular problems of composite beams, which may be time-consuming and unfavorable in applicability. Advances in computation and software have brought the finite element method into software packages which will significantly simplify the modeling and analyzing process. Nowadays, more and more academic researchers and engineers used these finite element commercial software packages to solve practical engineering problems.

As early as 1980, Hirst and Yeo [35] have used the standard finite element packages to analyze composite beams with partial and full shear connection, in which a quadrilateral element was employed to simulate discrete stud shear connectors. Recently, Thevendran et al. [36], Baskar et al. [37] and Liang et al. [38] utilized the commercial software ABAQUS to predict the ultimate load behavior of steel-concrete composite beams. In their approaches, the stud shear connectors were modeled by a three-dimensional beam element. Based on another commercial finite element software ANSYS, Queiroz et al. [39] proposed a three-dimensional finite element model to simulate the overall flexural behavior of simply supported composite beams subjected to either concentrated or uniformly distributed loads. In this model, elastic-plastic shell element (SHELL43) and solid element (SOLID65) were used for the steel girder and the concrete slab, respectively, while nonlinear spring element (COMBIN39) was used for the shear connectors.

1.3.2.3 Effective width evaluation

Due to the action of in-plane shear strain in the concrete flange, the normal stress distribution is not uniform along the slab width, which is termed as “shear lag” [40]. In a steel-concrete composite beam system, the concrete flange width may not be fully effective in resisting compression due to the shear lag phenomenon. The concept of effective width was

then introduced in the hypothesis of linear-elastic component materials as a simplification of the shear lag problem. As shown in Fig.1.6, the effective width is defined as

$$B_e = a_{e,1} + a_{e,2} + d_0 \quad (1.1)$$

where d_0 is the width of the connection zone, $a_{e,1}$ and $a_{e,2}$ are analytically expressed as

$$a_{e,i} = \frac{\int_{d_0/2}^{b_i} \sigma dy}{\sigma_{\max}} \quad (i = 1, 2) \quad (1.2)$$

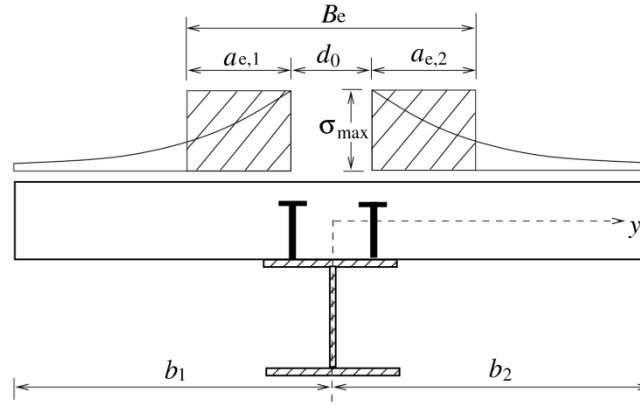


Fig. 1.6 The effective width definition of a composite beam

Estimation of effective width had been a challenging research topic, because it requires solutions of partial differential equations governing plate in-plane and bending behaviors. The effective width depends not only on the relative dimensions of the structure, but also on the type of loading, the support conditions and the considered cross section. However, in most codes of practice, very simple formulae are given for the calculation of effective width, though this may lead to some loss of economy. For example, for simply-support beams in buildings, the Eurocode [5] and the BS5400 [41] proposed that the effective width is 1/8 of span length, but not greater than half the distance to the next adjacent web, nor greater than the projection of the cantilever slab for edge beams. These limits are different in AASHTO [42] and the Chinese code provision [43] for the design of steel-concrete composite beams, in which the effective width of 1/4 and 1/6 of the span length is suggested respectively. A detail comparison in these provisions has been carried out by Ahn et al. [44].

Recently, Amadio and Fragiacomio [45] analyzed the effective width of steel-concrete composite beams by a parametric study carried out through the Abaqus code. Further, an experimental study by Amadio et al. [46] demonstrated that the effective width varies with loading conditions. By dividing the whole beam into the sagging bending moment zone and the hogging bending moment zone, a simple modification of Eurocode was then presented. Moreover, Chen and Zhang [47] evaluated the effective width of composite beams prestressed with external tendons by the finite element method. They concluded that the effective width of the beam prestressed with external tendons is slightly greater than the effective width when the beam is not prestressed. The influences by creep, shrinkage and the shear connection degree can be neglected in evaluation of the effective width.

1.3.3 Bonded steel and concrete composite beams

During the last fifty years, the adhesive bonding method has been developed for various reasons. On the one hand, the chemistry of polymers (epoxy resin or polyurethane) made it possible to produce adhesives being much more powerful and more durable. On the other hand, the development of manufacture technique made it possible to bond the concrete material and some metal materials tightly by adhesives.

Initially, the adhesive bonding method was used for repairing the damaged reinforced concrete beams and slabs by bonding many steel plates at the damage location. It was proven that the external bonding method is an efficient repair technique by virtue of its simplicity and facility in construction [48]. Afterwards, the adhesive bonding method was widely applied in both buildings and bridges to enhance the flexural capacity or the shear capacity by bonding steel plates to the tension face or side-faces of the structure [49-51]. In recent years, plate bonding to the concrete beam has gained new impetus with the use of lightweight fiber-reinforced polymer (FRP) composite materials [52-57]. Numerical simulations showed that the maximum shear stress increases with increases in the amount of fibers aligned in the beam's longitudinal axis, the modulus of the adhesive material and the number of laminate layers. However, the maximum peel-off stress decreases with increasing thickness of the adhesive layer.

The first experimental attempt of using the adhesive bonding method to assembly a steel and concrete composite beam was implemented by Miklofsky et al. [58] at the beginning of the 1960s. Two composite beams, including one traditional beam and one beam bonded by an epoxy adhesive, were tested to study the applicability of the adhesive bonded composite beam. At the same time, other experimental works by Kriegh and Endebrock [59] explored the technological features of epoxy resins and testified the validity of using this technique in composite beams. The research works [60, 61] also showed the adhesive bonding method can restrict the risk of cracking and thus increase the durability of structures. To ensure a better connection, Hick and Baar [62] carried out ten push-out tests to choose the type of gravel and the quantity of adhesive. The results showed that the 8/16 crushed porphyry and a 2.5mm thickness layer of Araldite AW132 epoxy adhesive are preferable. Then, a two-stage manufacture procedure was proposed. First, the upper surface of the steel beam in contact with the concrete is sanded, degreased and coated by a layer of adhesive in which the aggregates are set up. Second, 24 hours later, the casting of the concrete slab is carried out. Following this procedure, the ruin usually occurs in the concrete slab near the adhesive under shearing.

Nordin and Täljsten [63] compared the composite beams which connected in two ways: casting by steel shear connectors and bonding by epoxy adhesive. The results from the four-point bending tests showed that the adhesive bonding connection worked better than the steel shear connection in the laboratory. However, they also pointed out that this technique would be more complicated because there is still lack of the guidance available for the design of this technique used in composite beams.

Si Larbi et al. [64] investigated the static and instantaneous behavior of the bonding connection in the context of composite beam by performing push-out tests under various conditions. Experimental results showed that the bonding connection exhibits a very high stiffness and nearly the same strength as mechanical connectors. The risk of cracking in the concrete slab is also significantly reduced, which may increase the durability of bonded steel-concrete composite structures compared with ones equipped with mechanical connectors.

Bouazaoui et al. [65] studied the mechanical behavior and the parameter effect of bonded steel-concrete composite beams. The experimental tests showed that the connection between the steel girder and the concrete slab ensured by epoxy adhesive is perfect. The results also revealed the influence of the variation in adhesive thickness on the mechanical behavior and ultimate force is negligible.

Zhao and Li [66] used the finite element method to study the nonlinear mechanical behavior and failure process of bonded steel-concrete composite beams. Based on the numerical simulative results, the authors concluded three major reasons for the failure of the composite beam, namely cracking of the concrete caused by the local tensile stress, crushing of the concrete caused by the compressive stress, and extensive yielding of the steel beam under the global bending moment.

The above literature investigation showed that using the adhesive bonding as connection in steel and concrete composite beams is quite efficient. The adhesive bonding technique can be considered as an alternative method to the traditional mechanical connection. In conclusion, the advantages of the adhesive bonding connection over the traditional metal shear connectors are listed as follows.

- ① The adhesive bonded composite beam obtains a continuous transfer of the effort and thus decreases the appearance of shear stress concentration.
- ② Reduction in the total weight of the composite structure.
- ③ The adhesive bonding method makes it possible to eliminate the welding of the shear connectors which may deteriorate the mechanical performance of steel girder.
- ④ The bonded adhesive layer is impermeable and thus protects the joint of steel girder against corrosion.
- ⑤ The capacity of dissipation of the polymers which constitute the adhesives makes it possible to damp out the vibrations.
- ⑥ The opportunity of employing prefabricated concrete slabs instead of fresh concrete running on the steel girder is very interesting for the mixed construction industry. The traditional methods of connection between the concrete slab and the steel girder are not

or little appropriate for fast implementation.

However, it should also be noted that the tensile strength of the adhesive is rather low, and the adhesive bonding method is a relatively complex and expensive technique. Therefore, it is necessary to have good knowledge of the adhesive for efficiently using this method, which implies the solution of the following problems:

- ① Preparation of the surface to be bonding. The treatments to the surface of steel girder and concrete by mechanical or physicochemical operations are in general expensive but essential to eliminate the impurities, to increase the energy of surface and the mechanical fixing by creating roughness, and to support damping in order to facilitate the spreading out of the adhesive.
- ② The behavior of the adhesive bonding layer under constraints is different from that of the traditional assemblies, and it is also different from that of concrete beams strengthened by steel plate or FRP. The failure mechanisms are still not fully understood, and the influences of several parameters are not yet investigated very clearly.

1.4 REVIEW OF STRUCTURAL OPTIMIZATION DESIGN

In this section, a review to structural deterministic optimization, topology optimization and non-deterministic optimization under uncertainty is given.

1.4.1 Structural optimization

Since the advent of high speed computing in the 1950s, numerical techniques, such as the finite element method and the mathematical programming theory, provided an opportunity to improve existing designs and identify better designs early in the design process of machines and structures. The process of improvement of these designs basically forms the scope of *structural optimization design*. The application of the structural optimization has been extended to a wide range of design problems involving in the fields of civil construction, transportation, aerospace and national defense [67-69].

A general structural optimization problem is usually stated as to minimize an objective function subject to inequality and equality constraints insuring the feasibility of the structural design:

$$\begin{aligned} \min_{\mathbf{d}} \quad & f(\mathbf{d}) \quad (\mathbf{d} \in \mathbb{R}^N) \\ \text{s.t.} \quad & g_i(\mathbf{d}) \leq 0 \quad (i = 1, 2, \dots, N_g), \\ & h_j(\mathbf{d}) = 0 \quad (j = 1, 2, \dots, N_h), \end{aligned} \quad (1.3)$$

where $\mathbf{d} = [d_1, d_2, \dots, d_N]^T$ denotes the vector of design variables. These design variables can be either continuous, for example dimensions of a beam, or discrete, for example number of strands in a cable, type of material, or a combination of the two. $f(\mathbf{d})$ is the objective function, which typically is the structural cost or performance. $g_i(\mathbf{d}) \leq 0$ and $h_j(\mathbf{d}) = 0$ are the inequality constraints and equality constraints respectively, such as the requirements on stress, displacement or frequency. N_g and N_h are the constraint numbers.

An optimization problem is said to be linear when both the objective function and the constraints are linear functions of the design variables, which can be solved by a linear programming method. Otherwise, the optimization is said to be nonlinear. For the nonlinear optimization, we need to search the optimum by moving the design point from one to another. While there are many numerical search techniques available, most of them proceed through four basic steps in performing the move.

- ① The first step is the selection of the active constraint set discussed in the structural optimization model.
- ② The second step is the calculation of a search direction based on the objective function and the active constraint set. Some methods (such as the gradient projection method) look for a direction which is tangent to the active constraint boundaries. Other methods, such as the feasible direction or the interior penalty function method, seek to move away from the constraint boundaries.
- ③ The third step is to determine how far to go in the direction found in the previous step. This is often done by a process called a *one dimensional line search* because it seeks the

magnitude of a single scalar which is the distance to be travelled along the given search direction.

- ④ The last step is the convergence criterion check which determines whether additional moves are required.

1.4.2 Structural topology optimization

Three types of structural optimization problems at the level of macroscopic design can be categorized: sizing optimization, shape optimization and topology optimization. The sizing optimization (Fig.1.7) provides the means to generate optimal designs by modifying structural dimensions, while shape optimization (Fig.1.8) achieves this goal by adjusting geometrical position. Therefore the topology of the structure is predefined and remains unchanged throughout sizing and shape optimization process. The topology optimization (Fig.1.9), however, does not pre-specify an initial topology as requirement. In a topology design process, by giving an arbitrary design domain, loads, and boundary conditions, the connectivity and solid material distribution of the structure are gradually emerged during the design process itself. In simple terms, the aim of topology design is to characterize the indicator function by determining the distribution of solid material (or multiple phases of material) within the available domain. Therefore, the topology optimization is most valuable as preprocessing tools for sizing and shape optimization [70].

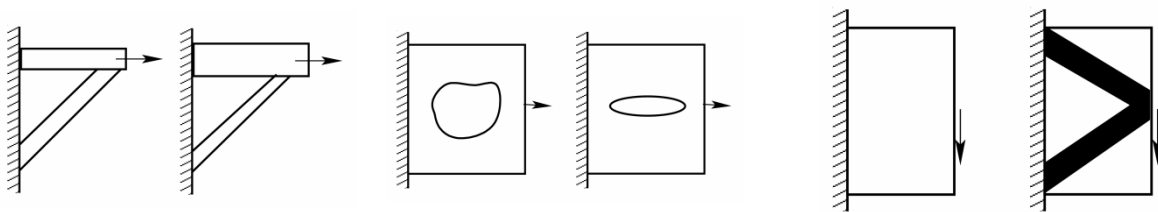


Fig. 1.7 Sizing optimization

Fig. 1.8 Shape optimization

Fig. 1.9 Topology optimization

Depending on the type of a structure, there exist two types of topology optimization, namely discrete or continuous. For discrete structures, such as truss structures, the topology

design problem aims to determine the optimum number, positions and mutual connectivity of the structural members within a predefined ground structure (Fig.1.10). The earliest design theory for the topology of discrete structures can be traced back to 1904 by Michell [71]. Subsequently, this area of research has been active for several decades and the interested readers are referred to the comprehensive review papers by Ringertz [72], Kirsch [73] and Rozvany et al [74].

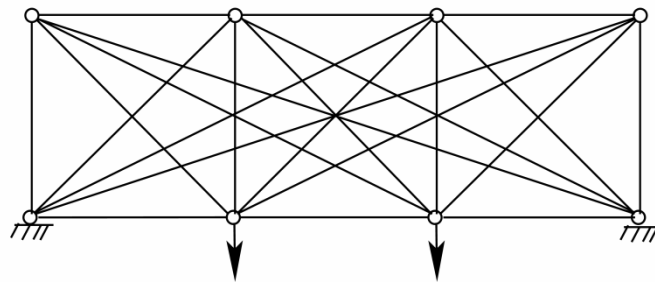


Fig. 1.10 Ground structure

In the topology optimization of continuum structures, it is assumed that the loading is prescribed and that a given amount of structural material is specified within a given 2D or 3D design domain with given boundary conditions. Then by using certain solution strategy, the shape of external as well as internal boundaries and the number of inner holes are optimized simultaneously with respect to a predefined design objective. Since Bendsøe and Kikuchi [75] first introduced the homogenization method into the optimal material distribution problem in late 1980s, the topology optimization of continuum structures has become an extremely active research field in the structural optimization community during the last two decades. There are several research activities going on throughout the world, and many different practical numerical methods have been developed and applied successfully to a variety of structural and multidisciplinary topology design problems [76, 77].

(1) Homogenization-based optimization method

In homogenization-based optimization (HBO) method, topology optimization is transformed to the problem of material redistribution within a design domain constructed by

composite material with microstructures. The effective material properties of the composite material are calculated using the theory of homogenization [75, 78, 79].

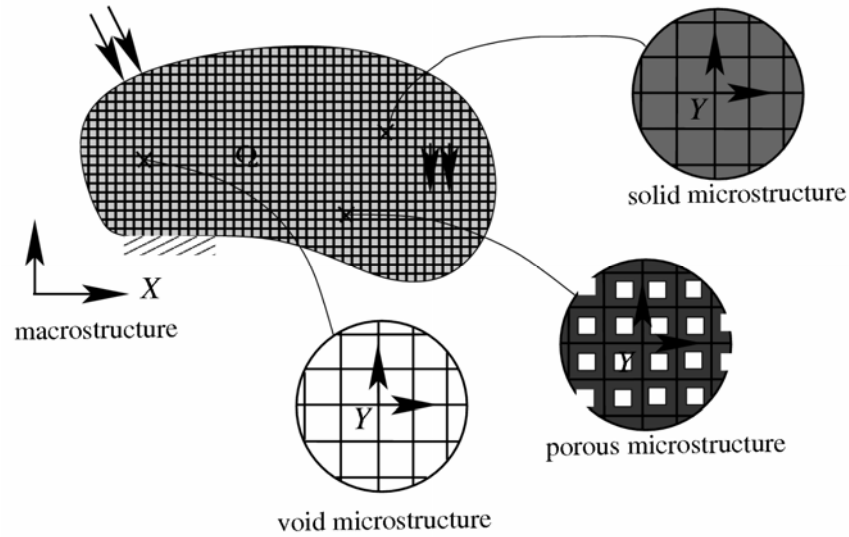


Fig. 1.11 Schematic representation of material microstructure [79]

The homogenization based optimization method first assumed that a periodic microstructure exists in the vicinity of an arbitrary point of a linearly elastic structure, and then introduced the concept of composite porous media. By introducing a material model with periodic, perforated microstructure, namely the *hole-in-cell* microstructure, the topology optimization problem is regularized via relaxation (extension) of the design space. The periodicity of the micro-structural model implies that the macroscopic mechanical properties of the structure can be determined by the microstructural parameters by means of the homogenization techniques. As shown in Fig.1.11, the design domain is composed of infinite micro-voids and then re-distributes a pre-specified amount of material by controlling the size and orientation of the voids. Two coordinate systems, X and Y , are defined to describe the material on the macroscopic scale and on the microscopic scale, respectively. The design variables of the topology optimization model are the dimensions of these microstructures. If the hole is full of the entire cell, the cell is void. Contrarily, if the hole reduces to zero, the cell represents solid.

(2) Density function method

The density function approach proposed by Mlejnek and Schirmacher [80], Yang and Chuang [81] has become a very popular approach for determining structural layout because of its simplicity and efficiency. In this approach, individual elements are considered to be of isotropic material. Unlike the homogenization method, in which the size and orientation of the voids are design variables, the material density of each finite element is selected as the design variable and the intermediate density is penalized (Fig.1.12). A comparison of the topology optimization based on the density and the homogenization is given in reference [82].

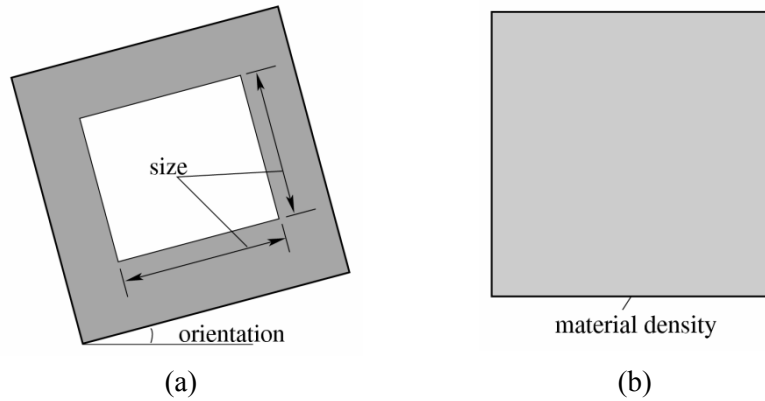


Fig. 1.12 Comparison of cell configurations for topology optimization
(a) Homogenization method; (b) Density function approach

The effective material properties can be evaluated using the relationships between the material density and Young's modulus, which is called material model. Some familiar material models including the Solid Isotropic Material with Penalization (SIMP) [83, 84] and Rational Approximation of Material Properties (RAMP) [85], have been applied to a wide range of structural as well as multidisciplinary design problems. Both SIMP and RAMP introduce the penalization power to force the topology design toward limiting values, 0 denotes void and 1 denotes solid, and thereby prompt the creation of more distinctive 0-1 topology designs.

(3) *Evolutionary Structural Optimization*

The evolutionary structural optimization (ESO) proposed by Xie and Steven [86] seeks the optimum design by removing the lowest stressed material from an oversized structure in

an evolutionary manner. Each time elements are removed, the structure is re-analyzed to obtain the new load paths. This is repeated until the result is a fully stressed design where all the members support the same maximum stress.

The ESO method requires a very small structural modification per cycle, and thus the computational cost is expensive. The new technique developed was the bidirectional ESO (BESO) method [87, 88], which involves adding material where the structure is over-stressed and simultaneously removing material where the structure is under-stressed in an iterative manner until a fully stressed design is achieved.

This kind of evolutionary optimization techniques is known as the hard kill optimization method. Without element elimination, Mattheck and Burkhardt [89], Baumgartner et al [90] suggested a soft kill option (SKO) method. In the SKO method, by setting the Young's modulus equal to the effective stress of elements in an optimization process, the optimal topology that represents an efficient load-carrying mechanism in the design domain can be characterized by the variation in its modulus.

(4) Level Set Method

The level set method was proposed by Osher and Sethian [91] in 1988 for tracing the propagation of the interfaces by driving one or several higher dimensional level set functions. The level set method was firstly introduced into the structural topology optimization by Sethian and Wiegmann [92]. In essence, the method employs the implicit moving material interface models or the level set vectors to represent complex interfaces, and the movement of the material interfaces is governed by a Hamilton-Jacobi type partial differential equation, whose robust numerical algorithm can handle topology merging or breaking naturally during the topology optimization process. For an overview, see also references [93, 94].

Other approaches such as the bubble method [95], the genetic algorithm [96], the neural networks algorithm [97], the bionics method [98] and the independent continuous mapping method [99], also have been employed to solve a wide range of topology optimization problems. In this paper, the density function method associated with SIMP model is used to design the topology layout of the steel and concrete composite beam.

1.4.3 Structural optimization design under uncertainty

Deterministic structural optimization searches for minimum cost without considering the uncertainties in design, manufacturing and operating processes. However, in a practical engineering design problem, as a rule, the uncertain scatter of structural parameters about their nominal values is unavoidable. For example, the applied loads may fluctuate dramatically during its service life-cycle, and the parameters defining the structure, such as geometrical dimensions and material properties, are also subject to inaccuracies or deviations. The structural performance always exhibits some degree of variations due to uncertainties of material properties, loading conditions, geometric dimensions, etc. Therefore, accounting for the inherent uncertainties of structures, non-deterministic structural optimization is attracting increasing attentions both in theoretical research and practical applications.

1.4.3.1 Probabilistic reliability-based approach

Conventionally, uncertainties in structures are inherently modeled as stochastic variables (or random fields/ processes) with certain probability distribution. Based on the classical probability theory, the probabilistic reliability theory provides a powerful methodology to take into account those uncertainties in the analysis and design of structures [100, 101]. The purpose of this methodology is to assess the structural reliability or the failure probability in presence of stochastic uncertainties.

A fundamental problem in structural probabilistic reliability theory is the computation of a multi-fold probability integral, which led to the development of various approximation methods [102]. As widely accepted by the engineering community, the first order reliability method (FORM) [103, 104] is one of the most efficient computational methods for the probabilistic structural reliability. The FORM constructs an approximation to the limit-state surface by a linear function, accuracy problems occur when the performance function is strongly nonlinear. The second order reliability method (SORM) [105-107] was then proposed as an attempt to improve the accuracy of FORM by approximating the limit-state surface using a quadratic surface. In general, FORM and SORM are sufficiently accurate for engineering purposes. However, these gradient based methods, which require the derivatives

of limit-state function with respect to the uncertain variables, were hardly effective when direct or analytical differentiation is impossible. The response surface method [108, 109] emerged as an alternative. Since the response surface commonly presents a simple form even an explicit expression, the computational operation cost can be reduced. Moreover, many classical procedures, such as Monte Carlo method, gradient projection method, were easily applied to improve the efficiency of the response surface [110-113].

Based on the probabilistic reliability theory, non-deterministic structural optimization, including Reliability-Based Design Optimization (RBDO) [114, 115] and structural robust design optimization [116-118], is attracting increasing attentions both in theoretical research and practical applications. While robust design aims at minimizing variation of the objective performance, RBDO puts more emphasis on reliability of the constraints. Robust design and RBDO are highly desirable because they have huge implications in commercial applications such as gaining greater market share for higher profits in the long run. In particular, RBDO is an effective approach to avoid structural failure and to enhance safety in the presence of uncertain parameters.

In the conventional RBDO method [119, 120], the probabilistic constraints are stated in terms of the reliability indices. This is the reliability index approach (RIA). At every iteration in the RIA, the reliability indices are calculated by determining the most probable point (MPP) from the FORM. The computational requirements are costly because numerous reliability analyses should be performed. Furthermore, the MPP search is very expensive for highly nonlinear constraints. Recently, a new approach, called the performance measure approach (PMA), has been introduced by Tu et al. [121]. To estimate the probabilistic constraints, the PMA employs probabilistic performance measures which satisfy target reliability indices. The PMA is reported to be more robust and efficient than the conventional RIA [122] and enhanced by techniques such as sequential optimization and reliability assessment [123] and the hybrid mean value method [124].

Some previous studies have shown that uncertain variations of both structural parameters [125] and material microstructures [126] may have considerable effects on the structural layout design. Thus, the Reliability-Based Topology Optimization (RBTO) [125], which

integrates the probabilistic reliability concept into the topology design of continuum structures, has been investigated by many authors for the conceptual design of large deformation structures [127], micro-electromechanical systems (MEMS) [128-131], heat transfer devices [132], and multi-physics coupled systems [133]. These studies showed that structures designed under specific reliability constraints may have different optimal topologies compared with conventional deterministic optimal designs.

1.4.3.2 Non-probabilistic approach based on convex model

The analysis of the probabilistic reliability requires precise information on the distribution of the uncertainties involved in the design. These data are hardly available in some practical engineering applications where there are only a limited number of samples or the uncertainties are inherently non-probabilistic. Studies on the construction of probabilistic models on the basis of incomplete information can be dated back to five decades ago. A long tradition in probability theory is to use the maximum entropy approach for setting up target distributions in the absence of sufficient sample data [134, 135]. The basic assumption of this approach is that the distribution of maximum entropy under constraints of first statistical moments matching is the least-biased estimation of the real distribution. The maximum entropy approach tends to produce a distribution that is closest to uniform.

However, it is noticed that the probabilistic reliability may be sensitive to the description of the random parameters and thus just small errors in the inputs may yield misleading results [136]. These, to some extent, prevent the conventional probabilistic methods from wider applications in practical engineering designs. Consequently, the quantification of various uncertainties in realistic systems is still a challenge problem [137] and a number of attempts have been made to apply non-probabilistic models, such as convex model and fuzzy randomness model, for mathematical description of the uncertainty in non-deterministic structural analysis and optimization problems with limited uncertainty information [138, 139].

In many circumstances, the bounds of the uncertainties, compared with the precise probability distribution data, are more easily available. The convex model, which provides an objective description of the boundary of the parameter variations without considering the

inner distribution, is suitable to treat those uncertain-but-bounded parameters in the optimization of uncertain structures. In the 1990s, Ben-Haim [140, 141] and Elishakoff [142] first discussed the concept of non-probabilistic reliability based on the convex model theory. The principal assumption behind this concept is that: a structural system is considered to be more reliable when it allows for a greater extent of uncertainties, and vice versa. In this context, the reliability of a structural system is measured with the maximum extent of uncertainties it permits. Following this idea, researchers have developed a variety of formulations and numerical techniques for implementing the non-probabilistic design optimization, which serves as an alternative to the well-established RBDO approaches when complete information on the uncertainty distribution is not available. Qiu and Elishakoff [143, 144], Elishakoff et al. [145] studied the optimal design of truss structures with uncertain-but-bounded parameters using the interval set modelling combined with a so-called anti-optimization technique. The interval set was also employed by Tabakov and Walker [146] to model the manufacturing tolerances in the ply angle optimization of a laminated composite shell using the GA algorithm. Lombardi and Haftka [147], Pantelides and Ganzerli [148] applied the anti-optimization technique to the optimization of structures with uncertain loading conditions. To avoid the expensive anti-optimization computations, Ganzerli and Pantelides [149] developed a convex model superposition technique.

Among the existing studies, the frequently used convex models are the interval model and the ellipsoid model. A principle characteristic of the interval model is that all the uncertain-but-bounded variables vary independently and thus may reach their extreme values simultaneously. For this reason, a pure interval model is often criticized for providing an over-conservative description of the system variability. On the other hand, the ellipsoid model considers all the variables to be correlated with each other, which excludes extreme combination of uncertain parameters and thus avoids over-conservative designs. It should be noted that in most cases only part of these uncertain-but-bounded variables are actually correlated while some others vary independently. Therefore, a more realistic way is to divide all the uncertain-but-bounded quantities into groups and treat them with a multi-ellipsoid convex model. The optimal structural design based on the multi-ellipsoid convex model for

grouped uncertainties has been investigated by Ben-Tal and Nemirovski [150], Luo et al [151].

1.4.3.3 Probabilistic and non-probabilistic mixed approach

In the risk assessment of engineering structures, a frequently encountered case is that: some of the uncertainties can be characterized with certain probability distributions and other uncertainties need to be treated as bounded ones due to their inherent natures or lack of sufficient sample data. A combination of stochastic variables and uncertain-but-bounded variables has been suggested for applications in such circumstances [152]. Penmetsa and Grandhi [153] presented a function approximation technique for the lower and upper bounds estimation of the structural reliability in the presence of both stochastic and interval variables. Similar problems have also been studied by Kreinovich et al. [154] and Qiu et al. [155]. Moreover, Du et al. [156] investigated the reliability-based design optimization of structures characterized by random and interval-valued parameters. In these studies, the upper bounds of the failure probability are determined numerically and used for measuring the structural reliability. Expensive interval arithmetic is usually involved for this task. Recently, the fuzzy set theory has also been combined with the probability theory for handling structural systems involving epistemic uncertainties arising from linguistic or subjective measures [157-159].

CHAPTER 2:
NONLINEAR FINITE ELEMENT SIMULATION OF
BONDED COMPOSITE BEAMS

2.1 INTRODUCTION

In comparison with laboratory tests which are highly time and cost demanding, the numerical simulation is cheaper, time-saving, not so dangerous and more information. As the computational power has intensely increased, numerical methods, in particular the finite element method (FEM), have also been resorted for analysis of many practical engineering problems. During the past three decades, numerous finite element programs have been developed which are able to solve linear, nonlinear, static, dynamic, elastic, plastic, steady state as well as transient problems.

In bonded steel and concrete composite beams, the debonding of the adhesive layer is one of the principal causes for deterioration or damage and the steel/concrete interfacial bonding shear strength plays an important role. However, the bonding shear strength depends not only on the mechanical properties of the component materials, but also on the surface properties of the steel and the concrete. Therefore, to effectively simulate the mechanical behavior of bonded composite beams, the interfaces should be distinguishingly modelled and the bonding shear strength is needed to be tested in advance.

In this chapter, the push-out test is first implemented to determine the shear strength of the adhesive bonding connection. Then, a three-dimensional nonlinear finite element model is proposed for analysis the bonded steel and concrete composite beams. This model takes into account the nonlinearity of the structure and also the effect of the concrete/adhesive interface. After being validated by existing experimental tests, this model is used to investigate the effects of some important parameters on the mechanical performance of the composite beams, including the elastic modulus of adhesive, the thickness of adhesive layer, the bonding strength and the bonding area.

2.2 PUSH-OUT TEST

The push-out test is a test for the mechanical connection of two different materials. It is widely used in the traditional steel and concrete composite structures for assessing the

interfacial shear strength of shear connectors. Herein, the push-out test has been implemented for studying the shear behavior of bonded composite beams.

2.2.1 Push-out specimen

A total of three uniform specimens were constructed. Each specimen consists of two concrete slabs and one steel girder. The geometry and the dimensions of the specimens have been chosen in reference to Bouazaoui et al. [65], as shown in Fig.2.1. The concrete parts contain some constructional reinforcement to strengthen concrete. The bonding area is 110 mm×350 mm on each face of the steel girder and the required thickness of adhesive layer is 5mm.

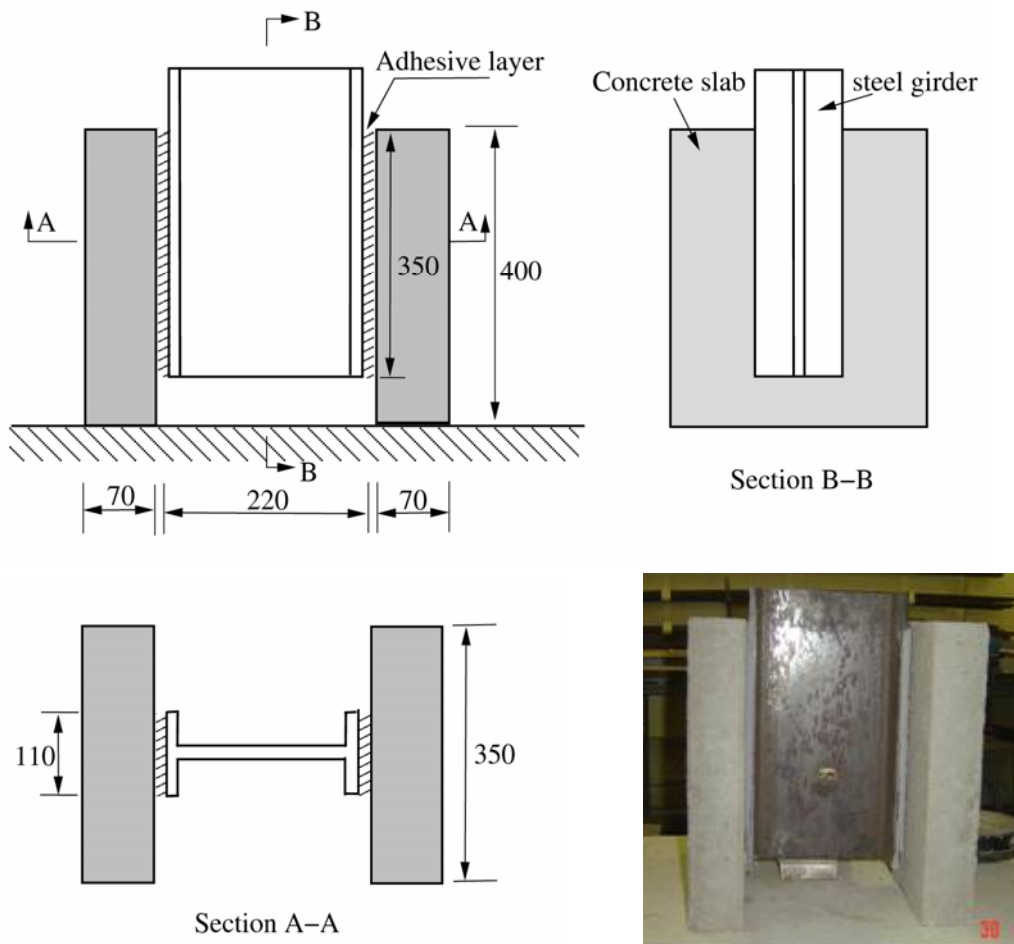


Fig. 2.1 Dimensions of push-out specimen (unit: mm)

2.2.2 Materials

The used concrete slabs were cast at the same time and stored in the same ambient conditions. The cement type was Portland Cement CEM I 52.5 and the compositions of the concrete were listed in Table 2.1. The compressive mechanical characteristics, strength and elastic modulus, of the concrete were determined after cure for 28 days by means of standard tests performed on two $\Phi 16 \times 32$ cm cylindrical specimens. The value of the elastic modulus obtained was 36,600 MPa and the average compressive strength was 71 MPa. The tensile strength obtained by bending tests on a parallelepiped concrete specimen of dimensions $10 \times 10 \times 40$ cm was 5.0 MPa.

Table 2.1 Composition proportion in one cubic meter concrete

Composition	Proportion (kg/m ³)
Coarse aggregate	1050
Sand	681
Cement	400
Silicafume	30
Water	150.5
Additives (sike viscosifier)	3.2

The steel girder used in construction of the specimen was 400 mm in length cut from an IPE 220 rolled beam, having a depth of 220 mm, a flange width of 110 mm, and a linear weight of 26.2 kg/m. The steel's material properties were tested by an MST 250 kN tensile testing machine. The average values obtained from the test for the elastic modulus and yield strength were 205,000 MPa and 470 MPa, respectively. The ultimate tensile strength was 570 MPa.

The adhesive layer was made of an epoxy resin which has a rigid behavior at the working temperature $[-30\text{ }^{\circ}\text{C}, +60\text{ }^{\circ}\text{C}]$. This epoxy resin can offer a good strength of adhesion but less flexibility. Its viscosity allows direct application on the steel surface. The measured mechanical properties of epoxy adhesive were listed in Table 2.2.

Table 2.2 Mechanical properties of epoxy adhesive

Properties	Value
Young's modulus (MPa)	12,300
Poisson's ratio	0.34
Ultimate strength (MPa)	19.5
Ultimate strain	0.0016

2.2.3 Test preparation

Before bonding the steel girder to concrete slabs, the surface treatment was necessary not only for removing any particles and impurities, but also for modifying the microcosmic nature of the surface and thus increasing its surface energy to improve the bonding quality. In this process, the concrete surface in contact with the adhesive was treated by means of corundum sandblasting to expose the coarse aggregates (Fig.2.2a), and then cleaned by an acetone solvent. The steel surface of the flanges was also sandblasted (Fig.2.2b).

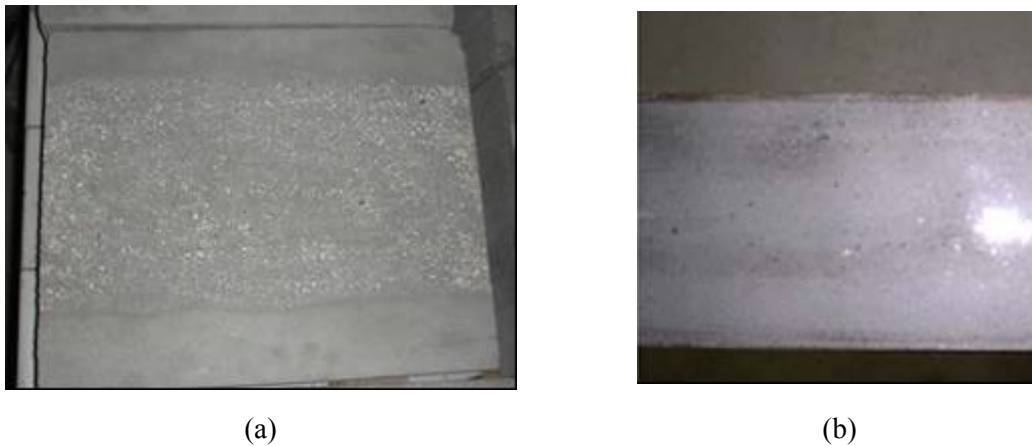


Fig. 2.2 The surface treatment before bonding

(a) The concrete slab; (b) The steel girder

24 hours after the surface treatment, the epoxy adhesive was coated on the steel surfaces of the two flanges along the length of the steel girder. It should be ensured that the coated

thickness of the epoxy adhesive was about 2 mm more than the final required thickness. After setting the required thickness of the adhesive layer (5 mm), the concrete slabs were tightly put upon the two faces of the steel girder. The remaining adhesive should immediately cleaned by a spatula.

Two days after the bonding operation, measuring instrumentations can be equipped on. During the test, the vertical displacement at loading point was continuously recorded by a Linear Variable Differential Transformers (LVDT). With the aim of measuring the evolution of the strains of the steel girder, a total of 3 strain gauges (G1, G2 and G3) were installed on the web of steel girder in the vertical direction. The location of these instrumentations was shown in Fig.2.3. Herein, the measuring data from the LVDT and strain gauges were recorded by using a data acquisition system connected to a computer.

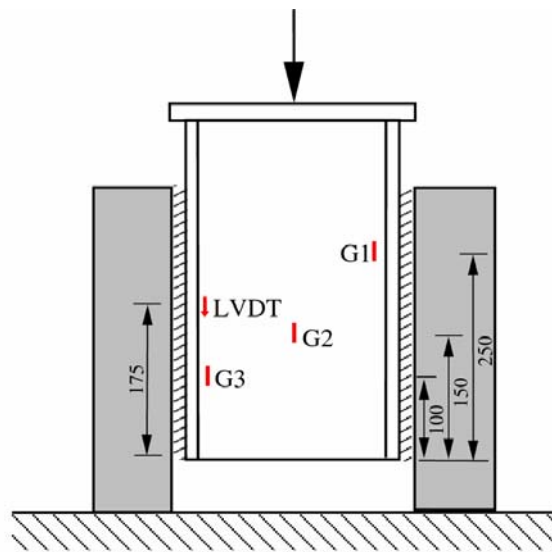


Fig. 2.3 Location of instrumentations (unit: mm)

The prepared push-out specimen was loaded by using the loading equipment with a capacity of 800 kN (Fig.2.4). To ensure the specimen was properly seated and all the instruments were working well, a small preload of 20 kN was applied on the push-out specimen and removed gradually before the actual test. After this pre-operation, a continuously increasing load at a uniform rate was then applied to the specimen up to failure.



Fig. 2.4 Push-out loading equipment

2.2.4 Push-out results



Fig. 2.5 Failure mode of push-out specimen

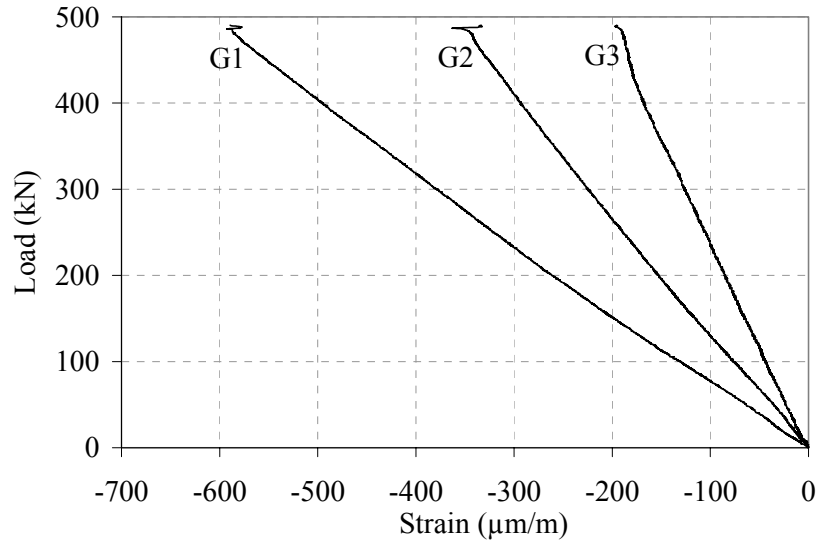


Fig. 2.6 Load versus strain in the web of steel girder

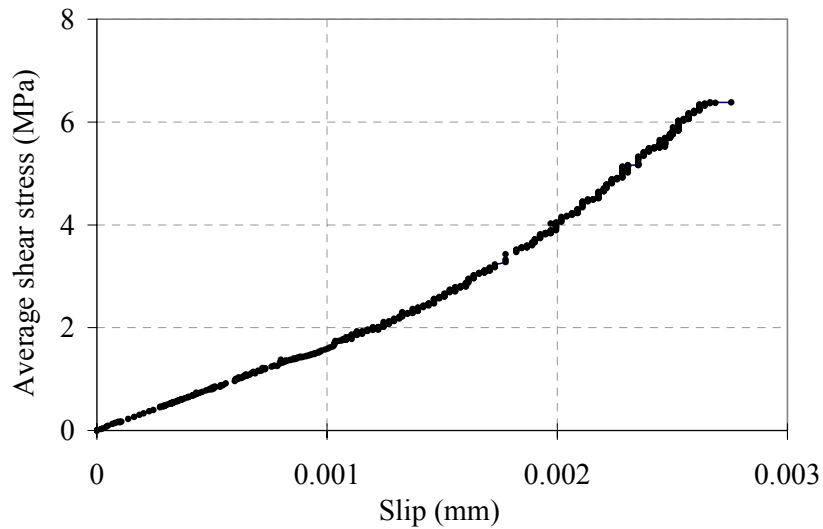


Fig. 2.7 Average shear stress versus slip curve

The failure mode of the push-out specimen is shown in Fig.2.5. It can be observed that the failure occurred within the first 2-5 mm of the concrete from the steel/concrete interface. Although the epoxy adhesive was subjected to a large shear force, no cracks were observed in the adhesive layer. This failure mode indicates a good bonding connection between the steel

and the concrete. The linear strain curves obtained by strain gauges showed that the steel girder is still in the stage of elastic deformation (Fig.2.6).

Fig.2.7 shows the evolution of the relative slip according to the applied average shear stress. The behavior of the bonding connection is close to linear elastic until a brittle failure, with the ultimate shear strength of 6.36 MPa and a very small ultimate slip. The curve of shear stress versus slip shows the bonding connection by epoxy adhesive can be considered as rigid.

2.3 FINITE ELEMENT MODEL OF BONDED COMPOSITE BEAMS

Using the finite element package ANSYS [160], a three-dimensional finite element model was developed to simulate the nonlinear behaviour of the bonded steel and concrete composite beams. The concrete slab was modeled by the 8-node concrete solid element (SOLID65), which is capable of cracking in tension and crushing in compression. Reinforcing steel bars in concrete were represented by the 3D beam element (BEAM188). The adhesive layer and the steel girder were modeled by the 8-node solid element (SOLID45).

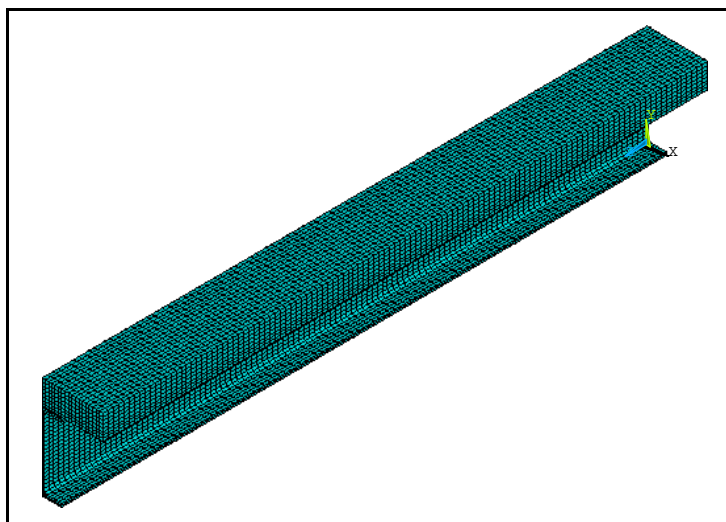


Fig. 2.8 Finite element mesh for a quarter of the composite beam

When the steel and the concrete were bonded by the epoxy adhesive, the previous push-out test showed that the debonding failure occurs through a thin layer of concrete near to the adhesive layer, while the adhesive layer itself is not cracking since the shear strength of the adhesive are usually higher than that of concrete. In view of this special failure phenomenon, a nonlinear spring element (COMBIN39) was employed to simulate the shear debonding characteristic of concrete/adhesive interface, whereas the steel/adhesive interface was assumed to be perfectly bonded. Due to symmetry of the problem, only a quarter of the simply supported composite beam was modeled by imposing an appropriate boundary condition on the symmetric areas, as shown in Fig.2.8.

2.3.1 Concrete/adhesive interface modeling

For the bonded steel and concrete composite beam, the interface of concrete slab and adhesive layer, where the debonding failure may occur, must be modeled specially. As shown in Fig.2.9, the nonlinear springs were added between the adjacent concrete element and adhesive element to model the shear resistance of concrete/adhesive interface, which has zero thickness. In this model, the normal nodal displacements were considering as coincident in the interface.

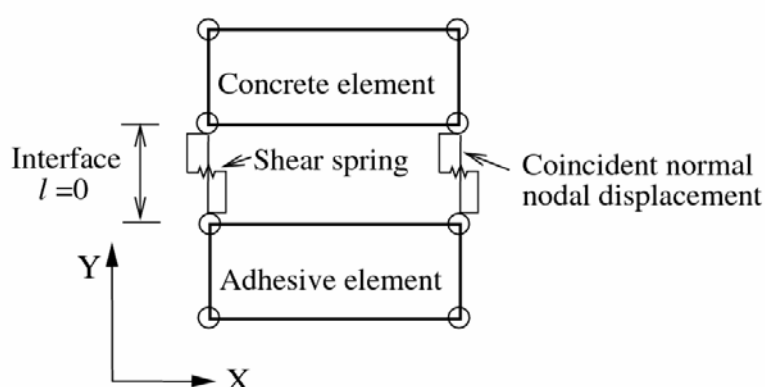


Fig. 2.9 Schematic illustration of concrete/adhesive interface modeling

The element COMBIN39 is a one-dimensional element defined by two nodes and a generalized force-deflection curve. The two nodes may be anywhere in space (including the

node-coincident case). The points on the force-deflection curve (denoted by $D1$, $F1$, etc.) represent force versus relative translation for structural analyses. Therefore, the shear behavior of the concrete/adhesive interface can be evaluated quantitatively by the force-deflection curve. Using the average shear stress versus slip curve in Fig.2.7 obtained from the available push-out test, a table of force values F and relative slip values D for the nonlinear springs can be defined as follows.

$$\begin{aligned} F &= \tau \times A_i \\ D &= s \end{aligned} \quad (2.1)$$

where A_i is the bonding area corresponding to the i th nonlinear spring, τ and s are the average shear stress and slip, respectively.

2.3.2 Concrete modeling

The concrete slab was modeled by a smeared crack model using the von Mises yield criterion with an isotropic hardening assumption. The concrete element is capable of cracking in tension and crushing in compression. In this model, if cracking or crushing behavior is predicted, the stress-strain relation is then adjusted associated with the integration points according to conditions.

(1) Compressive behaviour

Concrete in compression is considered to be an elastic-plastic and strain-softening material. The elastic modulus and the compressive strength of concrete slab, measured at the 28th day after concreting by means of standard cylindrical specimen tests, are denoted by E_c and f'_c , respectively. The stress-strain curve is assumed to be linear up to $0.4f'_c$, and the nonlinear stress-strain relationship for concrete in uniaxial compression can be expressed as an equation which was proposed by Carreira and Chu [161].

$$\sigma_c = \frac{f'_c \gamma_m \left(\varepsilon_c / \varepsilon'_c \right)}{\gamma_m - 1 + \left(\varepsilon_c / \varepsilon'_c \right)^{\gamma_m}} \quad (2.2)$$

where σ_c is the concrete compressive stress, ϵ_c is the concrete strain, ϵ_c' is the strain corresponding with the compressive strength f_c' , and γ_m is a modified material parameter defined by

$$\gamma_m = \frac{1}{1 - f_c' / (\epsilon_c' E_c)} \quad (2.3)$$

If the material at an integration point fails in compression, the material is assumed to be crushed at that point. In the concrete element, crushing is defined as the complete deterioration of all the strength characteristics of the material. In this paper, the crushing capability of the concrete element is disabled for improving convergence.

(2) Tensile behaviour

Concrete in tension was considered as a linear-elastic material up to the uniaxial tensile cracking stress, which is defined as the function of the compressive strength, that is $f_{ct}' = 0.6225\sqrt{f_c'}$. In the model, the presence of a crack at an integration point is represented through modification of the stress-strain relations by introducing a plane of weakness in a direction normal to the cracking face. Thus, the tensile stress decreases to zero immediately after concrete cracking. A typical asymmetry between the compressive and the tensile behaviour for concrete is shown in Fig.2.10.

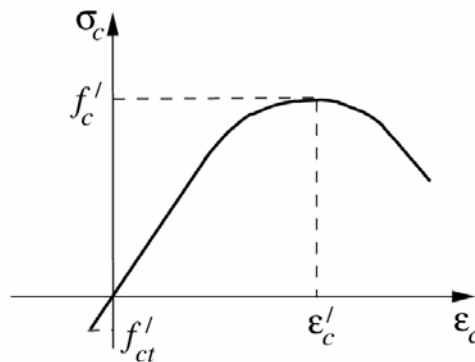


Fig. 2.10 Concrete stress-strain curve for uniaxial loading

(3) Crack shear transfer

The reduction in shear strength was taken into account as the crack opens. It is obvious that a considerable amount of shear stress can be transferred across the crack faces of concrete due to the surface nature of the crack face. Therefore, a “shear transfer coefficient” γ_t for an open crack is introduced which represents a shear strength reduction factor for shear sliding across the crack face. On the other hand, if the crack closes, then all compressive stresses normal to the crack plane are transmitted across the crack and a “shear transfer coefficient” γ_c for a closed crack is also introduced. The value of shear transfer coefficients is between 0 and 1, where 0 represents a smooth crack (complete loss of shear transfer) and 1 represents a very rough crack (no loss of shear transfer). The coefficients considered herein are $\gamma_t = 0.35$ and $\gamma_c = 0.75$.

2.3.3 Adhesive and steel modeling

The adhesive layer composed of epoxy resin or polyurethane was assumed to be linear elastic, isotropic material up to failure. The stress-strain relationship for the adhesive layer is expressed as

$$\sigma = \begin{cases} E_a \varepsilon & \varepsilon \leq \varepsilon_{au} \\ 0 & \varepsilon > \varepsilon_{au} \end{cases} \quad (2.4)$$

where σ , ε , E_a and ε_{au} are the actual stress, the actual strain, the elastic modulus and the ultimate strain in the adhesive, respectively.

For the steel I-girder, an elastic-plastic isotropic hardening rule and the von Mises yielding criterion were considered. A piece-wise linear stress-strain curve was used for steel girder in both compression and tension. The von Mises yield criterion was also used for the internal reinforcing steel in the concrete slab, and an isotropically hardening material is assumed, with perfectly plastic after the elastic limit.

2.4 VALIDATION OF THE FINITE ELEMENT MODEL

Two simply supported bonded steel-concrete composite beams (denoted by beam P1 and beam P2) tested to failure by Bouazaoui et al. [65], were analyzed by using the proposed nonlinear finite element model for the validation purpose. The span of the composite beams was 3486mm and the loads were applied to the mid-span of the beams. These two beams, with the only difference in the material properties of the adhesive layer (epoxy resin for beam P1 and polyurethane for beam P2, respectively), have the same dimensions as shown in Fig.2.11. The material properties for the composite beams are given in Table 2.3. In the FE model, a total of 24554 elements are used for modeling a quarter of the composite beam.

Table 2.3 Material properties of the composite beams

Material	Properties	Value
Concrete slab	Young's modulus (MPa)	36,600
	Poisson's ratio	0.28
	Compressive strength (MPa)	68
	Strain in compressive strength	0.003
Steel girder	Young's modulus (MPa)	205,000
	Poisson's ratio	0.3
	Yield stress (MPa)	470
	Ultimate strength (MPa)	570
	Ultimate strain	0.1
Reinforcing steel	Young's modulus (MPa)	205,000
	Poisson's ratio	0.3
	Yield stress (MPa)	500
Epoxy resin adhesive	Young's modulus (MPa)	12,300
	Poisson's ratio	0.34
	Ultimate strength (MPa)	19.5
	Ultimate strain	0.0016
Polyurethane adhesive	Young's modulus (MPa)	38.3
	Poisson's ratio	0.38
	Ultimate strength (MPa)	9.2
	Ultimate strain	0.24

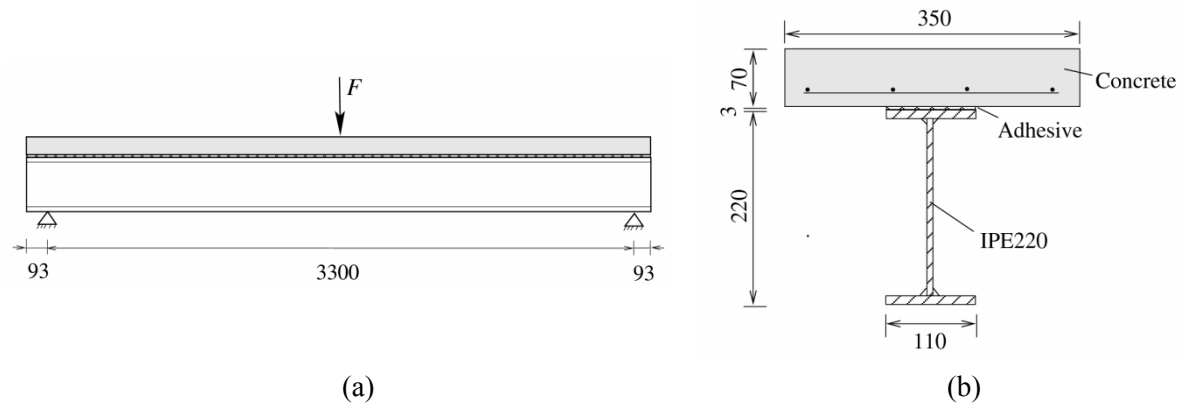


Fig. 2.11 Sketch of the composite beams

(a) Overall dimensions; (b) Cross-section dimensions (mm)

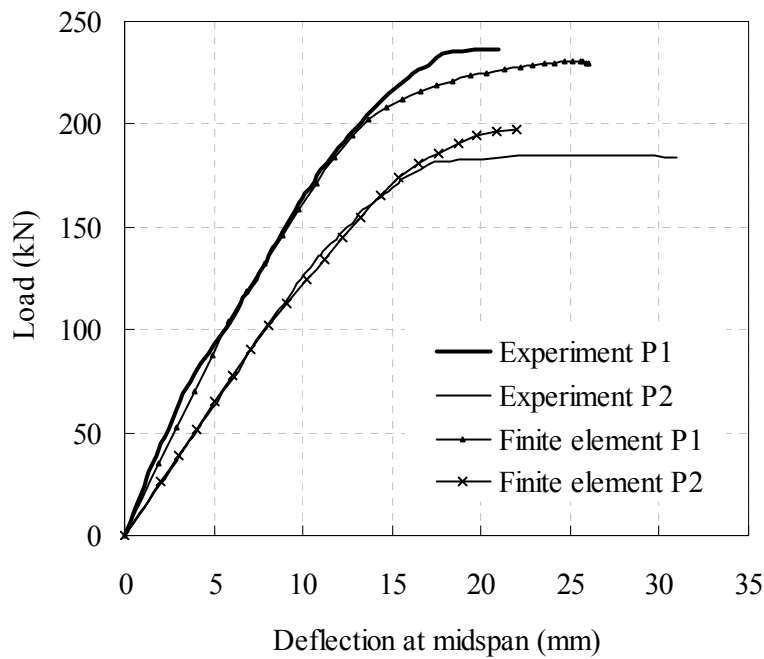


Fig. 2.12 Load-deflection curves from finite element model and test results

The curves of load versus mid-span deflection predicted by the proposed finite element model are compared with the corresponding test results in Fig.2.12. A good agreement between the numerical and experimental results was obtained not only in the initial stiffness

but also in the ultimate strength. The ultimate loads obtained by the present model are 230.5kN for beam P1 and 197kN for beam P2, which are 3.2% lower and 6.5% higher than the experimental ultimate value, respectively. The nonlinear numerical simulation also confirmed the experimental observation that the failure of bonded composite beams is caused by the concrete slab cracking and the steel girder yielding, without the debonding of adhesive connection. Therefore, it can be concluded from these comparisons that the finite element model developed in this paper is capable of predicting the nonlinear behavior of bonded steel and concrete composite beams.

2.5 EFFECTS OF PARAMETERS

2.5.1 Effects of the elastic modulus of adhesive

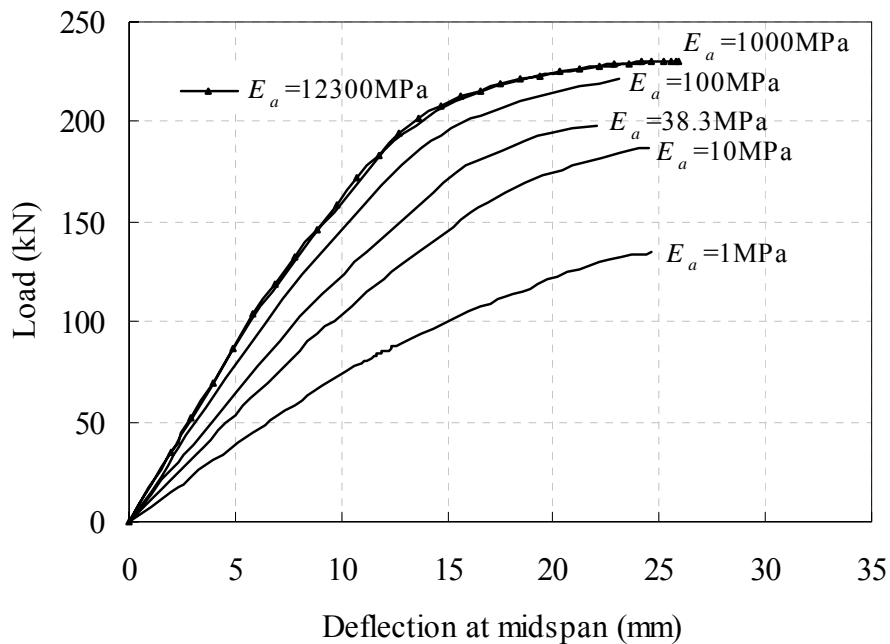


Fig. 2.13 Load-deflection curves of composite beams for various elastic modulus of adhesive

As can be observed in Fig.2.12, the initial stiffness and the ultimate strength of beam P2 are much lower than those obtained in the beam P1. This shows that the mechanical behavior

of the bonded composites beam highly depends on the adhesive's material properties. The proposed model was further used to investigate the behavior of bonded steel and concrete composite beams with various elastic modulus of adhesive, whereas other conditions remained unchanged.

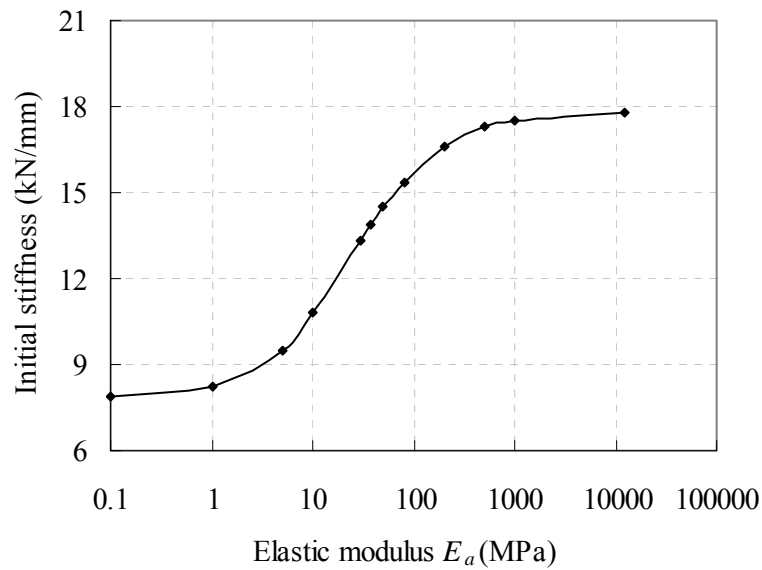


Fig. 2.14 Relationship between the initial stiffness and elastic modulus of adhesive

The load-deflection curves of composite beams with various elastic modulus are shown in Fig.2.13. It can be observed that the initial stiffness and the ultimate strength increase with the elastic modulus of the adhesive layer. Moreover, the nonlinear relationship between the initial stiffness of load-deflection curve and the elastic modulus of the adhesive layer is shown in Fig.2.14. According to the correlative level, three parts can be divided in this relation. In the first part ($0 < E_a < 1 \text{ MPa}$), the bonding effect by adhesive is much feeble because it cannot prevent the slip between the concrete slab and the steel girder at all. The mechanical behaviour of the bonded composite beam with adhesive property among this part is the same as the beam without any connection. In the second part ($1 \text{ MPa} \leq E_a \leq 1,000 \text{ MPa}$), a strong interaction between the initial stiffness and the elastic modulus is observed. The performance of bonded connection depends strongly on the elastic modulus of the adhesive. However, in

the third part ($E_a > 1,000$ MPa), the initial stiffness is almost not affected by the elastic modulus of adhesive. The adhesive bonding can effectively prevent the slip between the concrete slab and the steel girder in this part. Therefore, it is worth pointing out that the elastic modulus of adhesive material should be taken among the third part in order to ensure the desired performance of the bonded steel and concrete composite beams. Therefore, the advisable minimal value of the elastic modulus of the adhesive is 1000 MPa.

2.5.2 Effects of the adhesive layer thickness

In the practical operation condition, it is always difficult to control the thickness of the adhesive layer in a regular required thickness due to the complexity of construction in situ. In this section, a detailed investigation on the effects of adhesive thickness is carried out by the proposed nonlinear finite element analysis. The investigated composite beams have different adhesive layer thickness, whereas all other structural and material parameters are the same as beam P1.

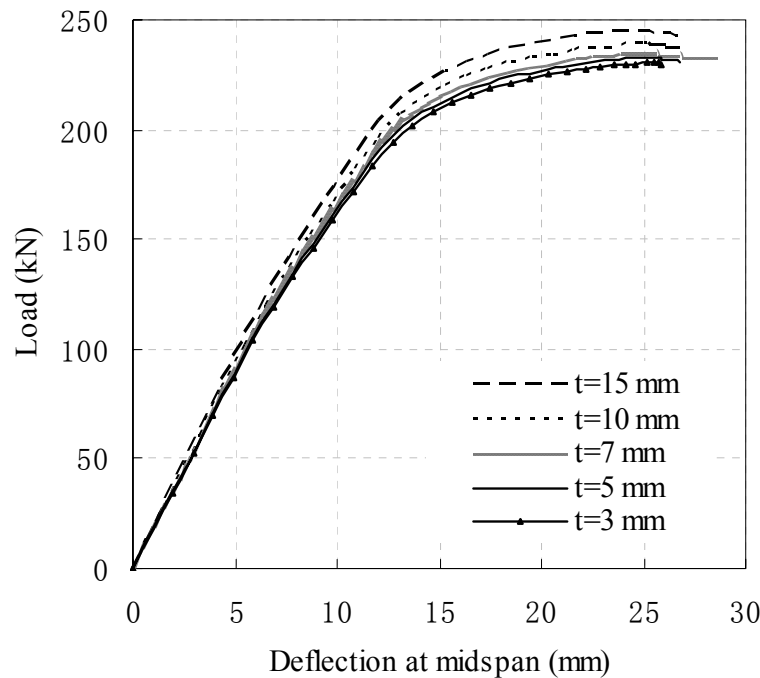


Fig. 2.15 Load-deflection curves of composite beams for various adhesive thicknesses

The corresponding load-deflection curves of composite beams with the adhesive thickness of 3mm, 5mm, 7mm, 10mm and 15mm are shown in Fig.2.15. It appears from the figure that the initial stiffness of the bonded composite beam is barely influenced by the adhesive thickness and the ultimate load slightly increases with an increase of the adhesive thickness. When the adhesive thickness increases from 3mm to 15mm, the ultimate load only increases by 6.3%.

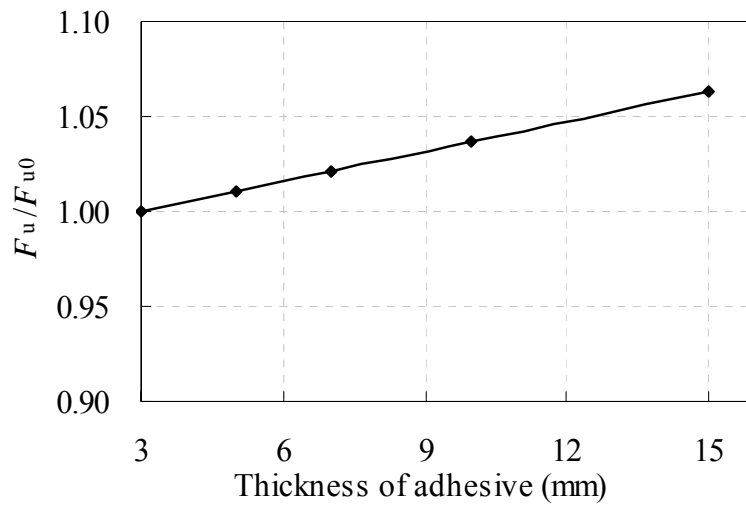


Fig. 2.16 Relationship between relative ultimate load and adhesive layer thickness

The relationship between the relative ultimate load F_u / F_{u0} and the adhesive layer thickness t is shown in Fig.2.16. A linear regression with a very low growth rate is then obtained as

$$\frac{F_u}{F_{u0}} = 0.0053(t - 3) + 1, \quad (t \geq 3\text{mm}) \quad (2.5)$$

where t is in mm, F_u is the ultimate load, F_{u0} is the ultimate load of beam P1 with $t = 3\text{mm}$. It can be concluded that the effects of adhesive thickness on the performance of composite beams are relative small.

2.5.3 Effects of the bonding strength

The debonding failure of the bonded steel and concrete composite beams depends on the bonding strength of concrete/adhesive interface, *i.e.* the ultimate shear stress τ_u . In generally, the bonding strength is determined mainly by the strength of concrete, the properties of adhesive, the technology of surface treatment and the quality control in construction. In this section, we investigate the debonding behaviour of composite beams with various bonding strengths, ranging from 0.5 MPa to 6.0 MPa. The material properties given in Table 2.3 for beam P1 were used for all cases.

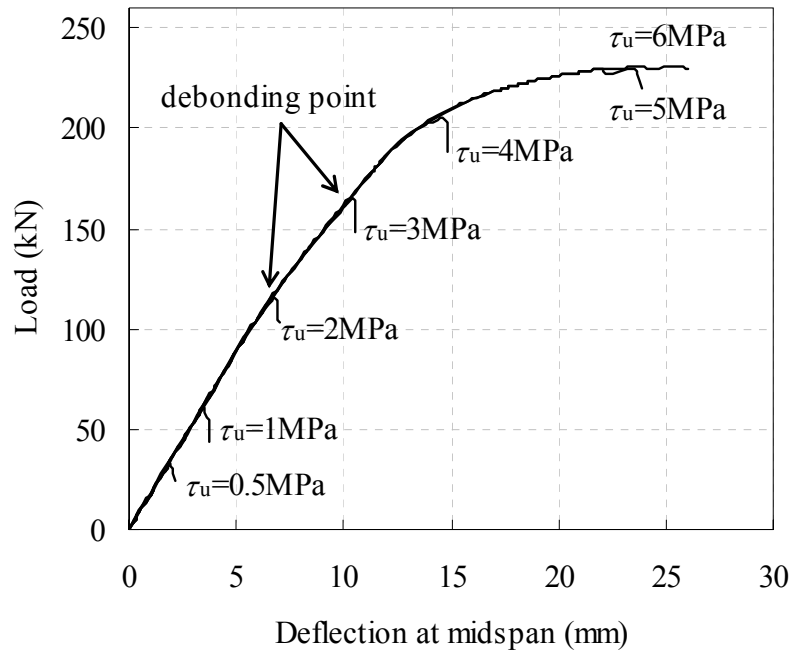


Fig. 2.17 Load-deflection curves of composite beams for various bonding strengths

In Fig.2.17, the ultimate loads when the debonding failure occurs can be observed. The debonding failure is a typical brittle destroy process with a catastrophic failure of the composite beams when an ultimate load is reached. Thus, an important issue in the design of the bonded composite beams is to avoid the failure in debonding mode. Furthermore, a nonlinear relationship between the ultimate load and the bonding strength for those fully bonded composite beams is plotted in Fig.2.18. It can be observed that the debonding failure

will occur if the value of bonding strength locates in $\tau_u \leq 5.0$ MPa and the ultimate load increases rapidly with the bonding strength. When $\tau_u > 5.0$ MPa, the adhesive bonding connection is sufficient and the debonding failure will not occur for this fully adhesive bonded composite beam.

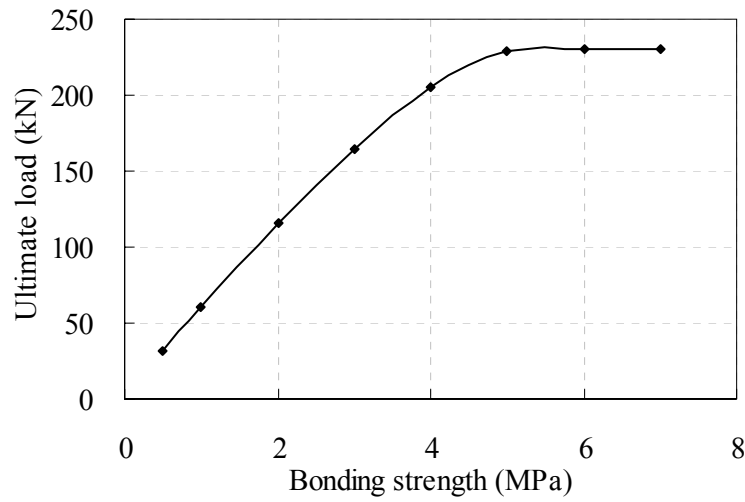


Fig. 2.18 Relationship between ultimate load and bonding strength

2.5.4 Effects of the bonding area

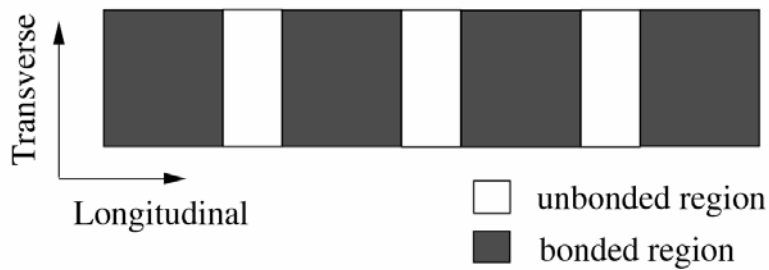


Fig. 2.19 Distribution of the bonded region

Another key factor that influences the debonding behavior of the bonded composite beam is the bonding area. In the present study, a relative bonding area χ , which is the

percent ratio of the actual adhesive bonding area to the maximal possible bonding area, was used. Here we assumed the actual bonded region is distributed evenly in subsection along the length of beam (see Fig.2.19). To quantify its effects, the simply supported composite beams similar as the beam P1 but with various relative bonding areas, ranging from 50% to 100%, were analyzed.

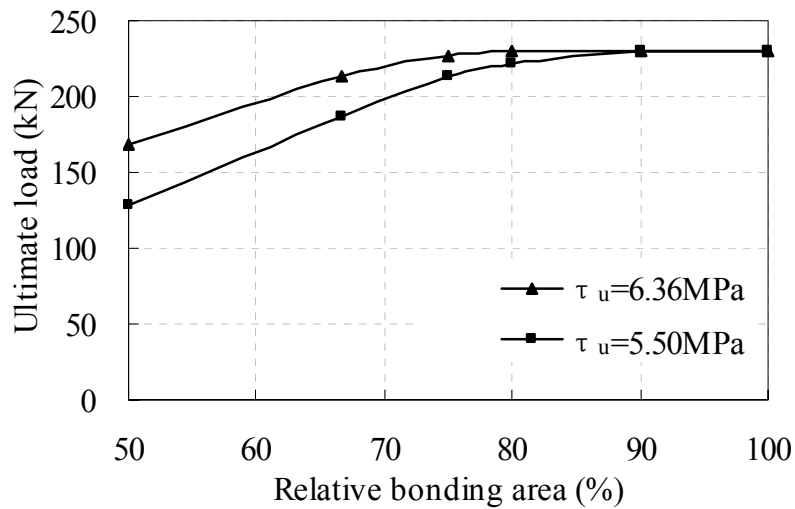


Fig. 2.20 Relationship curves between ultimate load and relative bonding area

The curves of the ultimate load versus the relative bonding area are plotted in Fig.2.20. For the composite beam with the bonding strength 6.36MPa, the higher relative bonding area ($\chi \geq 80\%$) resulted in a perfect connection without the debonding failure. However, when the relative bonding area $\chi < 80\%$, the composite beam will fail in debonding. For the case of the bonding strength $\tau_u = 5.5 \text{ MPa}$, the critical value of the bonding area, χ_c , is 90%. Below the critical bonding area, the ultimate load of the steel-concrete composite beam is influenced by the bonding area.

It is worth noting here that the debonding failure is mainly determined by an average bonding strength, which equals to the relative bonding area multiplying the bonding strength, namely $\bar{\tau}_u = \chi \tau_u$. Therefore, combining the effects of bonding strength and bonding area, an

approximate value of average bonding strength $\bar{\tau}_u \approx 5.0\text{MPa}$ is needed to be ensured for this bonded composite beam in order to avoid the debonding failure.

2.6 SUMMARY

This chapter first carried out an experimental push-out test to study the debonding failure mode and determine the bonding strength. Then, a validated three-dimensional nonlinear finite element model based on the finite element package ANSYS was proposed to predict the parametric effect of bonded steel and concrete composite beams. From the experimental and numerical results, the following conclusions can be drawn:

- The epoxy adhesive bonding connection between the steel girder and the concrete slab provided a bonding strength of 6.36MPa and a rather small ultimate slip. The debonding failure takes place within the first 2-5 mm of the concrete from the adhesive/concrete interface.
- The mechanical behaviour of the bonded composite beam depended strongly on the adhesive's material properties. The elastic modulus of adhesive material should exceed 1,000MPa in order to ensure the desired performance of bonded steel and concrete composite beams.
- The ultimate load of the bonded composite beam depends linearly on the thickness of the adhesive layer. However, this influence is relative small in practical engineering.
- The debonding failure of the bonded steel and concrete composite beam mainly depends on the bonding strength and the bonding area. In view of their effects, an average bonding strength $\bar{\tau}_u \approx 5.0\text{MPa}$ should be ensured in order to avoid the debonding failure.

CHAPTER 3:
TOPOLOGY DESIGN OF THE BONDED COMPOSITE
BEAM

3.1 INTRODUCTION

During a typical sizing or shape design process, the shape and dimensions of an otherwise complete structure with fixed topology are adjusted. In the steel and concrete composite beam, this initial fixed topology is often chosen intuitively or based on previous experience. Therefore, before we carry out the sizing design optimization of the bonded composite beam, a more reasonable topology configuration should be firstly determined. Topology optimization methods of continuum structure are the selection of the best configuration for the design of structures and thus are most valuable as preprocessing tools for sizing and shape optimization. In a topology design process, the connectivity and structural architecture is not pre-specified but emerges from the design process itself. It is widely accepted that topology optimization is of considerable practical importance because it achieves by far greater savings and design improvements than mere sizing or shape optimization.

In this chapter, a three-dimensional topology optimization methodology is presented for the design of the bonded steel and concrete composite beam. Following the SIMP approach, an artificial material model with penalization for elastic constants is assumed and elemental density variables are used for describing the structural layout. The considered problem is thus formulated as to find the optimal structural topology that minimizes the structural cost (material volume) under specified displacement constraints. In this context, an adjoint variable method is used for the sensitivity analysis and the Method of Moving Asymptotes (MMA [162]) is employed to update the design variables. Finally, the optimal topology of the steel and concrete composite beam is obtained.

3.2 TOPOLOGY DESIGN OF THE BONDED COMPOSITE BEAM

By giving a design domain, loads, and boundary conditions, the connectivity and solid material distribution of the structure are gradually emerged during the topology design process. Denoting the whole design domain by Ω and the body occupied by the structural

solid material by Ω_{solid} , the concept of material topology optimization can be described using a discrete function ϕ defined at each point \mathbf{s} as

$$\phi(\mathbf{s}) = \begin{cases} 1 & \forall \mathbf{s} \in \Omega_{\text{solid}}, \\ 0 & \forall \mathbf{s} \in \Omega \setminus \Omega_{\text{solid}}. \end{cases} \quad (3.1)$$

The structural topology optimization problem is mapped into a discrete material distribution problem finding the discrete indicator function $\phi(\mathbf{s})$ that minimizes an objective (or objectives) subject to constraints (see Fig.3.1).

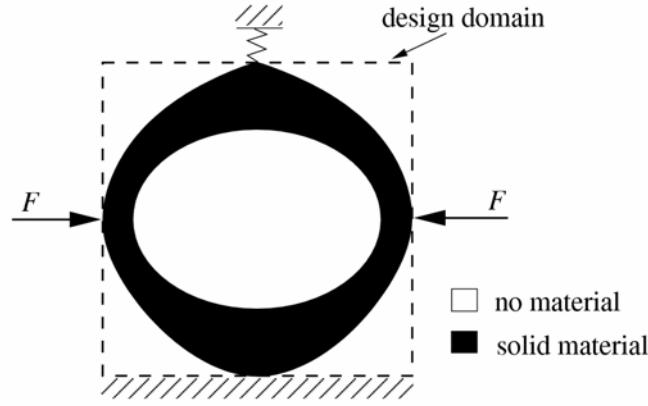


Fig. 3.1 Schematic illustration of material topology optimization

In the considered topology optimization problem, the composite beam structure is designed to minimize the total material volume while still satisfying constraints on specified global behaviors such as structural displacements. Based on the material defining at each point of design domain, the topology optimization of continuum structures with displacement constraints is stated as

$$\begin{aligned} \min_{\phi(\mathbf{s})} \quad & \int_{\Omega} \phi(\mathbf{s}) d\Omega \\ \text{s.t.} \quad & g_j = U_j - U_{\max,j} \leq 0 \quad (j = 1, 2, \dots, m), \\ & \phi(\mathbf{s}) = 0 \text{ or } 1, \quad \forall \mathbf{s} \in \Omega \end{aligned} \quad (3.2)$$

where U_j is the displacement in the j th constraint, and $U_{\max,j}$ is the maximum allowable value of the corresponding displacement.

For the topology optimization of the considered bonded steel and concrete composite beam, a linear elastic response is assumed in this preprocessing design. The design domain of the bonded composite beam is depicted in Fig.3.2. Herein, only the steel part undergoes topological optimization design, while the concrete part is regarded as a non-optimized region. For the purpose of simplification, the adhesive layer is ignored and the steel girder and the concrete slab are assumed to be connected perfectly.

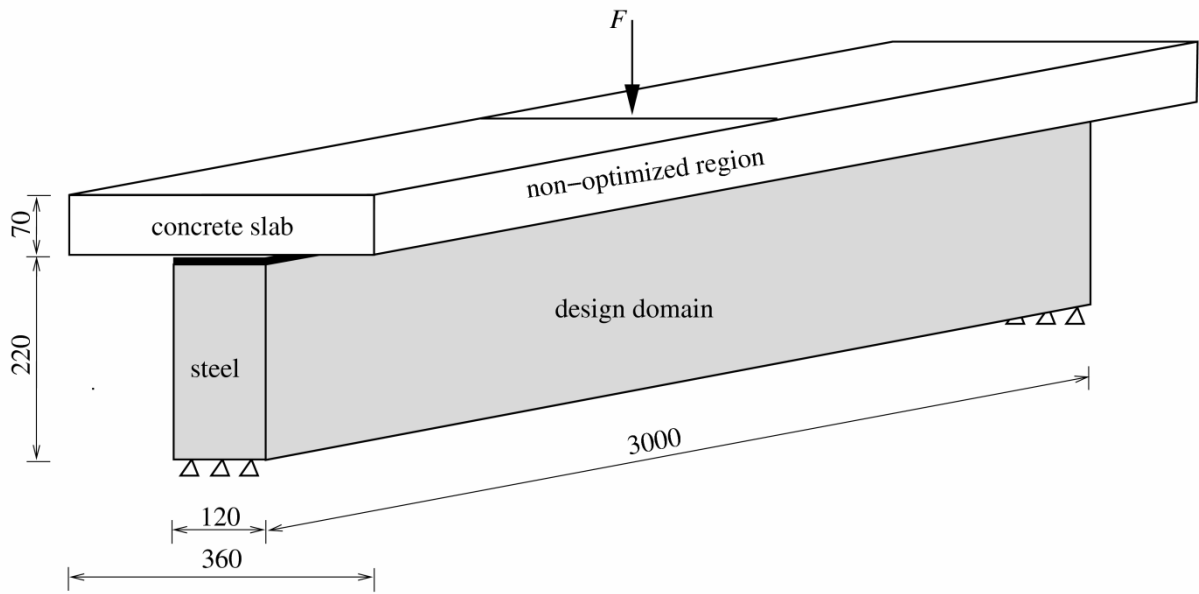


Fig. 3.2 Design domain of the bonded composite beam (Unit: mm)

Herein, all the materials are assumed to be linear, elastic and isotropic. The Young's modulus and the Poisson's ratio of the steel and the concrete material selected from experimental values are the following: $E_s = 205,000\text{MPa}$, $\nu_s = 0.3$, $E_c = 36,600\text{MPa}$, $\nu_c = 0.28$. The composite beam is simply supported and an external concentrated force F , with the magnitude of 200kN, is applied to the concrete slab at the mid-span of beam in downward direction. In this topology optimization design, a vertical displacement constraint $U_{\text{mid}} \leq 10\text{mm}$ is imposed on the loading point.

3.3 SOLUTION STRATEGY

3.3.1 SIMP approach

The topology optimization problem (3.2) is by definition a discretized 0-1 programming one and in general cannot be solved analytically. A frequently used method to relax the formulation is the SIMP approach (Bendsøe [83]; Zhou and Rozvany [84]), which introduces an artificial isotropic material model and replaces the binary topology design variables with element-wise material density variables. The material density variable takes the value 1 in solid domain Ω_{solid} and 0 elsewhere. In the method, by dividing the whole design domain Ω into finite elements, a penalized interpolation scheme between the material properties and the density variables is assumed for suppressing intermediate density values in the resulting optimal design. Using the SIMP approach, the optimization problem is rewritten as

$$\begin{aligned} \min_{\boldsymbol{\rho}} \quad & V = \sum_{e=1}^N \rho_e V_e \\ \text{s.t.} \quad & \mathbf{KU} = \mathbf{P}, \\ & g_j(\boldsymbol{\rho}) = U_j(\boldsymbol{\rho}) - U_{\max,j} \leq 0 \quad (j = 1, 2, \dots, m), \\ & \mathbf{0} < \boldsymbol{\rho}_{\min} \leq \boldsymbol{\rho} \leq \mathbf{1}, \end{aligned} \quad (3.3)$$

where $\boldsymbol{\rho} = [\rho_1, \rho_2, \dots, \rho_N]^T$ is the vector of elemental relative densities which are taking as design variables, V is the total material volume, N is the total number of elements, ρ_e and V_e are the relative density and the volume of the e th element, respectively. \mathbf{K} is the global stiffness matrix, \mathbf{U} is the nodal displacement vector, \mathbf{P} is the external force vector and $\mathbf{KU} = \mathbf{P}$ defines the linear equilibrium state of the finite element model. In order to avoid numerical difficulties caused by zero densities, a lower-bound limit $0 < \rho_{\min} \ll 1$ is imposed on the density variables.

In the artificial material model, the Young's modulus for each element is expressed as a function of the relative density variable, namely

$$E_e = \rho_e^p E_0 \quad (e = 1, 2, \dots, N), \quad (3.4)$$

where $p > 1$ is the penalization factor, E_0 is the elastic modulus for the fully solid material. Fig.3.3 shows the relative stiffness ratio E_e/E_0 versus relative density ρ_e for different values of the penalization factor p , and illustrates that the nonlinearity of the SIMP model implicitly penalized intermediate densities toward limiting values $\rho = 0$ (void) and $\rho = 1$ (solid) and thereby leads approximately to a “0-1” material distribution in the design domain. In this paper, the penalty factor is set to be $p = 3$, which is a usual value used by many topology optimization studies (Bendsøe and Sigmund [163]).

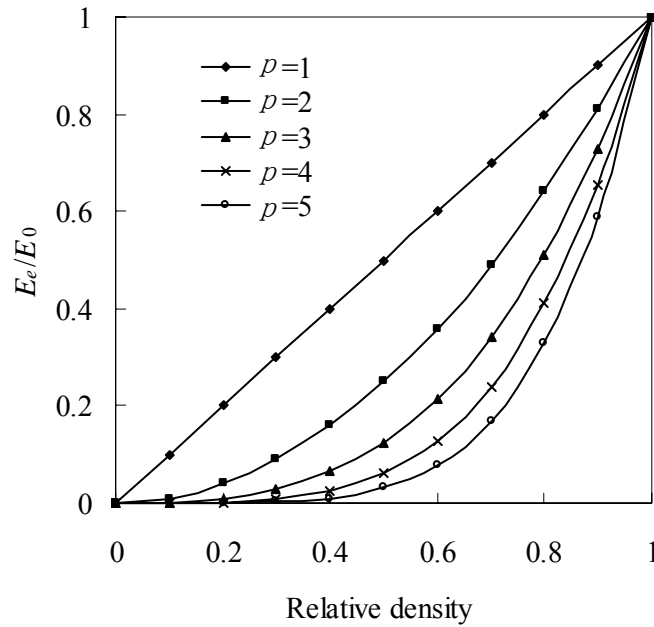


Fig. 3.3 The penalty effect with different penalization factors in SIMP model

It is a drawback of the SIMP approach that the obtained topology results may not only exhibit checkerboard patterns, but also dependent on the orientation and refinement of the mesh. Many additional regularization methods, such as the perimeter method [164], the slope control approach [165], the higher-order finite element method [166] or the filtering method [167], were developed to augment the formulation of the optimization problem. In this study, the well-known sensitivity filtering technique [168], which restricts the discontinuity of the

optimized material distribution by smoothing the gradients of objective and constraints, is employed. The sensitivity filtering formula is expressed as

$$\frac{\widehat{\partial g}}{\partial \rho_e} = \frac{1}{\rho_e \sum_{e'=1}^{N_e} \hat{H}_{e'}} \sum_{e'=1}^{N_e} \hat{H}_{e'} \rho_{e'} \frac{\partial g}{\partial \rho_{e'}} \quad (e=1,2,\dots,N), \quad (3.5)$$

where $\partial g / \partial \rho_{e'}$ is the original sensitivity and $\widehat{\partial g} / \partial \rho_e$ is the modified or smoothed sensitivity. The weight factor $\hat{H}_{e'}$ is written as

$$\hat{H}_{e'} = \begin{cases} r_{\min} - d(e, e'), & d(e, e') \leq r_{\min} \\ 0, & d(e, e') > r_{\min} \end{cases} \quad (3.6)$$

where $d(e, e')$ is defined as the distance between centre of element e and centre of element e' , r_{\min} is a given filter radius and is set as 1.5 times the length of element. Eq.(3.6) denotes that the weight factor decays linearly with the distance from element e to e' and is zero outside the filter area. Instead of the original sensitivities, the modified sensitivities are used in the optimization update. It should be noticed that this sensitivity filtering technique has not yet been proven to ensure existence of solutions. However, numerous applications have shown that the filter improves the checkerboard pattern and produces mesh-independent design in practice.

3.3.2 Solving algorithm of optimization problem

The SIMP approach leads to a smooth constrained optimization problem, which can be efficiently solved by gradient-based optimization algorithms. For complex topology optimization problems, the number of optimization variables is typically large as the resolution of the structural geometry increases with the number of finite elements in the design domain. Several mathematical programming methods, such as sequential linear programming (SLP), sequential quadratic programming (SQP), sequential convex programming (SCP), have been advocated. In this study, the convex approximation-based

MMA algorithm [162], which is particularly applicable for large-scale topology optimization, was successfully employed.

Based mainly on gradient information, MMA approximates the original implicit optimization problem into a series of strictly convex and explicit sub-problems, which implies that there is always a unique optimal solution. The process is expounded as follows.

We first assumed a general form of the nonlinear constraint optimization problem

$$\begin{aligned}
 \min \quad & f_0(\mathbf{z}) + a_0 r_0 + \sum_{i=1}^M (c_i r_i + \frac{1}{2} d_i r_i^2) \\
 \text{s.t.} \quad & f_i(\mathbf{z}) - a_i r_0 - r_i \leq 0 \quad (i=1, \dots, M), \\
 & z_{j,\min} \leq z_j \leq z_{j,\max} \quad (j=1, \dots, L), \\
 & r_i \geq 0 \quad (i=1, \dots, M), \\
 & r_0 \geq 0,
 \end{aligned} \tag{3.7}$$

where $\mathbf{z} = [z_1, \dots, z_L]^T$ are the true optimization variables, $\mathbf{r} = [r_1, \dots, r_M]^T$ and r_0 are the artificial optimization variables, f_0, f_1, \dots, f_M are continuously differentiable real-valued functions, $z_{j,\min}$ and $z_{j,\max}$ are the lower and upper limits of design variables, a_0, a_i, c_i and d_i are given real numbers, which satisfy $a_0 > 0$, $a_i \geq 0$, $c_i \geq 0$, $d_i \geq 0$ and $c_i + d_i > 0$. By chosen those real numbers appropriately, the general form (3.7) can be put into many particular optimization problems. For the ordinary nonlinear programming in this study, we chose $a_0 = 1$, $a_i = 0$, $r_0 = 0$, $c_i = 10000$, $d_i = 0$.

In the k -th iteration, the current iteration point $(\mathbf{z}^{(k)}, \mathbf{r}^{(k)}, r_0^{(k)})$ is obtained. Based on the current iteration point, an approximating explicit sub-problem is then generated as

$$\begin{aligned}
 \min \quad & \tilde{f}_0^{(k)}(\mathbf{z}) + a_0 r_0 + \sum_{i=1}^M (c_i r_i + \frac{1}{2} d_i r_i^2) \\
 \text{s.t.} \quad & \tilde{f}_i^{(k)}(\mathbf{z}) - a_i r_0 - r_i \leq 0 \quad (i=1, \dots, M), \\
 & \xi_{j,L}^{(k)} \leq z_j \leq \xi_{j,U}^{(k)} \quad (j=1, \dots, N), \\
 & r_i \geq 0 \quad (i=1, \dots, M), \\
 & r_0 \geq 0,
 \end{aligned} \tag{3.8}$$

Obviously, in the above sub-problem, the functions $f_i(\mathbf{z})$ are replaced by their first-order approximating convex functions, namely

$$\tilde{f}_i^{(k)}(\mathbf{z}) = \sum_{j=1}^N \left(\frac{p_{ij}^{(k)}}{u_j^{(k)} - z_j} + \frac{q_{ij}^{(k)}}{z_j - l_j^{(k)}} \right) + \varepsilon_i^{(k)} \quad (i = 0, 1, \dots, M), \quad (3.9)$$

where

$$\begin{aligned} p_{ij}^{(k)} &= \left(u_j^{(k)} - z_j^{(k)} \right)^2 \left(\left(\frac{\partial f_i}{\partial z_j}(\mathbf{z}^{(k)}) \right)^+ + \kappa_{ij}^{(k)} \right), \\ q_{ij}^{(k)} &= \left(z_j^{(k)} - l_j^{(k)} \right)^2 \left(\left(\frac{\partial f_i}{\partial z_j}(\mathbf{z}^{(k)}) \right)^- + \kappa_{ij}^{(k)} \right), \\ \varepsilon_i^{(k)} &= f_i(\mathbf{z}^{(k)}) - \sum_{j=1}^n \left(\frac{p_{ij}^{(k)}}{u_j^{(k)} - z_j^{(k)}} + \frac{q_{ij}^{(k)}}{z_j^{(k)} - l_j^{(k)}} \right), \end{aligned} \quad (3.10)$$

and

$$\begin{aligned} \left(\frac{\partial f_i}{\partial z_j}(\mathbf{z}^{(k)}) \right)^+ &= \max \left\{ 0, \frac{\partial f_i}{\partial z_j}(\mathbf{z}^{(k)}) \right\}, \\ \left(\frac{\partial f_i}{\partial z_j}(\mathbf{z}^{(k)}) \right)^- &= \max \left\{ 0, -\frac{\partial f_i}{\partial z_j}(\mathbf{z}^{(k)}) \right\}, \\ \kappa_{ij}^{(k)} &= 10^{-3} \cdot \left| \frac{\partial f_i}{\partial z_j}(\mathbf{z}^{(k)}) \right| + \frac{10^{-6}}{u_j^{(k)} - l_j^{(k)}}, \quad (i = 0, 1, \dots, M; j = 1, 2, \dots, L). \end{aligned} \quad (3.11)$$

In Eqs.(3.10) and (3.11), $l_j^{(k)}$ and $u_j^{(k)}$ are the lower asymptotes and the upper asymptotes, respectively. The asymptotes are used to adjust the convex properties of sub-problems. The default rules for updating the asymptotes are as follows.

When in the first two iterations ($k = 1, 2$),

$$\begin{aligned} l_j^{(k)} &= z_j^{(k)} - 0.5(z_{j,\max} - z_{j,\min}), \\ u_j^{(k)} &= z_j^{(k)} + 0.5(z_{j,\max} - z_{j,\min}). \end{aligned} \quad (3.12)$$

When $k \geq 3$,

$$\begin{aligned} l_j^{(k)} &= z_j^{(k)} - \gamma_j^{(k)} (z_j^{(k-1)} - l_j^{(k-1)}), \\ u_j^{(k)} &= z_j^{(k)} + \gamma_j^{(k)} (u_j^{(k-1)} - z_j^{(k-1)}), \end{aligned} \quad (3.13)$$

where

$$\gamma_j^{(k)} = \begin{cases} 0.7 & \text{if } (z_j^{(k)} - z_j^{(k-1)})(z_j^{(k-1)} - z_j^{(k-2)}) < 0, \\ 1.2 & \text{if } (z_j^{(k)} - z_j^{(k-1)})(z_j^{(k-1)} - z_j^{(k-2)}) > 0, \\ 1 & \text{if } (z_j^{(k)} - z_j^{(k-1)})(z_j^{(k-1)} - z_j^{(k-2)}) = 0. \end{cases} \quad (3.14)$$

According to the lower asymptotes $l_j^{(k)}$ and the upper asymptotes $u_j^{(k)}$, the lower limits $\xi_{j,L}^{(k)}$ and the upper limits $\xi_{j,U}^{(k)}$ of the design variables in sup-problem (3.8), which satisfy $l_j^{(k)} < \xi_{j,L}^{(k)} \leq z_j^{(k)} \leq \xi_{j,U}^{(k)} < u_j^{(k)}$, can be determined.

$$\begin{aligned} \xi_{j,L}^{(k)} &= \max \left\{ z_{j,\min}, 0.9l_j^{(k)} + 0.1z_j^{(k)} \right\}, \\ \xi_{j,U}^{(k)} &= \min \left\{ z_{j,\max}, 0.9u_j^{(k)} + 0.1z_j^{(k)} \right\}. \end{aligned} \quad (3.15)$$

After solved the strictly convex sub-problem, a unique optimal solution $(\mathbf{z}^*, \mathbf{r}^*, r_0^*)$ can be obtained. Letting $(\mathbf{z}^{(k+1)}, \mathbf{r}^{(k+1)}, r_0^{(k+1)}) = (\mathbf{z}^*, \mathbf{r}^*, r_0^*)$, then a new sub-problem is generated. This process will continue up to the convergent criteria is satisfied.

3.3.3 Sensitivity analysis

It is worth mentioning that, when the number of the design variables is less than that of the structural behaviour constraints, the direct variable method is suitable for calculating the derivatives of the constraint function with respect to the design variables. Otherwise, the adjoint variable sensitivity analysis method is computationally more efficient. In topology optimization of continuum structures, the number of design variables is typically much larger than that of structural behavior constraints. As a common practice in such circumstances, the

adjoint variable method is employed for an efficient sensitivity analysis. The associated computational scheme is given as follows.

The linear equilibrium equation for a structure under static loads reads

$$\mathbf{K}\mathbf{U} = \mathbf{P} \quad (3.16)$$

where \mathbf{K} is the global stiffness matrix, \mathbf{U} is the nodal displacement vector and \mathbf{P} is the external force vector.

Differentiating the equilibrium equation with respect to the e th elemental design variable ρ_e , it yields

$$\mathbf{K} \frac{d\mathbf{U}}{d\rho_e} = \frac{d\mathbf{P}}{d\rho_e} - \frac{d\mathbf{K}}{d\rho_e} \mathbf{U} \quad (e = 1, 2, \dots, N). \quad (3.17)$$

One obtains the following relation from (3.17)

$$\begin{aligned} \frac{\partial g_j(\boldsymbol{\rho})}{\partial \rho_e} &= \left[\frac{\partial g_j}{\partial \mathbf{U}} \right]^T \frac{d\mathbf{U}}{d\rho_e} \\ &= \left[\frac{\partial g_j}{\partial \mathbf{U}} \right]^T \mathbf{K}^{-1} \left(\frac{d\mathbf{P}}{d\rho_e} - \frac{d\mathbf{K}}{d\rho_e} \mathbf{U} \right) \quad (e = 1, 2, \dots, N). \end{aligned} \quad (3.18)$$

Introducing an adjoint vector $\boldsymbol{\lambda}$, which is the solution to the equation

$$\mathbf{K}\boldsymbol{\lambda} = \frac{\partial g_j}{\partial \mathbf{U}}, \quad (3.19)$$

the sensitivity of the j -th constraint value can be given as

$$\frac{\partial g_j(\boldsymbol{\rho})}{\partial \rho_e} = \boldsymbol{\lambda}^T \left(\frac{d\mathbf{P}}{d\rho_e} - \frac{d\mathbf{K}}{d\rho_e} \mathbf{U} \right) \quad (e = 1, 2, \dots, N). \quad (3.20)$$

The derivative of the global stiffness matrix in (3.20) can be easily calculated at the elemental level in the considered topology optimization problem, thus (3.20) becomes

$$\frac{dg_j}{d\rho_e} = \boldsymbol{\lambda}^T \frac{d\mathbf{P}}{d\rho_e} - (\boldsymbol{\lambda}^e)^T \frac{\partial \mathbf{K}^e}{\partial \rho_e} \mathbf{U}^e \quad (e = 1, 2, \dots, N), \quad (3.21)$$

where λ^e and \mathbf{U}^e are the elemental adjoint vector and the elemental displacement vector, respectively; \mathbf{K}^e is the elemental stiffness matrix. Using the SIMP material interpolation relation in Eq.(3.4), the derivative of \mathbf{K}^e with respect to the density design variables is given by

$$\frac{\partial \mathbf{K}^e}{\partial \rho_e} = p \rho_e^{p-1} \mathbf{K}_0^e \quad (e = 1, 2, \dots, N), \quad (3.22)$$

where \mathbf{K}_0^e is the elemental stiffness matrix computed with unit density. If no topology-dependent loading conditions are considered, the first term on the right-hand side of (3.21) vanishes, otherwise it can be computed with special treatments [169], but this is beyond the scope of this study.

3.4 OPTIMAL STRUCTURAL LAYOUT

In view of the symmetry, one quarter of the whole composite beam is modeled with 14400 eight-node 3-D solid elements, in which 9900 elements are occupied by the design domain. Accordingly the symmetry constraints were put on the symmetry areas. The topology optimization process starts with a homogeneous material density distribution $\rho_e = 0.5$ ($e = 1, 2, \dots, 9900$).

The iteration history of the structural topology design problem plotted in Fig.3.4 shows a steady decrease of the objective function during the optimization process. The optimal structural layout obtained by the topology optimization approach is presented in Fig.3.5 and Fig.3.6. Herein, Fig.3.5(a,b) show the front view and the side view respectively. Both figures show the distribution of smoothed nodal densities, which are computed by averaging the density values of neighboring elements. In the figures, the black areas denote the solid regions in the resulting structural topology; the white areas indicate the void regions and the grey areas represent the regions with intermediate densities. The corresponding 3-D colorful distribution of the relative densities is presented in Fig.3.6(a). After deleted the low density

elements ($\rho_e < 0.8$), the optimal topology of the bonded steel and concrete composite beam is then revealed in Fig.3.6(b) distinctly.

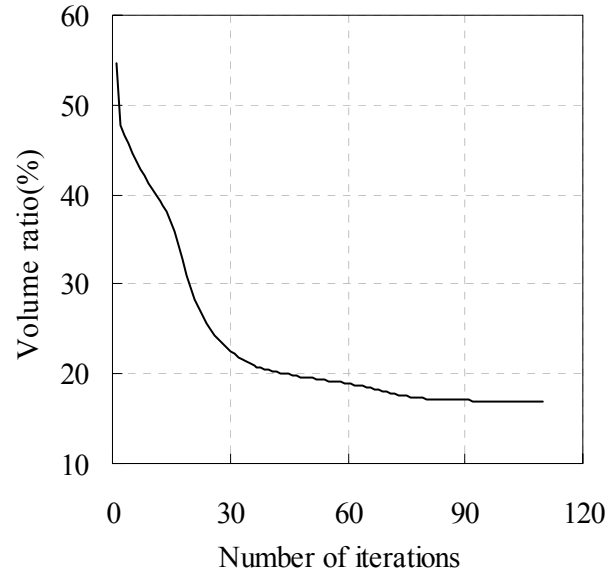


Fig. 3.4 Iteration history of the topology optimization

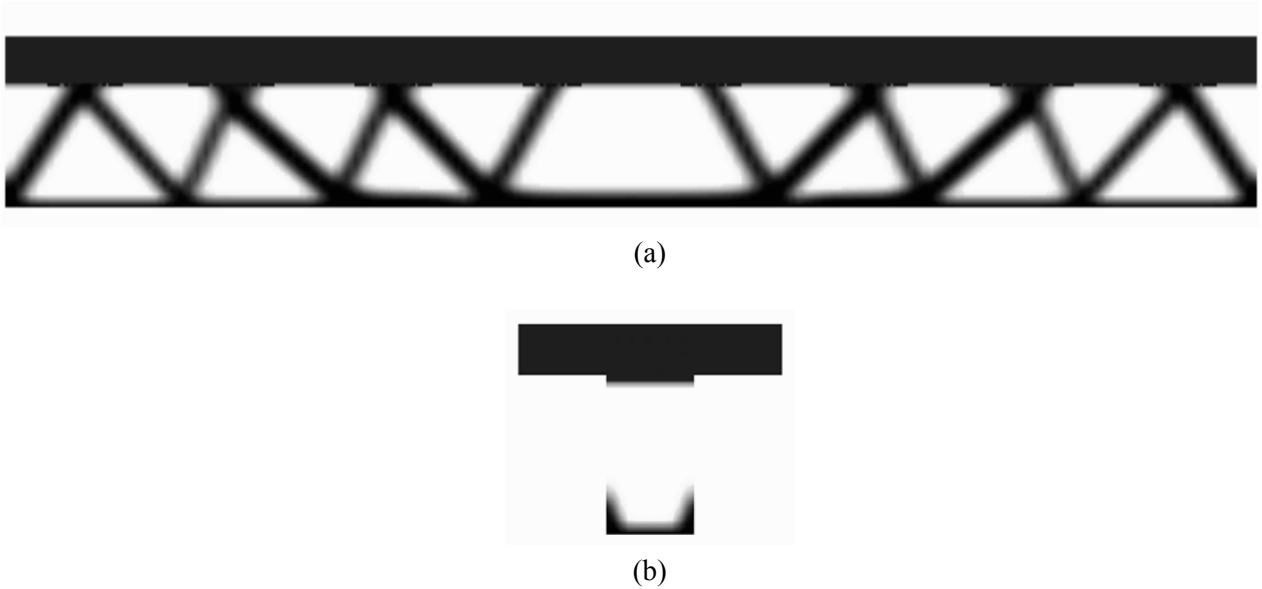
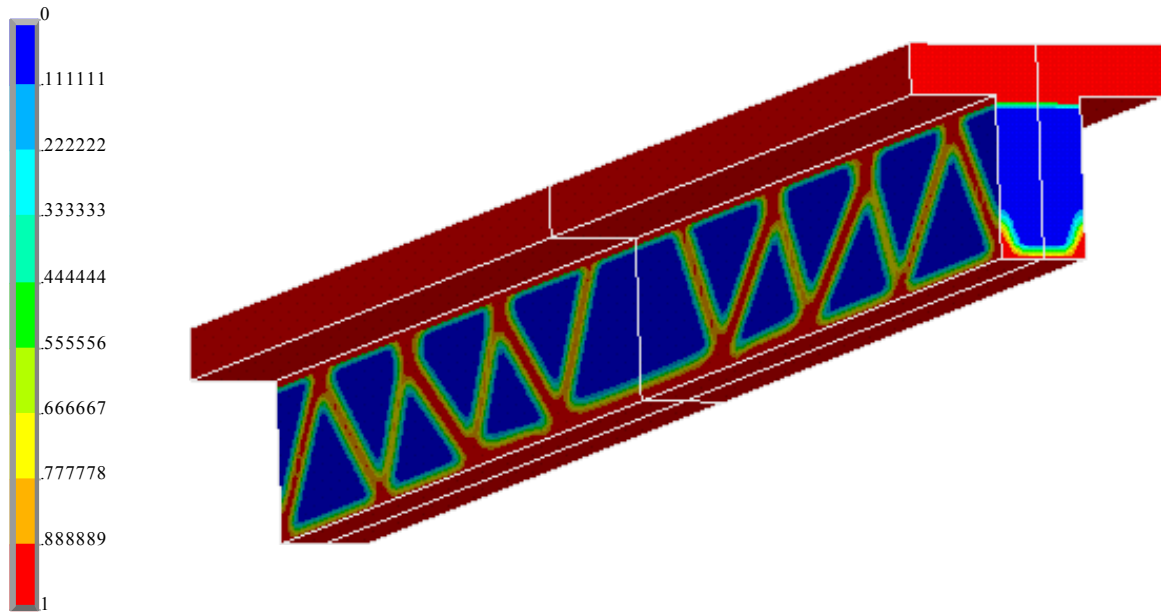
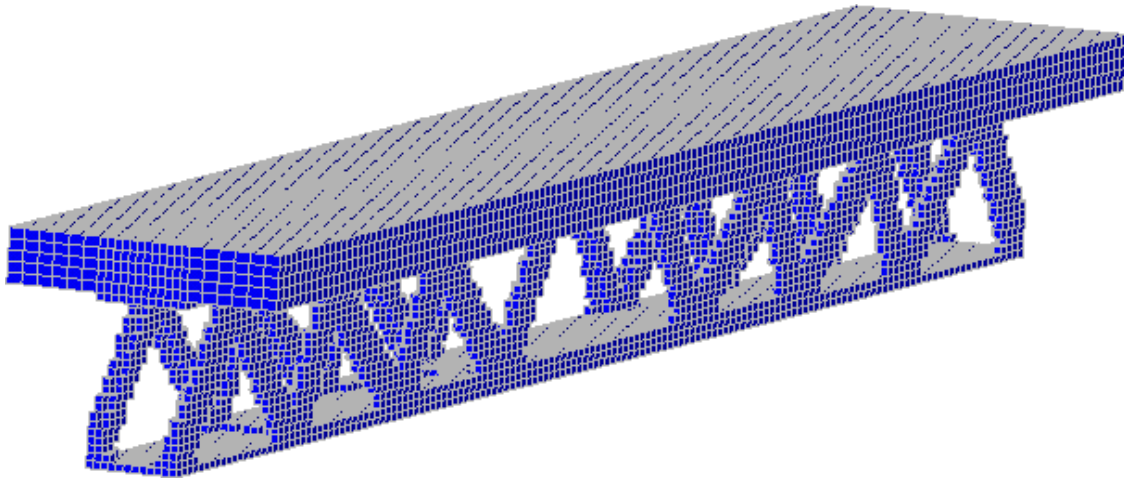


Fig. 3.5 Plan views of the optimal structural layout

(a) The front view; (b) The side view



(a)



(b)

Fig. 3.6 3-D optimal layout of the bonded composite beam

(a) Distribution of the relative densities; (b) Solution with relative densities less than 0.8 removed

Compared with the conventional composite beam composed by concrete slab and I-girder, the topology optimization solution suggests a distinct different structural layout. It should be noted that it will be more economical in this specific problem to design the bonded

composite beam based on the optimal layout than merely to augment the dimension of the beam.

3.5 SUMMARY

In the design of bonded steel and concrete composite beam, a topology optimization in the early stage is of considerable practical importance. Based on the SIMP approach, this chapter presented a three-dimensional topology optimization methodology of the bonded composite beam. By using the adjoint variable method for the sensitivity analysis, the optimization problem is efficiently solved by the gradient-based optimization algorithm (MMA). The proposed topology approach presented a new structural topology of the bonded steel and concrete composite beam.

CHAPTER 4:
STRUCTURAL RELIABILITY ASSESSMENT BASED ON
PROBABILITY AND CONVEX SET MIXED MODEL

4.1 INTRODUCTION

In a practical engineering problem, including the bonded steel and concrete composite beam, the structural performance may exhibit some degree of degradation due to inherent uncertainties in material properties, geometrical dimensions and loading conditions. Conventionally, uncertainties in structural systems are modeled as stochastic variables (or random fields/ processes) with certain probability distribution. Based on the classical probability theory, the probabilistic reliability theory provides a powerful methodology to take into account those uncertainties in the analysis and design of structures. The purpose of this methodology is to assess the structural reliability or the failure probability in presence of stochastic uncertainties.

A probability-based reliability assessment requires precise probabilistic characteristics of the random inputs. These data, however, are sometimes practically difficult to obtain, especially when only a limited number of input samples are available or the uncertainties are inherently non-probabilistic. With the limited available information, it is relatively easy to construct a conservative set-valued model that is consistent with the uncertainties, even if an accurate probabilistic model cannot be set up. A typical example of such uncertainties is the geometrical dimensions of a manufactured product, the variation range of which is controlled by specified tolerance bounds. In such cases, the set theory-based convex model [170], which bounds all possible values of the uncertainties within a convex set without assuming any probability distributions, is attractive for representation of those uncertain-but-bounded variables.

In the risk assessment of engineering structures, a frequently encountered case is that: some of the uncertainties can be characterized with certain probability distributions and other uncertainties need to be treated as bounded ones due to their inherent natures or lack of sufficient sample data. A combination of stochastic variables and uncertain-but-bounded variables has been suggested for applications in such circumstances. As the previous literature survey reveals, a number of attempts have been made for mixed uncertainty quantification. However, most of the existing papers focus on the combination of stochastic randomness and

interval set, which is the simplest instance of the convex model. Apparently, the reliability definition based on combination of probability and convex set models (in particular, multi-ellipsoid convex model), as well as systematic numerical techniques for associated reliability evaluation, has not been fully explored in the literature.

In this chapter, we first present a brief introduction to the conventional probabilistic model and the multi-ellipsoid convex model as a prerequisite. Then, a definition of structural reliability under mixed model representation with stochastic variables and uncertain-but-bounded variables is proposed. Therein, the multi-ellipsoid model is employed for representing these bounded uncertainties. The calculation of the corresponding reliability index is mathematically stated as a constrained minimization problem. Two solution approaches, namely the mathematical programming method and a direct iterative approach, are presented for seeking the worst-case point and the most probable failure point (MPP). To demonstrate the applicability of the proposed mixed model and the efficiency of the numerical techniques for the associated reliability analysis, two simple examples are presented and the results obtained by different approaches are compared. To this end, the proposed mixed model is employed to assess the reliability of a forenamed bonded steel and concrete beam.

4.2 GENERAL CONCEPTS OF PROBABILISTIC MODEL AND CONVEX MODEL

4.2.1 Probabilistic model

When considering a total number of m stochastic variables denoted by a vector $\mathbf{x} = \{x_1, x_2, \dots, x_m\}^T$, the structural failure state is characterized by a limit-state function or performance function $G(\mathbf{x})$, and $G(\mathbf{x}) = 0$ denotes the limit-state surface. The m -dimensional uncertainty space is thus divided into a safe region ($\Omega_s = \{\mathbf{x} : G(\mathbf{x}) > 0\}$) and a failure region ($\Omega_f = \{\mathbf{x} : G(\mathbf{x}) \leq 0\}$).

In probabilistic reliability theory, the failure probability of a structure is expressed as the multi-variate integral

$$P_f = \Pr\{G(\mathbf{x}) \leq 0\} = \int_{\Omega_f} f_x(\mathbf{x}) d\mathbf{x}, \quad (4.1)$$

where P_f is the structural failure probability, $\Pr\{\cdot\}$ denotes a probability, $f_x(\mathbf{x})$ is the joint Probability Density Function (PDF) of the random variables \mathbf{x} . (Fig.4.1)

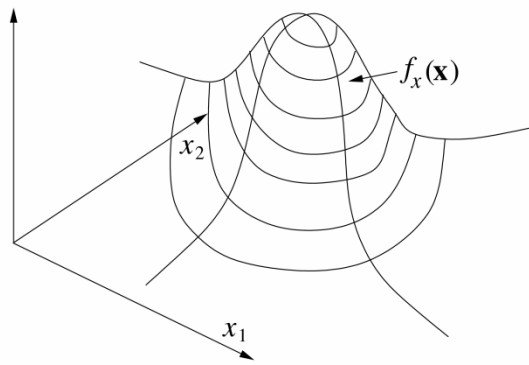


Fig. 4.1 Joint probability density function

As mentioned previously, the multi-fold integration in Eq.(4.1) can be implemented with various numerical methods, among which the FORM is one of the most familiar approaches. For normal random variables \mathbf{x} , the FORM requires a linear transformation of \mathbf{x} into standard normal random variables \mathbf{u} by

$$u_i = \frac{x_i - \bar{x}_i}{\sigma_i} \quad (i = 1, 2, \dots, m), \quad (4.2)$$

where \bar{x}_i and σ_i are the mean value and the standard deviation of x_i , respectively.

For problems with non-Gaussian random variables, there are many available techniques, such as Rosenblatt's transformation [171] and Rackwitz-Fiessler transformation [104], for transforming the distribution into approximately equivalent normal distribution. For instance, when the variables are mutually independent, the Rackwitz-Fiessler transformation can be expressed by

$$u_i = \Phi^{-1} \left[F_{x_i}(x_i) \right], \quad (4.3)$$

where $F_{x_i}(x_i)$ is the non-Gaussian cumulative distribution function for x_i , $\Phi^{-1}(\cdot)$ is the inverse of the standard normal cumulative distribution function.

In the standard \mathbf{u} -space, the limit-state function is symbolically expressed as $g(\mathbf{u})$, where $\mathbf{u} = \{u_1, u_2, \dots, u_m\}^T$ is the standard normal vector of \mathbf{x} . Thus the probabilistic reliability index β is defined as the shortest distance from the origin to the failure surface $g(\mathbf{u}) = 0$, namely

$$\begin{aligned} \beta &= \min_{\mathbf{u}} \sqrt{\mathbf{u}^T \mathbf{u}} \\ \text{s.t. } g(\mathbf{u}) &= 0, \end{aligned} \quad (4.4)$$

and the structural failure probability P_f can be written as

$$P_f = \Phi(-\beta) = 1 - \int_{-\infty}^{\beta} \frac{1}{\sqrt{2\pi}} \exp\left(-\frac{1}{2}u^2\right) du. \quad (4.5)$$

4.2.2 Non-probabilistic convex model

When a convex set is defined to describe the bounded uncertain variables, it is referred to as convex modeling of uncertainties. Many types of the convex sets such as the interval set and the ellipsoid set can be used to describe those so-called uncertain-but-bounded variables. In practical situations, some considered uncertainties arising from different sources (e.g. the imprecision of geometry, the scattering of material properties, the fluctuation of loading conditions, etc) may vary independently and thus it is more realistic to divide them into groups. For this realistic reason, the multi-ellipsoid convex model [151] is employed in this study. The mathematical definition of the multi-ellipsoid convex model is described in what follows.

Supposing N_E groups of bounded uncertainties (the total number is n) are considered, the vector of uncertain variables is expressed by

$$\mathbf{y}^T = \{\mathbf{y}_1^T, \mathbf{y}_2^T, \dots, \mathbf{y}_{N_E}^T\}, \quad (4.6)$$

where $\mathbf{y}_i \in \mathbb{R}^{n_i}$ ($i = 1, 2, \dots, N_E$) represents the i th group of uncertainties and $\sum_{i=1}^{N_E} n_i = n$.

The multi-ellipsoid convex model treats each group of uncertain variables with an individual ellipsoid set, respectively, as

$$\mathbf{y} \in \mathbb{E} = \left\{ \mathbf{y} : (\mathbf{y}_i - \mathbf{y}_i^c)^T \mathbf{W}_i (\mathbf{y}_i - \mathbf{y}_i^c) \leq \theta_i^2, i = 1, 2, \dots, N_E \right\}, \quad (4.7)$$

where \mathbf{y}_i^c denotes the nominal values of \mathbf{y}_i , $\mathbf{W}_i \in \mathbb{R}^{n_i \times n_i}$ is a symmetric positive-definite real matrix defining the orientation and aspect ratio of the i th ellipsoid set and it is referred to as the characteristic matrix, θ_i is a positive real number defining the magnitude of the variability. These parameters of the ellipsoid sets can be determined from measurement results or the manufacturing tolerance specifications.

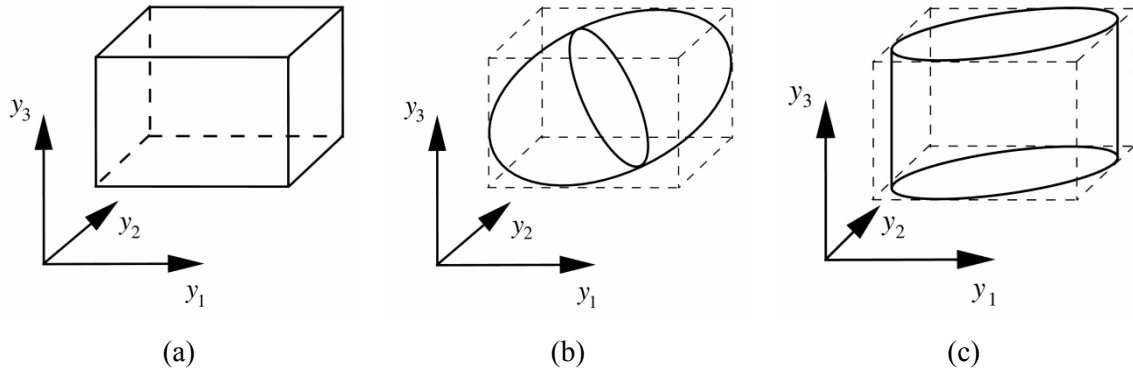


Fig. 4.2 Specific cases of convex models for three uncertain variables

(a) Three-dimensional interval model. (b) Three-dimensional single-ellipsoid model.

(c) Multi-ellipsoid convex model defined by an ellipsoid (for y_1 and y_2) and an interval (for y_3)

It should be noted that the multi-ellipsoid set in (4.7) degenerates into a conventional interval model when each uncertainty group consists of only one uncertain variable. Hence, the multi-ellipsoid convex model provides a unified representation accommodating both conventional ellipsoid sets and interval sets that co-exist in the uncertainty model of a structural system. The interval model and the single-ellipsoid model can be regarded as two

specific instances of the multi-ellipsoid convex model. For illustrative purpose, three cases of convex models for a problem with three uncertain-but-bounded variables are shown in Fig.4.2.

It is convenient to transform the vector \mathbf{y} into a dimensionless vector $\boldsymbol{\delta} \in \mathbb{R}^n$, of which the components are related by

$$\delta_i = (y_i - y_i^c) / y_i^c \quad (i = 1, 2, \dots, n). \quad (4.8)$$

Then the multi-ellipsoid set (4.7) can be denoted by a dimensionless form

$$\boldsymbol{\delta} \in \mathbb{E} = \{ \boldsymbol{\delta} : \boldsymbol{\delta}_i^T \hat{\mathbf{W}}_i \boldsymbol{\delta}_i \leq \theta_i^2, i = 1, 2, \dots, N_E \}, \quad (4.9)$$

where $\hat{\mathbf{W}}_i$ is the dimensionless characteristic matrix.

In Eq.(4.9), a linear transformation of uncertain variables into a normalized space would be beneficial. To achieve this, we first solve the following eigenvalue problems:

$$\hat{\mathbf{W}}_i \mathbf{Q}_i = \mathbf{Q}_i \boldsymbol{\Lambda}_i \quad (i = 1, 2, \dots, N_E), \quad (4.10)$$

where \mathbf{Q}_i is an orthogonal matrix comprising the normalized eigenvectors and $\boldsymbol{\Lambda}_i$ is a diagonal matrix consisting of the eigenvalues of $\hat{\mathbf{W}}_i$.

Introducing normalized vectors \mathbf{v}_i defined by

$$\mathbf{v}_i = (1/\theta_i) \boldsymbol{\Lambda}_i^{1/2} \mathbf{Q}_i^T \boldsymbol{\delta}_i \quad (i = 1, 2, \dots, N_E), \quad (4.11)$$

the original multi-ellipsoid convex model becomes

$$\mathbb{E} = \{ \mathbf{v} : \mathbf{v}_i^T \mathbf{v}_i \leq 1 \text{ (or } \|\mathbf{v}_i\|_2 \leq 1) \quad i = 1, 2, \dots, N_E \}, \quad (4.12)$$

and it forms multiple spheres of unit radius in each individual sub-dimensional space spanned by \mathbf{v}_i . For example, three specific cases of multi-ellipsoid convex models in Fig.4.2 are then normalized as Fig.4.3. Here $\|\cdot\|_2$ denotes the $L-2$ norm.

After the transformation of the original grouped bounded uncertain parameters $\mathbf{y}^T = \{\mathbf{y}_1^T, \mathbf{y}_2^T, \dots, \mathbf{y}_{N_E}^T\}$, as expressed by Eq.(4.11), the limit-state function $G(\mathbf{y})$ can be rewritten as $g(\mathbf{v})$ in the normalized space. Fig.4.4 illustrates the 3-dimensional normalized

space for the case of two grouped ellipsoid set, in which one group consists of two uncertain parameters (v_1, v_2) while the other one consists of only one parameter v_3 . In the figure, the solid cylinder represents the normalized convex set of the uncertainties and the grey surface denotes the limit-state surface $g(\mathbf{v})=0$. The normalized space is thus divided into a safe region ($g(\mathbf{v}) > 0$) and a failure region ($g(\mathbf{v}) < 0$).

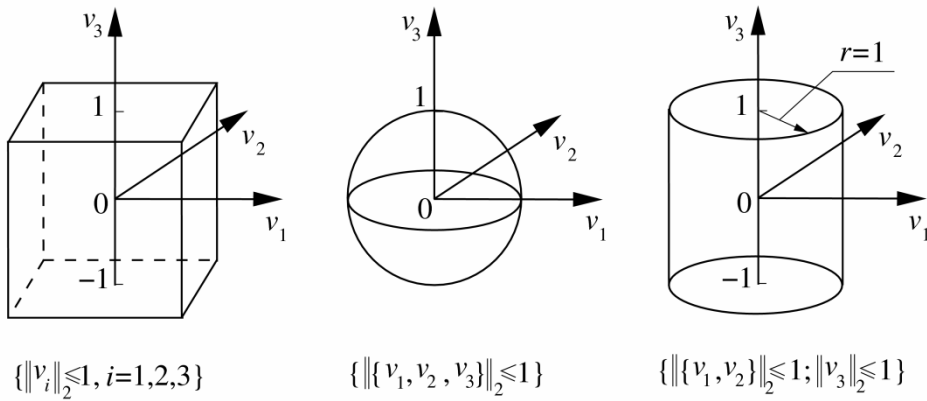


Fig. 4.3 Three specific normalized multi-ellipsoid convex model

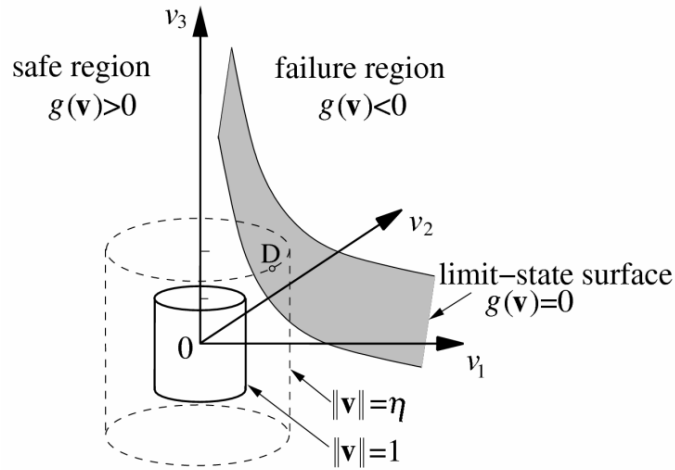


Fig. 4.4 Schematic illustration of the non-probabilistic reliability index in the normalized space

For simplicity in the following discussion, we define the **length** of a vector \mathbf{v} ($\mathbf{v}^T = \{\mathbf{v}_1^T, \mathbf{v}_2^T, \dots, \mathbf{v}_{N_E}^T\}$) in the normalized space as

$$\|\mathbf{v}\| = \left| \sqrt{\mathbf{v}_1^T \mathbf{v}_1}, \sqrt{\mathbf{v}_2^T \mathbf{v}_2}, \dots, \sqrt{\mathbf{v}_{N_E}^T \mathbf{v}_{N_E}} \right|_{\infty} = \max \left(\sqrt{\mathbf{v}_1^T \mathbf{v}_1}, \sqrt{\mathbf{v}_2^T \mathbf{v}_2}, \dots, \sqrt{\mathbf{v}_{N_E}^T \mathbf{v}_{N_E}} \right), \quad (4.13)$$

where $|\cdot|_{\infty}$ denotes the $L-\infty$ norm.

Thus, the bounds of the normalized multi-ellipsoid convex set can be expressed as $\|\mathbf{v}\|=1$. As shown in Fig.4.4, expanding the cylinder proportionally in all directions, the maximum allowable uncertain degree is reached when the enlarged cylinder becomes tangent to the limit-state surface at point D. Note that among all the points in the limit-state surface, point D has the minimal *distance* in the sense of the length measure defined in Eq.(4.13). According to the concept of non-probabilistic reliability proposed by Ben-haim [140] and Elishakoff [142], which is defined as the maximum degree of uncertainty a structure can tolerate before its failure, it is reasonable to choose the *distance* from the origin to point D as the measurement of non-probabilistic reliability. Therefore, for the multi-ellipsoid model, the non-probabilistic reliability index η can be defined in the normalized space as the minimal *distance* from the origin to the limit-state surface, which can be expressed as

$$\eta = \text{sgn}(g(\mathbf{0})) \cdot \min_{\mathbf{v}} \|\mathbf{v}\| = \text{sgn}(g(\mathbf{0})) \cdot \min_{\mathbf{v}} \left\{ \max \left(\sqrt{\mathbf{v}_1^T \mathbf{v}_1}, \sqrt{\mathbf{v}_2^T \mathbf{v}_2}, \dots, \sqrt{\mathbf{v}_{N_E}^T \mathbf{v}_{N_E}} \right) \right\} \quad (4.14)$$

s.t. $g(\mathbf{v}) = 0$,

where the signum function $\text{sgn}(g(\mathbf{0}))$ is added to define a negative reliability index when the limit-state function is negative at the origin in the normalized space.

Obviously, the greater the non-probabilistic reliability index η is, the greater extent of parameter variation the structure will allow for. Particularly, $\eta = 1$ means that the structure is critical for the reference parameter uncertainties. For $\eta > 1$, all the possible values of the uncertainties lie within the safe region and therefore the structure has a safety margin. Though it might be argued that $\eta = 1$ is sufficient for a reliability requirement if the chosen ellipsoids

(or intervals) reflect well the actual variability of the structure, a greater value of η offers a specified safety margin, which is usually desirable in the practical engineering.

4.3 RELIABILITY ANALYSIS UNDER PROBABILITY AND CONVEX SET MIXED MODEL

In many cases, all the uncertain variables associated with the parameters and the external loads of a structural system can be classified into stochastic variables (denoted by $\mathbf{x} \in \mathbb{R}^m$) and grouped uncertain-but-bounded variables (denoted by $\mathbf{y} = \{\mathbf{y}_1^T, \mathbf{y}_2^T, \dots, \mathbf{y}_{N_E}^T\}^T \in \mathbb{R}^n$) as described in the previous section. To make better use of available information and avoid making any additional assumption, the stochastic variables are described by probability distribution functions while the uncertain-but-bounded variables are represented by a multi-ellipsoid convex model.

The limit-state function defines the failure mode of the structural system and it plays an essential role in the reliability evaluation. After the normalization of the original uncertain variables \mathbf{x} and \mathbf{y} into \mathbf{u} and \mathbf{v} as explained in section 4.2, the limit-state function $G(\mathbf{x}, \mathbf{y})$ is mapped into the corresponding normalized limit-state function $g(\mathbf{u}, \mathbf{v})$. In the conventional probabilistic model, the limit state $g(\mathbf{u}, \mathbf{v}) = 0$ forms an m -dimensional surface (called limit-state surface) in the standard \mathbf{u} -space and it divides the \mathbf{u} -space into two parts, namely a safe region and a failure region. However, for the proposed mixed model representation, the limit state $g(\mathbf{u}, \mathbf{v}) = 0$ presents a cluster of limit-state surfaces in the standard \mathbf{u} -space. Each individual limit-state surface corresponds to a possible realization of parameter combination $\mathbf{v} \in \mathbb{E}$. In other words, all the points that satisfying $g(\mathbf{u}, \mathbf{v}) = 0$ form a banded geometry in the \mathbf{u} -space. The whole \mathbf{u} -space Ω is thus divided into a safe region ($\Omega_s = \{\mathbf{u} : \min_{\mathbf{v} \in \mathbb{E}} g(\mathbf{u}, \mathbf{v}) > 0\}$), a critical region ($\Omega_c = \{\mathbf{u} : \exists \mathbf{v} \in \mathbb{E}, g(\mathbf{u}, \mathbf{v}) = 0\}$) and a failure region ($\Omega_f = \Omega \setminus (\Omega_s \cup \Omega_c)$). If N_F failure modes are considered, the safe region of

the problem becomes $\Omega_s = \Omega_{s,1} \cap \Omega_{s,2} \cap \dots \cap \Omega_{s,N_F}$. Fig.4.5 illustrates the 2-dimensional \mathbf{u} -space for the case of two stochastic variables (u_1, u_2) and n uncertain-but-bounded variables \mathbf{v} .

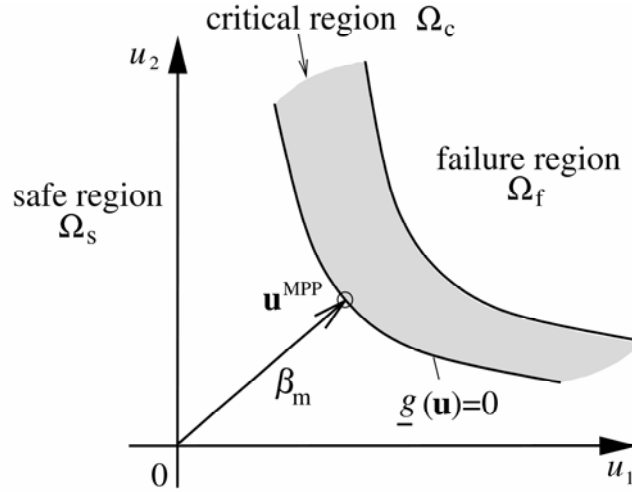


Fig. 4.5 Schematic representation of the reliability index under mixed model in the \mathbf{u} -space

The purpose of the reliability evaluation is to rationally quantify the degree of structural safety. It is recalled that the structural probability reliability is defined as the probability that the structure performs its desired functionality under given random system variations. By extending this concept, we define the reliability under probability and convex set mixed model as: the least probability that the structural behaviour satisfies the design requirements for all the possible values of the bounded uncertainties. This reliability measure provides a conservative assessment on the probability that a structure performs as designed in presence of bounded variations in addition to conventional randomness. Mathematically, by replacing the limit-state function in the conventional reliability function, we can express the structural reliability under mixed model as

$$P_m = \Pr\{\underline{g}(\mathbf{u}) > 0\}, \quad (4.15)$$

where $\underline{g}(\mathbf{u}) = \min_{\mathbf{v} \in \mathbb{E}} g(\mathbf{u}, \mathbf{v})$ and $\underline{g}(\mathbf{u}) = 0$ indicates the failure of the structure. The subscript $\langle m \rangle$ stands for the mixed model.

From (4.15) and the illustration in Fig.4.5, it is easily seen that the corresponding reliability index β_m can be defined as

$$\beta_m = \text{sgn}\left(g\left(\mathbf{0}, \mathbf{v}^*\right)\right) \cdot \sqrt{\left(\mathbf{u}^{\text{MPP}}\right)^T \mathbf{u}^{\text{MPP}}} \quad (4.16)$$

where the signum function $\text{sgn}(\cdot)$ is included here to yield a negative value when $g(\mathbf{0}, \mathbf{v}^*) < 0$, which indicates that the design violates the design requirement for the mean values of the probabilistic uncertainties under the worst-case combination of the bounded parameters. \mathbf{u}^{MPP} is the most probable failure point (MPP) of the limit-state surface $\underline{g}(\mathbf{u}) = 0$, and it is the solution to

$$\begin{aligned} \min_{\mathbf{u}} \quad & \{\mathbf{u}^T \mathbf{u}\} \\ \text{s.t.} \quad & g(\mathbf{u}, \mathbf{v}^*) = 0, \end{aligned} \quad (4.17)$$

and \mathbf{v}^* is referred to as the *worst-case point* which is found by solving the following minimization problem

$$\begin{aligned} \min_{\mathbf{v}} \quad & g(\mathbf{u}, \mathbf{v}) \\ \text{s.t.} \quad & \mathbf{v}_i^T \mathbf{v}_i \leq 1 \quad (i = 1, 2, \dots, N_E). \end{aligned} \quad (4.18)$$

Geometrically, the proposed reliability index β_m is the shortest distance from the origin to the critical region in \mathbf{u} -space. Obviously, when all the uncertainties can be provided with precise probabilistic distributions, this reliability index degenerates into a conventional probability reliability index. It is also worth mentioning that the signum function is added in (4.16) to yield a negative reliability index when the limit-state function takes a negative value for the mean values of the stochastic variables and the worst-case combination of the uncertain-but-bounded variables.

After the reliability index is calculated, the structural failure probability can be expressed by

$$P_f = \Phi(-\beta_m) = 1 - \int_{-\infty}^{\beta_m} \frac{1}{\sqrt{2\pi}} \exp\left(-\frac{1}{2}u^2\right) du. \quad (4.19)$$

4.4 SOLUTION STRATEGY FOR STRUCTURAL RELIABILITY INDEX

In this section, two computational procedures, respectively based on the mathematical programming method and a direct iterative scheme, for evaluating the proposed reliability index under mixed model are elaborated.

4.4.1 Mathematical programming method

The reliability analysis expressed by (4.17) and (4.18) appears as a nested optimization problem. The outer loop aims to seek the MPP \mathbf{u}^{MPP} while the inner loop focuses on searching for the worst-case point \mathbf{v}^* . By combining the two sub-problems in (4.17) and (4.18), \mathbf{u}^{MPP} and \mathbf{v}^* in (4.16) can be found by solving the following single-loop minimization problem

$$\begin{aligned} \min_{\mathbf{u}, \mathbf{v}} \quad & \{\mathbf{u}^T \mathbf{u}\} \\ \text{s.t.} \quad & g(\mathbf{u}, \mathbf{v}) = 0, \\ & \mathbf{v}_i^T \mathbf{v}_i \leq 1 \quad (i = 1, 2, \dots, N_E). \end{aligned} \quad (4.20)$$

It is noted that the normalized stochastic variables \mathbf{u} and the normalized uncertain-but-bounded variables \mathbf{v} are treated as the design variables simultaneously in the above problem. The single-loop optimization (4.20) can be solved by many existing gradient-based mathematical programming algorithms. It is also worth mentioning here that a global optimum cannot be ensured when a standard mathematical programming algorithm such as the SQP method is employed. However, by using sequential linear approximations of the limit-state function, problem (4.20) can be treated by solving a sequence of approximate convex optimization problems. This would substantially raise the chance of finding the global

optimum and improve the convergence behaviour in the solution of problem (4.20). In the present study, the optimization package CFSQP [172], which is an implementation of the Sequential Quadratic Programming (SQP) algorithm, is used for solving this minimization problem.

4.4.2 Direct iterative approach

For the double-loop optimization problems (4.17) and (4.18), the outer loop and the inner loop can also be solved sequentially in an iterative manner until convergence is achieved. This procedure is described as follows.

Assume after the k -th iteration we get $\mathbf{u}^{(k)}$ and $\mathbf{v}^{(k)}$. By approximating the limit-state function with the first-order Taylor expansion about $\mathbf{v}^{(k)}$, we can write the inner problem (4.18) as

$$\begin{aligned} \min_{\mathbf{v}} \quad & g(\mathbf{u}^{(k)}, \mathbf{v}^{(k)}) + \sum_{i=1}^{N_E} (\mathbf{G}_{\mathbf{v}_i}^{(k)})^T (\mathbf{v}_i - \mathbf{v}_i^{(k)}) \\ \text{s.t.} \quad & \mathbf{v}_i^T \mathbf{v}_i \leq 1 \quad (i = 1, 2, \dots, N_E). \end{aligned} \quad (4.21)$$

where $\mathbf{G}_{\mathbf{v}_i}^{(k)} = \left. \frac{\partial g(\mathbf{u}, \mathbf{v})}{\partial \mathbf{v}_i} \right|_{(\mathbf{u}^{(k)}, \mathbf{v}^{(k)})}$.

In most practical engineering problems, the variability of the uncertain-but-bounded variables is small or moderate, so that the limit-state function can be assumed monotonic with respect to these quantities within their variation bounds. Hence, all the constraints in (4.21) will be active at the optimum. By applying the Karush-Kuhn-Tucker optimality conditions at \mathbf{v}^* , it yields

$$\begin{cases} \mathbf{G}_{\mathbf{v}_i}^{(k)} + 2\lambda_i \mathbf{v}_i = 0 \\ \mathbf{v}_i^T \mathbf{v}_i = 1 \end{cases} \quad (i = 1, 2, \dots, N_E), \quad (4.22)$$

where $\lambda_i > 0$ is the Lagrangian multiplier for the i th constraint. From above equations, we have

$$\begin{cases} \lambda_i = \sqrt{(\mathbf{G}_{\mathbf{v}_i}^{(k)})^T \mathbf{G}_{\mathbf{v}_i}^{(k)}} / 2 \\ \mathbf{v}_i = -\mathbf{G}_{\mathbf{v}_i}^{(k)} / \sqrt{(\mathbf{G}_{\mathbf{v}_i}^{(k)})^T \mathbf{G}_{\mathbf{v}_i}^{(k)}} \end{cases} \quad (i=1, 2, \dots, N_E). \quad (4.23)$$

Based on this observation, an intuitional scheme for updating $\mathbf{v}^{(k+1)}$ is suggested:

$$\begin{aligned} \mathbf{v}^{(k+1)} &= \left[(\mathbf{v}_1^{(k+1)})^T, (\mathbf{v}_2^{(k+1)})^T, \dots, (\mathbf{v}_{N_E}^{(k+1)})^T \right]^T \\ &= - \left[\left(\frac{\mathbf{G}_{\mathbf{v}_1}^{(k)}}{\sqrt{(\mathbf{G}_{\mathbf{v}_1}^{(k)})^T \mathbf{G}_{\mathbf{v}_1}^{(k)}}} \right)^T, \left(\frac{\mathbf{G}_{\mathbf{v}_2}^{(k)}}{\sqrt{(\mathbf{G}_{\mathbf{v}_2}^{(k)})^T \mathbf{G}_{\mathbf{v}_2}^{(k)}}} \right)^T, \dots, \left(\frac{\mathbf{G}_{\mathbf{v}_{N_E}}^{(k)}}{\sqrt{(\mathbf{G}_{\mathbf{v}_{N_E}}^{(k)})^T \mathbf{G}_{\mathbf{v}_{N_E}}^{(k)}}} \right)^T \right]^T \end{aligned} \quad (4.24)$$

Further, analogously as in the familiar HL-RF algorithm, which was originally developed for evaluating the probabilistic reliability index, the following updating scheme for the MPP search in the \mathbf{u} -space is employed:

$$\mathbf{u}^{(k+1)} = \frac{(\mathbf{G}_{\mathbf{u}}^{(k)})^T \mathbf{u}^{(k)} - g(\mathbf{u}^{(k)}, \mathbf{v}^{(k+1)})}{(\mathbf{G}_{\mathbf{u}}^{(k)})^T \mathbf{G}_{\mathbf{u}}^{(k)}} \mathbf{G}_{\mathbf{u}}^{(k)}, \quad (4.25)$$

where $\mathbf{G}_{\mathbf{u}}^{(k)} = \left. \frac{\partial g(\mathbf{u}, \mathbf{v})}{\partial \mathbf{u}} \right|_{(\mathbf{u}^{(k)}, \mathbf{v}^{(k+1)})}$.

The updating procedures in (4.24) and (4.25) are repeated until a convergence criterion is satisfied. The flowchart of the direct iteration process is given in Fig.4.6.

It should be noted that the standard HL-RF algorithm may suffer a poor convergence due to the zigzagging movement of iteration points in case of high nonlinearity of the limit-state function. In this case, some modifications suggested in references [122, 173, 174] can be embedded into the present iteration procedures for improving the convergence behaviour.

Compared with the mathematical programming method, the direct iteration algorithm approach is straightforward and convenient from computational point of view. However, similarly as in the HL-RF algorithm for the probabilistic reliability problem, the proposed iteration algorithm cannot guarantee obtaining the correct reliability index if the limit-state

function is non-convex or not smooth. In such a case, mathematical programming methods enhanced with special techniques such as multiple initial guesses and convex approximations should be resorted to.

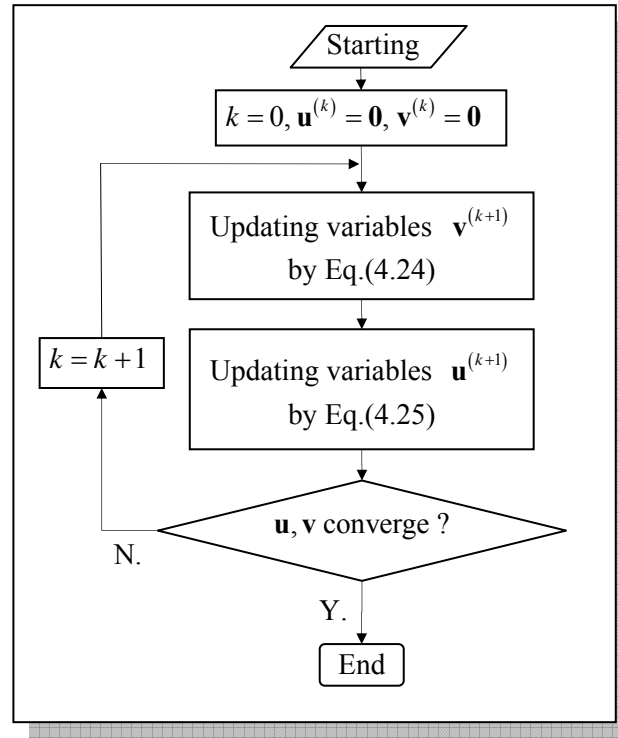


Fig. 4.6 Flowchart of the iteration process

4.5 NUMERICAL EXAMPLES

4.5.1 Example with explicit performance function

A relatively simple mathematical problem with three uncertain variables is treated in this example. Two performance functions G_1 and G_2 are considered respectively, which are given as

$$\begin{aligned} G_1 &= y - x_1 x_2 \\ G_2 &= 3y - x_1^2 x_2 \end{aligned} \quad (4.26)$$

where x_1 and x_2 are normally distributed variables with the mean values of $\bar{x}_1 = 3.0$ and $\bar{x}_2 = 2.0$, and the standard deviations $\sigma_1 = 0.3$ and $\sigma_2 = 0.2$, respectively. The variable y represents a bounded quantity and its value is restricted by $|y - 10.0| \leq 2.0$ or $y \in [8, 12]$. Obviously, $y^* = 8$ is the worst-case point in this specific problem.

The reliability indices β_m , obtained using the standard mathematical programming (MP) approach and the proposed direct iteration method, are both shown in Table 4.1. Both approaches produce identical results: $\beta_m = 2.1878$, $x_1^{\text{MPP}} = 3.464$, $x_2^{\text{MPP}} = 2.309$, $y^* = 8$ for the limit-state function G_1 and $\beta_m = 1.3550$, $x_1^{\text{MPP}} = 3.360$, $x_2^{\text{MPP}} = 2.126$, $y^* = 8$ for the limit-state function G_2 .

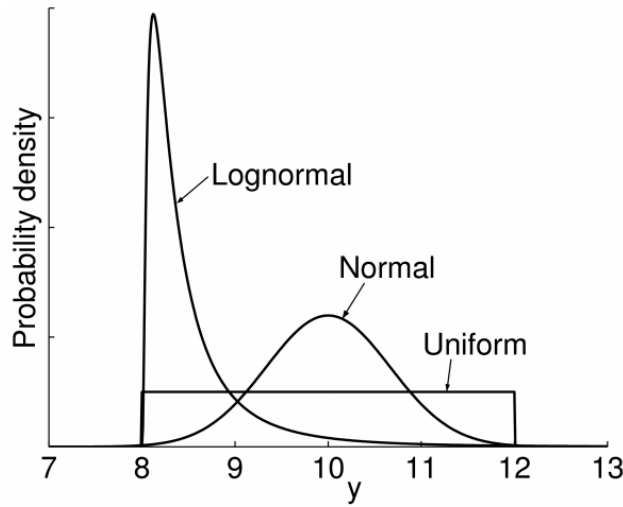


Fig. 4.7 Three assumed probabilistic distributions for uncertain variable y

For comparison purpose, a Monte Carlo simulation-based probabilistic reliability analysis is also run for three cases with assumed probabilistic distributions of y (lognormal distribution, normal distribution and uniform distribution). The lognormal distribution has a

mean of 8.55 and a standard deviation of 0.72, the normal distribution has a mean of 10 and a standard deviation of 2/3, while the uniform distribution is on the specified interval from 8 to 12. These distributions are schematically illustrated in Fig.4.7. In each case, a Monte Carlo simulation with 200,000 realizations is implemented for extracting the failure probability. These results, as well as the corresponding probabilistic reliability indices, are also listed in Table 4.1. As can be noted, the results for these three cases are quite different. This is natural since that the conventional probabilistic reliability analysis relies on the distribution characteristics of the inputs.

Table 4.1 Comparison of reliability results under mixed model and assumed distribution of y

Limit-state function	Reliability index β_m under mixed model (Failure probability)		Probabilistic reliability index β under assumed distribution (Failure probability)		
	By MP	By iteration	Lognormal	Normal	Uniform
G_1	2.1878 (0.0143)	2.1878 (0.0143)	2.54 (0.0055)	3.40 (0.0003)	3.03 (0.0012)
G_2	1.3550 (0.0877)	1.3550 (0.0877)	1.63 (0.0515)	2.37 (0.0089)	2.13 (0.0166)

It is also noted that for both limit-state functions the reliability indices predicted by the mixed model are less than those by pure probabilistic models, regardless the distribution type assumed in the reliability analysis. This confirms that the mix model provides a more conservative measure of the system safety without introducing subjective assumptions on the uncertainty distribution.

4.5.2 Reliability analysis of a cantilever beam

A cantilever beam subjected to a concentrated force P is shown in Fig.4.8. The beam has a length of L , a width of b and a height of h . The Young's modulus of the material is E . The structure becomes unsafe when the tip displacement is greater than 0.15 in. Thus the limit-state function is defined as

$$G = 0.15 - \frac{4PL^3}{Ebh^3} \quad (4.27)$$

In this example, E and P are considered as normal random variables, whereas L , b and h are represented by uncertain-but-bounded variables reflecting manufacturing errors. The uncertainty characteristics are summarized in Table 4.2.

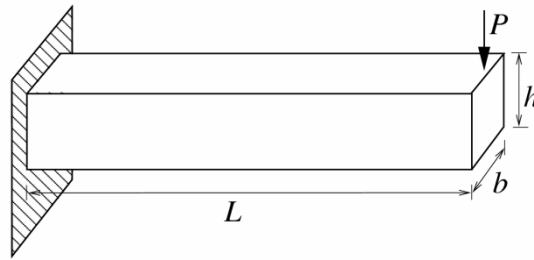


Fig. 4.8 A cantilever beam

Table 4.2 Uncertainty characteristics of the cantilever beam

Uncertain variable	Mean (nominal) value	COV	Convex model description
E (psi.)	10^7	0.05	--
P (lb.)	100	0.1	--
L (in.)	30	--	$-0.05 \leq \delta_L \leq 0.05$
b (in.)	0.8359	--	$[\delta_b \ \delta_h] \begin{bmatrix} 1 & 0 \\ 0 & 1 \end{bmatrix} \begin{bmatrix} \delta_b \\ \delta_h \end{bmatrix} \leq 0.05^2$
h (in.)	2.5093	--	

The reliability evaluation has been performed by the mathematical programming approach and the direct iteration method, respectively. The obtained results are listed in Table 4.3 and the iteration histories for both approaches are plotted in Fig.4.9. For both approaches, the initial guesses of the MPP and the worst-case point are the mean values or nominal values of the uncertainties, and the stopping criteria is that the relative difference between the objective function values of two adjacent iterations is less than 10^{-4} . The same reliability index $\beta_m = 2.8853$ is achieved, though the number of iteration steps involved in the

proposed direct iteration method is much less than that in the mathematical programming approach.

Table 4.3 Summary of results for the cantilever beam example

	Reliability index β_m	Total number of iterations	MPP and the worst-case point				
			E^{MPP} (10^6 psi.)	P^{MPP} (lb.)	L^* (in.)	b^* (in.)	h^* (in.)
By MP	2.8853	25	9.194	123.926	31.5	0.823	2.390
By iteration	2.8853	5	9.194	123.930	31.5	0.823	2.390

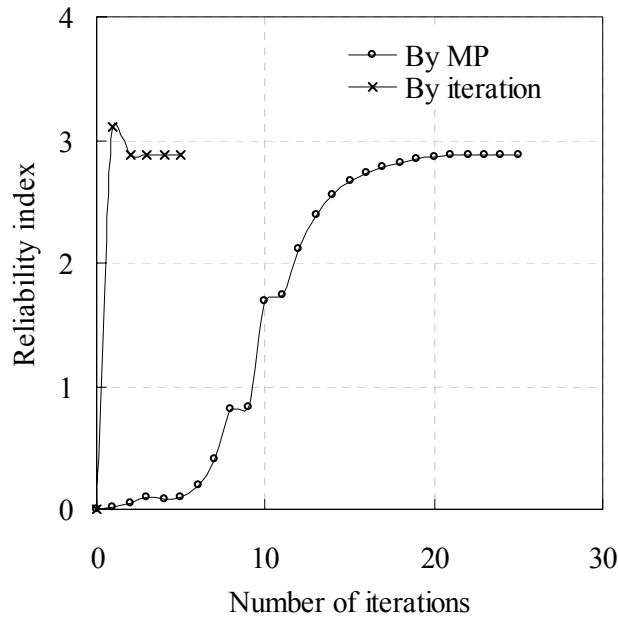


Fig. 4.9 Iteration histories of reliability evaluation for the cantilever beam

4.6 RELIABILITY ASSESSMENT OF THE BONDED COMPOSITE BEAM

In this section, the bonded steel and concrete composite beam, named P1 in Chapter 2, is considered. As shown in Fig.4.10, the composite beam consists of a concrete slab, an adhesive layer and a steel girder. It is simply supported and a concentrated load is applied to the mid-span of the beam. The Young's modulus and the permissible stresses of these materials are normally distributed random variables with the mean values given in Table 4.4 and the

coefficients of variation 0.08. The Poisson's ratios for the constituent materials of the concrete slab, the adhesive layer and the steel girder are 0.28, 0.34 and 0.30, respectively. The load magnitude F is also a normal random variable with the mean value of 150kN and the coefficient of variation of 0.1. Hence, there are six stochastic variables for material properties and one stochastic variable for load magnitude. In addition, nine cross-sectional dimensions (y_1, y_2, \dots, y_9) presented in Fig.4.10b are treated as interval-valued variables with the relative variation of 5% about their nominal values. Thus, a total number of 16 uncertain variables, including the aforementioned 7 stochastic variables and 9 interval variables, are considered in this problem. The structural failure is defined by $G = 15 - U_{\text{mid}} \leq 0$, where U_{mid} is the vertical displacement at the mid-span.

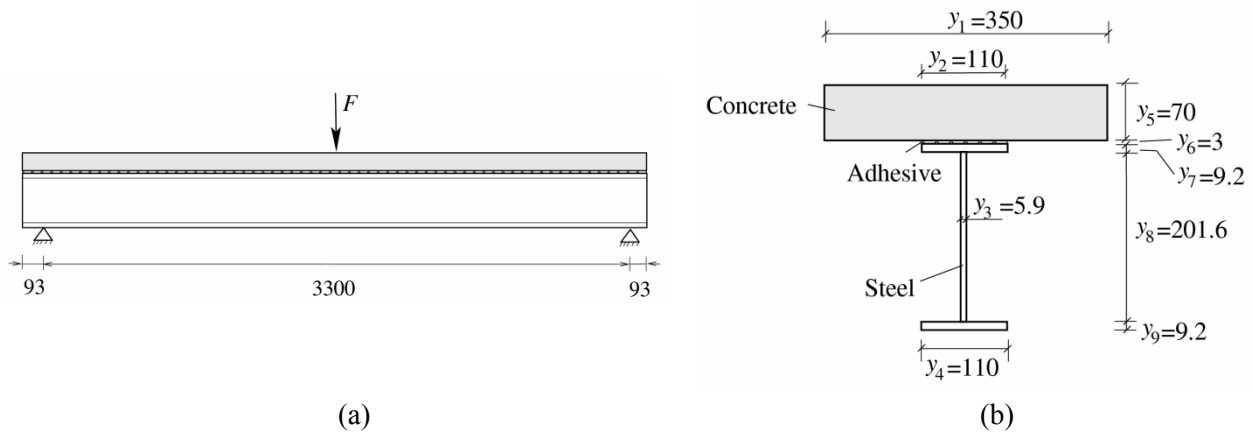


Fig. 4.10 The composite beam P1

(a) Overall dimensions; (b) Cross-section dimensions (Unit: mm)

Table 4.4 Mean values of the material properties for the composite beam P1

Material	Young's modulus (MPa)	Permissible von Mises stress (MPa)
Concrete	36,600	68.0
Adhesive	12,300	19.5
Steel	205,000	470

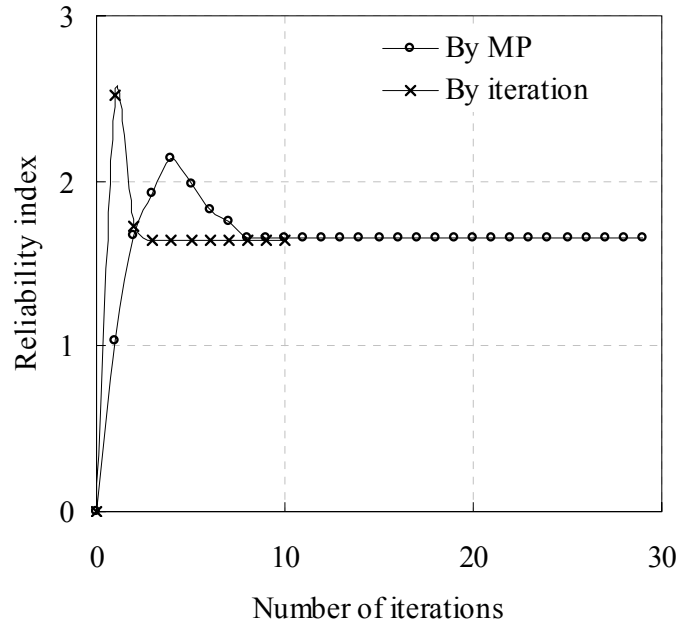


Fig. 4.11 Iteration histories of reliability evaluation for the composite beam P1

Making use of the symmetry, one fourth of the composite beam is discretized by using the nonlinear finite element model proposed in chapter 2. The mathematical programming approach and the proposed iteration method have been both applied to this problem. In the latter approach, a technique proposed by Lee et al. [122] is adapted for detecting and eliminating excessive zigzagging iterations. The reliability indices obtained by both approaches are $\beta_m = 1.652$ (failure probability 4.93%) and $\beta_m = 1.647$ (failure probability 4.98%), respectively. This insignificant difference may be due to a premature convergence of the mathematical programming solution. The iteration histories of the reliability evaluation are plotted in Fig.4.11. Again, it can be observed that the present iteration method is more efficient than the mathematical programming approach. This seems to confirm that the proposed iteration scheme behaves better than standard optimizers, especially for engineering problems involving a large number of uncertain parameters.

4.7 SUMMARY

In many real-life structural safety assessment problems, a pure probabilistic description for all the uncertain parameters is hardly obtainable due to lack of sufficient sample data, while the bounds of some uncertain parameters can be easily determined in consistence with available information. For structures exhibiting both probabilistic and bounded uncertainties, unjustified assumptions on distribution characteristics may give rise to misleading results, which makes a pure probabilistic reliability analysis questionable. In this chapter, based on the multi-ellipsoid convex model description for grouped uncertain-but-bounded variables, a combined probabilistic and set-valued description is presented. The reliability index is defined as the shortest distance from the origin to the critical region in the standard \mathbf{u} -space. Mathematically, the evaluation of the reliability index is formulated as a nested optimization problem. The original nested problem is then transformed into an equivalent single-loop constraint optimization problem, with the purpose to improve the computational efficiency in seeking the MPP and the worst-case point. In conjunction with the linear approximation of the limit-state function, a direct iteration algorithm is suggested for solving the minimization problem. The numerical examples confirm that both approaches are applicable but the direct iteration algorithm seems to be more efficient. It can be also seen that the mixed model tends to present a relatively conservative assessment of structural reliability. To this end, the proposed mixed model is employed to assess the reliability of a bonded steel and concrete beam. The assessed result showed that the failure probability of this bonded composite beam is about 5%.

There is no doubt that the reliability evaluation should be implemented in the conventional probabilistic framework when sufficient data are available for constructing accurate probabilistic models of the uncertainties. Nevertheless, the present formulation and numerical techniques provide an alternative approach for the reliability evaluation of structures subject to both stochastic and bounded variations.

CHAPTER 5:
RELIABILITY-BASED DESIGN OPTIMIZATION OF THE
BONDED COMPOSITE BEAM

5.1 INTRODUCTION

Along with the ever increasing computational power, the past two decades had seen a rapid development of structural optimization in both theories and industrial applications. In particular, the design optimization problem incorporating various uncertainties has been intensively studied. Among other non-deterministic optimal design formulations, the reliability-based design optimization provides an effective tool for seeking the best designs against structural failures in presence of system variations. Basically, the uncertainty models employed by a typical structural reliability analysis can be classified into two categories: the probabilistic model and non-probabilistic models. As the most mature uncertainty model, the probabilistic model describes the stochastic parameters and structural responses with random fields or discrete random variables that have certain statistical distribution characteristics. The probabilistic model has been successfully used in many real-life engineering applications for structural reliability-based design optimization as well as robust design optimization. In practical applications, the probabilistic distribution type and corresponding statistical parameters of inputs are usually attracted from a sufficient amount of measured data or assumed on the basis of engineering experiences.

In the bonded steel and concrete composite beam, some of the concerned uncertainties are probabilistic variables with precise probability distribution information, while others are only uncertain-but-bounded due to their inherent characteristic or lacking sufficient sample data. Therefore, it would be desirable to select the proposed probability and convex set mixed model to quantify these different types of uncertainties. Based on the structural reliability assessment method in chapter 4, it is useful to fully explore the reliability-based design optimization formulation using the probability and convex set mixed model.

This chapter aims to provide a systematic method to incorporate simultaneously randomness and uncertain-but-bounded uncertainties into the design optimization problem. Using the mathematical definition of structural mixed reliability index based on probabilistic model and convex set, a nested optimization model for reliability-based structural design problems with constraints on such mixed reliability indices is presented. To improve the

convergence of the inner loop, the performance measure approach (PMA) [121] is employed. Two approaches, namely the nested double-loop approach and the linearization-based approach, are employed to solve the optimization formula. Then, two mathematical and engineering design examples are presented to demonstrate the applicability of the proposed model and the efficiency of the numerical techniques. Finally, based on the optimal topology layout in chapter 3, a sizing design optimization of the bonded steel and concrete composite beam incorporating reliability constraints is mathematically formulated.

5.2 RELIABILITY-BASED STRUCTURAL OPTIMIZATION WITH PROBABILITY AND CONVEX SET MIXED MODEL

5.2.1 Optimization problem and performance measure approach

A structural optimization problem usually aims to seek the least cost for satisfying certain structural behaviour requirements. Under the mixed model, the structural behaviours can be expressed as the performance functions of the design variables \mathbf{d} , the normalized probabilistic variables \mathbf{u} and the normalized uncertain-but-bounded variables \mathbf{v} , namely $g_j(\mathbf{d}, \mathbf{u}, \mathbf{v})$ ($j = 1, 2, \dots, N_g$). It should be noted that the design variables can be also defined as the mean values or the nominal values of the uncertain variables. In the present paper, the reliability-based design optimization problem under the probability and convex set mixed model is mathematically formulated as

$$\begin{aligned} \min_{\mathbf{d}} \quad & f(\mathbf{d}) \\ \text{s.t.} \quad & \beta_m[g_j(\mathbf{d}, \mathbf{u}, \mathbf{v})] \geq \underline{\beta}_{m,j} \quad (j = 1, 2, \dots, N_g) \\ & \mathbf{d}_L \leq \mathbf{d} \leq \mathbf{d}_U \end{aligned} \quad (5.1)$$

and

$$\begin{aligned} \beta_m[g_j(\mathbf{d}, \mathbf{u}, \mathbf{v})] &= \text{sgn}(g(\mathbf{d}, \mathbf{0}, \mathbf{v}^*)) \cdot \min_{\mathbf{u}} \{\sqrt{\mathbf{u}^T \mathbf{u}}\} \\ \text{s.t.} \quad & g_j(\mathbf{d}, \mathbf{u}, \mathbf{v}^*) = 0 \end{aligned} \quad (5.2)$$

where $f(\mathbf{d})$ is the objective function to be minimized; $\beta_m[g_j(\mathbf{d}, \mathbf{u}, \mathbf{v})]$ is the mixed reliability index corresponding to the j th performance function; $\underline{\beta}_{m,j}$ is the prescribed target value of the reliability index; N_g is the number of constraints; \mathbf{d}_L and \mathbf{d}_U are the lower and upper bounds of the design variables, respectively. \mathbf{v}^* is the worst-case point and is defined by (4.18).

In the above reliability-based optimum design problem, the outer loop aims to minimize the cost function of the structural design, while the inner loop represents the reliability analysis. In the direct approach, the reliability-index-based approach, these two loops can be sequentially treated and the solution of the inner loop is used to determine whether or not the reliability constraints in the outer loop are satisfied. However, the design sensitivity analysis of the reliability index presents an *optimum sensitivity* problem, which is extremely difficult to be solved, especially when a large number of design variables are involved. In addition, the strong coupling between the outer and inner loop as well as the high nonlinearity of the problem may lead to iteration instability and poor convergence. In order to circumvent these difficulties, a recently introduced performance measure approach (PMA), which was proposed by Tu et al. [121] and enhanced by Youn et al. [124], is employed in this chapter.

In contrast to the direct method relying on the comparison between the current reliability index value and its prescribed target value, the performance measure approach checks the satisfaction of a reliability constraint according to the target performance value at a target point in the uncertain parameter space. The primary idea of the performance measure approach is to transform the design problem (5.1) into an equivalent optimization problem expressed by

$$\begin{aligned} \min_{\mathbf{d}} \quad & f(\mathbf{d}) \\ \text{s.t.} \quad & \alpha_j(\mathbf{d}) \geq 0 \quad (j = 1, 2, \dots, N_g) \\ & \mathbf{d}_L \leq \mathbf{d} \leq \mathbf{d}_U \end{aligned} \quad (5.3)$$

where $\alpha_j(\mathbf{d})$ is the target performance value and defined as the minimal value of $g_j(\mathbf{d}, \mathbf{u}, \mathbf{v}^*)$ that yields the prescribed target reliability index $\underline{\beta}_{m,j}$, namely

Taking the case with two probabilistic variables $\mathbf{u} = \{u_1, u_2\}$ and uncertain-but-bounded variables \mathbf{v} as an example, Fig.5.1 schematically illustrates the basic idea of the performance measure approach mentioned above. In the \mathbf{u} -space plotted in the figure, the solid circle represents the boundary of the probabilistic variables characterized by a radius of the desired reliability index $\underline{\beta}_m$. Among all the points lying on the solid circle, the point at which the limit-state function $g(\mathbf{u}, \mathbf{v}^*)$ takes its minimum value is denoted by \mathbf{B} . Here the target performance $\alpha = g(\mathbf{u}^*, \mathbf{v}^*)$ is defined as the limit-state function value at this point. Obviously, the feasibility of the design is satisfied if and only if α is positive. If $\alpha = 0$, the reliability index equals to $\underline{\beta}_m$ and therefore the structure is in a critical state, while $\alpha < 0$ means that there exists within the solid circle certain parameter combinations that will result in a performance failure. Consequently, the constraint $\alpha \geq 0$ is equivalent to the reliability index constraint $\beta_m \geq \underline{\beta}_m$ as appeared in the original optimization problem (5.1).

Note that the position of the target point varies with the design point during the entire optimization. In general, the computational costs involved in seeking the target point and in calculating the reliability index are different. The former minimization problem has the simpler expression of the cost function and the constraints, whereas the latter could result in solution instability due to the implicit and design variable-dependent constraint condition. Researches showed that the performance measure approach is inherently robust and superior in view of both computational efficiency and numerical stability (Lee et al. [122]).

5.2.2 Design sensitivity analysis of the target performance

When a gradient-based optimization algorithm is employed in solving the design optimization problem (5.3), the computation of the design sensitivity of the objective function and the constraints is necessitated. In the context of the proposed method, the derivative of the target performance α_j with respect to the design variable is expressed by

$$\frac{d\alpha_j}{d\mathbf{d}} = \frac{d g_j(\mathbf{d}, \mathbf{u}^*, \mathbf{v}^*)}{d\mathbf{d}}, \quad (5.7)$$

where \mathbf{u}^* is the target point in the \mathbf{u} -space, \mathbf{v}^* is the worst-case point. \mathbf{u}^* and \mathbf{v}^* are the optimum of the minimization problem (5.6) and are thus implicitly dependent upon the design variable \mathbf{d} . In fact, calculation of the derivative $d\alpha_j/d\mathbf{d}$ is an optimum sensitivity problem. However, as can be seen from what follows, it can be easily evaluated in this particular circumstance.

For the sake of convenience in the subsequent derivation, the concerned performance problem can be rewritten as following

$$\begin{aligned} \min_{\mathbf{u}, \mathbf{v}} \quad & g(\mathbf{d}, \mathbf{u}, \mathbf{v}) \\ \text{s.t.} \quad & \mathbf{u}^T \mathbf{u} = \underline{\beta}_m^2 \\ & \mathbf{v}_i^T \mathbf{v}_i \leq 1 \quad (i = 1, 2, \dots, N_E) \end{aligned} \quad (5.8)$$

Using the Karush-Kuhn-Tucker optimality conditions, the following relations at point $(\mathbf{u}^*, \mathbf{v}^*)$ can be obtained

$$g_{,u_l} + 2\lambda \mathbf{u}^T \frac{\partial \mathbf{u}}{\partial u_l} = 0 \quad (l = 1, 2, \dots, m), \quad (5.9)$$

$$g_{,v_l} + 2 \sum_{i \in I} \lambda_i \mathbf{v}_i^T \frac{\partial \mathbf{v}_i}{\partial v_l} = 0 \quad (l = 1, 2, \dots, n), \quad (5.10)$$

$$\lambda \geq 0, \lambda_i \geq 0 \quad i \in I(\mathbf{v}^*), \quad (5.11)$$

$$\mathbf{u}^T \mathbf{u} - \underline{\beta}_m^2 = 0 \quad (5.12)$$

$$\mathbf{v}_i^T \mathbf{v}_i - 1 = 0, \quad i \in I(\mathbf{v}^*), \quad (5.13)$$

where $g_{,u_l} = \partial g / \partial u_l$ and $g_{,v_l} = \partial g / \partial v_l$ denote the partial derivative of the limit-state function with respect to the uncertainty u_l and v_l , λ and λ_i are the Lagrange multiplier, $I(\mathbf{v}^*)$ is the index set of active constraints.

Using (5.7), (5.9) and (5.10), the derivative $d\alpha/d\mathbf{d}$ can be given as

$$\begin{aligned}
\frac{d\alpha}{d\mathbf{d}} &= \frac{\partial g(\mathbf{d}, \mathbf{u}^*, \mathbf{v}^*)}{\partial \mathbf{d}} + \sum_{l=1}^m \left(g_{,u_l} \frac{du_l}{d\mathbf{d}} \right)_{\mathbf{u}=\mathbf{u}^*} + \sum_{l=1}^n \left(g_{,v_l} \frac{dv_l}{d\mathbf{d}} \right)_{\mathbf{v}=\mathbf{v}^*} \\
&= \frac{\partial g(\mathbf{d}, \mathbf{u}^*, \mathbf{v}^*)}{\partial \mathbf{d}} + \sum_{l=1}^m \left(-2\lambda \mathbf{u}^T \frac{\partial \mathbf{u}}{\partial u_l} \frac{du_l}{d\mathbf{d}} \right)_{\mathbf{u}=\mathbf{u}^*} + \sum_{l=1}^n \left(-2 \sum_{i \in I} \lambda_i \mathbf{v}_i^T \frac{\partial \mathbf{v}_i}{\partial v_l} \frac{dv_l}{d\mathbf{d}} \right)_{\mathbf{v}=\mathbf{v}^*}
\end{aligned} \tag{5.14}$$

The differentiation of (5.12) and (5.13) with respect to the design variables yields

$$\sum_{l=1}^m \mathbf{u}^T \frac{\partial \mathbf{u}}{\partial u_l} \frac{du_l}{d\mathbf{d}} = 0 \quad \text{for } \mathbf{u} = \mathbf{u}^*, \tag{5.15}$$

$$\sum_{l=1}^n \mathbf{v}_i^T \frac{\partial \mathbf{v}_i}{\partial v_l} \frac{dv_l}{d\mathbf{d}} = 0 \quad \text{for } \mathbf{v} = \mathbf{v}^*, \quad i \in I(\mathbf{v}^*). \tag{5.16}$$

Therefore, the last two terms in (5.14) vanish and the derivative $d\alpha/d\mathbf{d}$ further reduces to

$$\frac{d\alpha}{d\mathbf{d}} = \frac{\partial g(\mathbf{d}, \mathbf{u}^*, \mathbf{v}^*)}{\partial \mathbf{d}} \tag{5.17}$$

In the optimization problem (5.1), the design sensitivity analysis of the constraint function is extremely difficult. Nevertheless, using (5.17), the sensitivity of the target performance can be easily evaluated. In computer implementations, the semi-analytical method using either direct variables or adjoint variables can be employed for such a computation.

5.2.3 Solution strategy

The structural optimization problem incorporating reliability constraints under mixed modeling of probabilistic randomness and convex models presents a challenging problem with nested optimization. While a direct double-loop approach available, we proposed a single-loop approach based on linearization of limit-state function to reduce the computational cost.

(1) Nested double-loop approach

In the reliability-based optimization problem under mixed model, the inner-loop of the target performance evaluation is embedded in the overall outer-loop optimization. A

double-loop procedure, as depicted in Fig.5.2, is competent for solving the above nested problem (5.3) and (5.6). Herein, a modified programming scheme based on the optimization package CFSQP (Lawrence et al. [172]), which is an implementation of the Sequential Quadratic Programming (SQP) algorithm, is used to solve the problem.

Though the nested double-loop approach can be employed, this still requires prohibitively lengthy calculations. Since the inner loop evaluation of target performance needs many function evaluations of performance functions, and each iteration in the outer-loop optimization consists of a fulfillment of the inner-loop, the total number of function evaluations is usually very high.

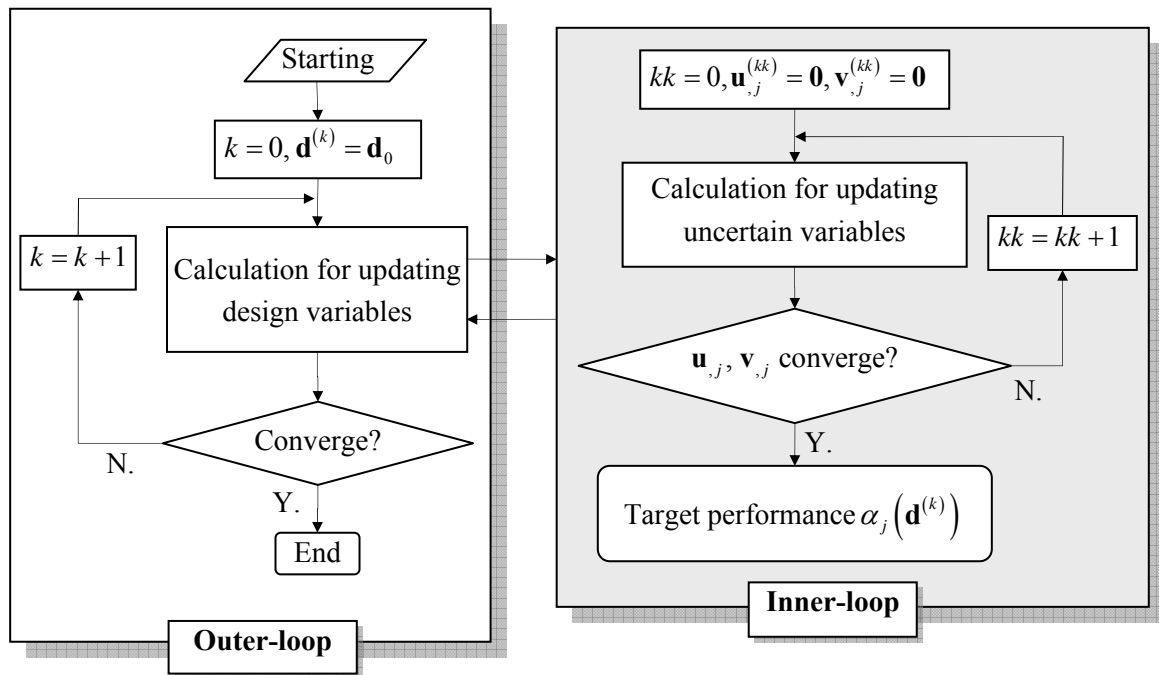


Fig. 5.2 Flow chart of the traditional nested double-loop approach

(2) Linearization-based approach

Various techniques have been developed to decouple the nested optimization problem involved in the conventional RBDO. In a sequential optimization strategy (Royset et al. [175]; Du and Chen [123]; Cheng et al. [176]), the inner-loop and outer-loop are implemented

sequentially and thus the optimum design is obtained by solving a sequence of sub-programming problems. In addition, a single-loop strategy (Chen et al. [177]; Kuschel and Rackwitz [178]; Liang et al. [179]), which allows the solution to be infeasible before convergence and satisfies the constraints only at the optimum, has also been developed. Numerical investigations suggested that those methods could considerably improve the efficiency in solving the RBDO problem. In this section, based a similar decoupling strategy as the single-loop method, a linearization-based approach is proposed to solve the specific reliability-based optimization problem under mixed model.

In most practical circumstances, the variability of the uncertain-but-bounded variables is relatively small or moderate. Therefore, it is reasonable to assume that the performance functions are monotonic with respect to these quantities within their variation bounds. In virtue of this, all the inequality constraints in (5.6) will be active at the optimum. Thus, an iteration scheme for solving the optimum $(\mathbf{u}_{,j}^*, \mathbf{v}_{,j}^*)$ is derived based on the optimality conditions in the following.

Denoting the approximate solution of Eq.(5.6) in the k -th iteration by $(\mathbf{u}_{,j}^{(k)}, \mathbf{v}_{,j}^{(k)})$, by approximating the limit-state function g_j with the first-order Taylor expansion about $(\mathbf{u}_{,j}^{(k)}, \mathbf{v}_{,j}^{(k)})$, we rewrite Eq.(5.6) as

$$\begin{aligned} \alpha_j(\mathbf{d}^{(k)}) &= \min_{\mathbf{u}, \mathbf{v}} \left\{ g_j(\mathbf{d}^{(k)}, \mathbf{u}_{,j}^{(k)}, \mathbf{v}_{,j}^{(k)}) + \mathbf{G}_{\mathbf{u}_{,j}}^T(\mathbf{u} - \mathbf{u}_{,j}^{(k)}) + \mathbf{G}_{\mathbf{v}_{,j}}^T(\mathbf{v} - \mathbf{v}_{,j}^{(k)}) \right\} \\ \text{s.t. } \mathbf{u}^T \mathbf{u} &= \underline{\beta}_{m,j}^2 \\ \mathbf{v}_i^T \mathbf{v}_i &= 1 \quad (i = 1, 2, \dots, N_E) \end{aligned} \quad (5.18)$$

where $\mathbf{d}^{(k)}$ denotes the k -th (current) iteration design variables, the subscript $(, j)$ stands for the j -th performance function. $\mathbf{G}_{\mathbf{u}_{,j}}^{(k)}$ and $\mathbf{G}_{\mathbf{v}_{,j}}^{(k)}$ are partial derivatives of the performance function, which are expressed by

$$\mathbf{G}_{\mathbf{u}_{,j}}^{(k)} = \frac{\partial g_j}{\partial \mathbf{u}} \bigg|_{\mathbf{d}^{(k)}, \mathbf{u}_{,j}^{(k)}, \mathbf{v}_{,j}^{(k)}}, \quad \mathbf{G}_{\mathbf{v}_{,j}}^{(k)} = \frac{\partial g_j}{\partial \mathbf{v}} \bigg|_{\mathbf{d}^{(k)}, \mathbf{u}_{,j}^{(k)}, \mathbf{v}_{,j}^{(k)}}, \quad (5.19)$$

Both derivatives can be either explicitly obtained or evaluated by using classical approaches such as the semi-analytical method.

Before deriving the iteration scheme for solving the above constrained minimization problem, a Lagrangian function is first constructed:

$$L = g_j(\mathbf{d}^{(k)}, \mathbf{u}_{,j}^{(k)}, \mathbf{v}_{,j}^{(k)}) + \mathbf{G}_{\mathbf{u}_{,j}^{(k)}}^T (\mathbf{u} - \mathbf{u}_{,j}^{(k)}) + \mathbf{G}_{\mathbf{v}_{,j}^{(k)}}^T (\mathbf{v} - \mathbf{v}_{,j}^{(k)}) + \lambda (\mathbf{u}^T \mathbf{u} - \underline{\beta}_{m,j}^2) + \sum_{i=1}^{N_E} \lambda_i (\mathbf{v}_i^T \mathbf{v}_i - 1), \quad (5.20)$$

where λ and λ_i are the Lagrangian multiplier for the corresponding constraints.

Applying the Karush-Kuhn-Tucker optimality condition at the optimum $(\mathbf{u}_{,j}^*, \mathbf{v}_{,j}^*)$, we have

$$\begin{cases} \left. \frac{\partial L}{\partial \mathbf{u}} \right|_{\mathbf{u}_{,j}^*} = \mathbf{G}_{\mathbf{u}_{,j}^{(k)}} + 2\lambda \mathbf{u}_{,j}^* = 0, \\ \frac{\partial L}{\partial \lambda} = (\mathbf{u}_{,j}^*)^T \mathbf{u}_{,j}^* - \underline{\beta}_{m,j}^2 = 0, \\ \left. \frac{\partial L}{\partial \mathbf{v}_i} \right|_{\mathbf{v}_{i,j}^*} = \mathbf{G}_{\mathbf{v}_{i,j}^{(k)}} + 2\lambda_i \mathbf{v}_{i,j}^* = 0, \\ \frac{\partial L}{\partial \lambda_i} = (\mathbf{v}_{i,j}^*)^T \mathbf{v}_{i,j}^* - 1 = 0 \quad (i = 1, 2, \dots, N_E). \end{cases} \quad (5.21)$$

After some manipulations, Eq.(5.21) leads to

$$\begin{cases} \mathbf{u}_{,j}^* = -\underline{\beta}_{m,j} \frac{\mathbf{G}_{\mathbf{u}_{,j}^{(k)}}}{\sqrt{\mathbf{G}_{\mathbf{u}_{,j}^{(k)}}^T \mathbf{G}_{\mathbf{u}_{,j}^{(k)}}}}, \\ \mathbf{v}_{i,j}^* = -\frac{\mathbf{G}_{\mathbf{v}_{i,j}^{(k)}}}{\sqrt{\mathbf{G}_{\mathbf{v}_{i,j}^{(k)}}^T \mathbf{G}_{\mathbf{v}_{i,j}^{(k)}}}} \quad (i = 1, 2, \dots, N_E). \end{cases} \quad (5.22)$$

Thus, a heuristic scheme for updating $(\mathbf{u}_{,j}^*, \mathbf{v}_{,j}^*)$ corresponding to the j th reliability constraint would be

$$\begin{aligned}
(\mathbf{u}_{,j}^{(k+1)}, \mathbf{v}_{,j}^{(k+1)}) &= (\mathbf{u}_{,j}^{(k+1)}, \mathbf{v}_{1,j}^{(k+1)}, \dots, \mathbf{v}_{N_E,j}^{(k+1)}) \\
&= - \left\{ \beta_{m,j} \frac{\mathbf{G}_{\mathbf{u}_{,j}^{(k)}}}{\sqrt{\mathbf{G}_{\mathbf{u}_{,j}^{(k)}}^T \mathbf{G}_{\mathbf{u}_{,j}^{(k)}}}}, \frac{\mathbf{G}_{\mathbf{v}_{1,j}^{(k)}}}{\sqrt{\mathbf{G}_{\mathbf{v}_{1,j}^{(k)}}^T \mathbf{G}_{\mathbf{v}_{1,j}^{(k)}}}}, \dots, \frac{\mathbf{G}_{\mathbf{v}_{N_E,j}^{(k)}}}{\sqrt{\mathbf{G}_{\mathbf{v}_{N_E,j}^{(k)}}^T \mathbf{G}_{\mathbf{v}_{N_E,j}^{(k)}}}} \right\}. \quad (5.23)
\end{aligned}$$

The flowchart of the optimization process using the linearization-based approach is given in Fig.5.3. The optimum structural design is searched in the design space by the optimizer, while $\mathbf{u}_{,j}^*$ and $\mathbf{v}_{,j}^*$ are updated simultaneously by Eq.(5.23). This process continues until the objective function becomes stable and all the target performance constraints are satisfied. With this procedure, the computational efficiency will be much higher than that of the nested double-loop approach because the expensive inner iterations are avoided.

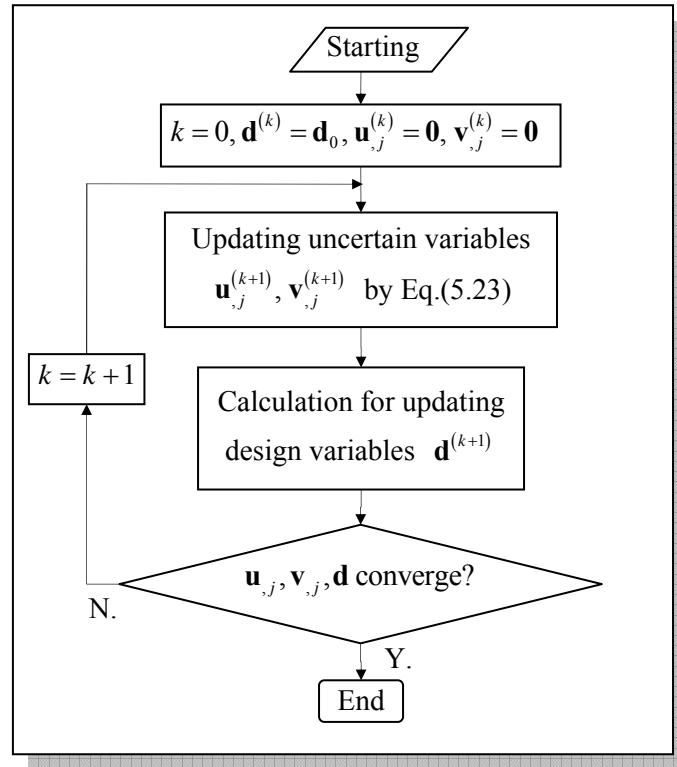


Fig. 5.3 Flowchart of the optimization process using the linearization-based approach

However, it should be noted that the suggested linearization-based approach relies on the assumption of the local monotonicity of performance function with respect to uncertainties. In addition, the global optimality cannot be guaranteed if the performance function is non-convex or not smooth. In such a case, the nested double-loop approach enhanced with special techniques such as multiple initial guesses and convex approximations can be resorted to.

5.2.4 Validation by numerical examples

To demonstrate the validity and effectiveness of the reliability-based optimization approach under mixed model, two examples regarding design optimization of a mathematical function and a truss structure are given in this section. We will also make comparisons between the computing efficiency of the nested double-loop approach and that of the linearization-based approach.

(1) Minimization of a mathematical function under reliability constraints

The first example considers minimization of an explicit performance function under reliability constraints. Two normally distributed random variables (denoted by x_1 and x_2) and two uncertain parameters (denoted by y_1 and y_2) bounded by an ellipsoid model are taken into account in the problem. The optimization problem is expressed as

$$\begin{aligned} \min_{\mathbf{d}} \quad & f(\mathbf{d}) = (d_1 + 3)^2 + (d_2 + 3)^2 \\ \text{s.t.} \quad & \beta_m [g_1(\mathbf{x}, \mathbf{y}) \geq 0] \geq \underline{\beta}_m, \\ & \beta_m [g_2(\mathbf{x}, \mathbf{y}) \geq 0] \geq \underline{\beta}_m, \\ & 0.01 \leq d_1 \leq 10, \quad 0.01 \leq d_2 \leq 10, \end{aligned} \quad (5.24)$$

in which

$$\begin{aligned} g_1(\mathbf{x}, \mathbf{y}) &= x_1(x_2 + y_1) - y_2, \\ g_2(\mathbf{x}, \mathbf{y}) &= x_1 - (x_2 + y_1)^2 y_2, \end{aligned} \quad (5.25)$$

where the design variables are $\mathbf{d} = \{d_1, d_2\}^T$, with d_1 and d_2 representing the mean values of x_1 and x_2 , respectively. The Coefficients of Variation (COV) for x_1 and x_2 are both

0.03. Another two variables y_1 and y_2 are described by an ellipsoid model expressed by $\mathbf{y} = \{y_1, y_2\}^T \in \mathbf{E} \equiv \left\{ \mathbf{y} \mid (\mathbf{y} - \mathbf{y}^c)^T \mathbf{W}_y (\mathbf{y} - \mathbf{y}^c) \leq 0.5^2 \right\}$, where the nominal values $\mathbf{y}^c = \{y_1^c, y_2^c\}^T = \{0.25, 2\}^T$ and $\mathbf{W}_y = \begin{bmatrix} 4 & 0 \\ 0 & 1 \end{bmatrix}$.

Table 5.1 Solutions for the mathematical example

	Linearization-based approach	Nested double-loop approach
Objective	55.9733	55.9733
Solution (d_1, d_2)	(3.5045, 0.6966)	(3.5045, 0.6966)
Nominal value $(\bar{x}_1, \bar{x}_2, y_1^c, y_2^c)$	(3.5045, 0.6966, 0.25, 2)	(3.5045, 0.6966, 0.25, 2)
$(x_1^*, x_2^*, y_1^*, y_2^*)$ for g_1	(3.2750, 0.6536, 0.0366, 2.2606)	(3.2752, 0.6536, 0.0365, 2.2600)
$(x_1^*, x_2^*, y_1^*, y_2^*)$ for g_2	(3.2901, 0.7426, 0.4699, 2.2380)	(3.2892, 0.7425, 0.4699, 2.2377)
Number of iterations for outer-loop	32	31
Average number of iteration for each inner-loop	1	9
Total number of performance function evaluations	64	558

The target reliability index of the constraints is $\underline{\beta}_m = 3.0$, which means the failure probability of the structure must be less than 0.135%.

When using the CFSQP to solve the minimization problems, the stop criterion of iterations is: the relative difference between the objective function values of two adjacent iterations is less than 10^{-4} , or the number of iteration steps exceeds 500. For initial values of the design variables $d_1^{(0)} = d_2^{(0)} = 5$, the obtained optimal solutions are listed in Table 5.1. The proposed linearization-based approach results in the identical optimal solutions as the nested double-loop approach. However, the former approach is much more efficient since it involves only one time of the limit-state function evaluation for each inner-loop. For testing the

dependency of the optimal solutions upon the initial guesses, three different initial values of design variables $d_i^{(0)} = 1, 3, 8$ ($i = 1, 2$) are also fed into the optimizer. From the iteration histories shown in Fig.5.4, it can be seen that the iterations converge to the same optimum, though the efficiency of the linearization-based approach is dependent on the initial design point.

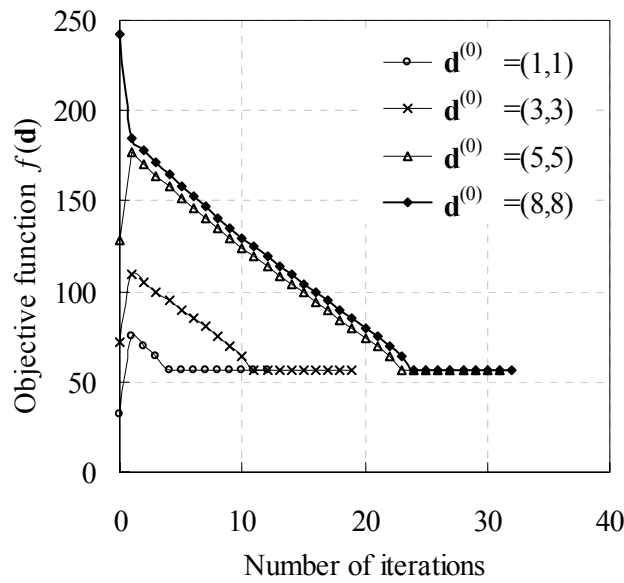


Fig. 5.4 Iteration histories of the optimization with different initial design points

(2) Reliability-based optimization of a ten-bar truss structure

Fig.5.5 shows a frequently studied planar ten-bar truss structure, which is to be optimized for minimum weight. The horizontal and vertical bar members have a length of $L = 360$. The mass density of the material is $\rho = 0.1$. Two external loads P are applied at node 2 and node 4. A constraint $U \leq 2.0$ is imposed on the vertical displacement of node 2. The bar cross-sectional areas A_i ($i = 1, 2, \dots, 10$) and the Young's modulus E of the material are Gaussian normal random variables, whereas the external load P is an uncertain-but-bounded variable. The uncertainty properties are summarized in Table 5.2.

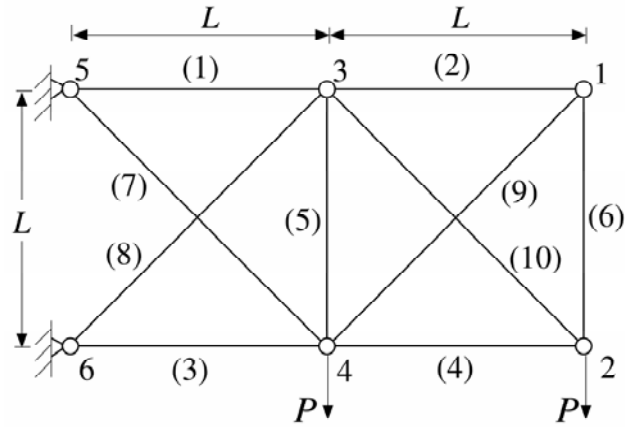


Fig. 5.5 The ten-bar truss structure

Table 5.2 Uncertainty properties for the ten-bar truss structure

Uncertainty	Section area $A_i (i = 1, 2, \dots, 10)$	Young's modulus E	External load P
Distribution	Normal distribution	Normal distribution	Uncertain-but-bounded
Nominal value	\bar{A}_i	10^7	10^5
COV	0.05	0.05	--
Variation range	--	--	15%

The mean values of the member sections $\bar{A}_i (i = 1, 2, \dots, 10)$ are taken as design variables, with lower bounds $\underline{d}_i = 0.1$ and initial values $d_i^{(0)} = 40.0 (i = 1, 2, \dots, 10)$. The target reliability index is set as $\beta_m = 3.0$.

The obtained optimal design by the proposed method based on the mixed model is listed in the second column of Table 5.3. Therein, a reliability index $\beta_m = 2.996$ is achieved. The iteration history plotted in Fig.5.6 shows a steady decrease of the objective function as well as a stable convergence during the optimization process.

For comparison purpose, the deterministic optimization based on nominal values, the reliability-based optimization in the probabilistic framework (Conventional RBDO) and the worst-case scenario approach using pure non-probabilistic description were also run. The

well-known PMA approach is employed for solving the conventional RBDO problem, where all the uncertainties are assumed to have a Gaussian normal distribution with the Coefficient of Variation being 0.05 and the probabilistic reliability is required to be 3.0. In the worst-case scenario approach, all the uncertain parameters are described by interval variables. Therein, the variation ranges of A_i ($i=1,2,\dots,10$) and E about their nominal values are assumed to be 15%, i.e. three times that of the corresponding Coefficient of Variation.

Table 5.3 Optimal solutions using different approaches

Member number	Optimal cross-sectional area \bar{A}_i			
	Proposed method using mixed model	Deterministic optimization	Conventional RBDO	Worst-case scenario approach
1	42.91	31.37	39.23	49.83
2	0.10	0.10	0.10	0.10
3	29.32	21.48	26.81	34.16
4	21.01	15.46	19.23	24.57
5	0.10	0.10	0.10	0.10
6	0.10	0.10	0.10	0.10
7	3.38	2.83	3.21	4.19
8	30.81	22.56	28.18	35.81
9	29.94	21.86	27.36	34.75
10	0.10	0.10	0.10	0.10
Total weight	6638.0	4880.4	6076.9	7729.8
β_m	2.996	<0	1.502	5.332

The optimal solutions using the above three methods are also listed in Table 5.3. For these optimal designs, the corresponding reliability indices evaluated under the mixed model parameters are given in the last row of the table. The deterministic optimization presents a design with the least structural weight, though the reliability requirement is not accounted for. The conventional RBDO solution has a reliability index of $\beta_m = 1.502$ and therefore also violates the reliability constraint. The design obtained by the worst-case scenario approach

demands for the most volume of material. With a corresponding reliability index $\beta_m = 5.332$, it turns out to be an over-conservative design. It is also noted that there are considerable differences between the optimal solutions by RBDO and by the worst-case scenario approach. This implies that it may be dangerous to treat probabilistic uncertainties with non-probabilistic models, and vice versa. The importance of the proposed method based on the mixed model is thus highlighted.

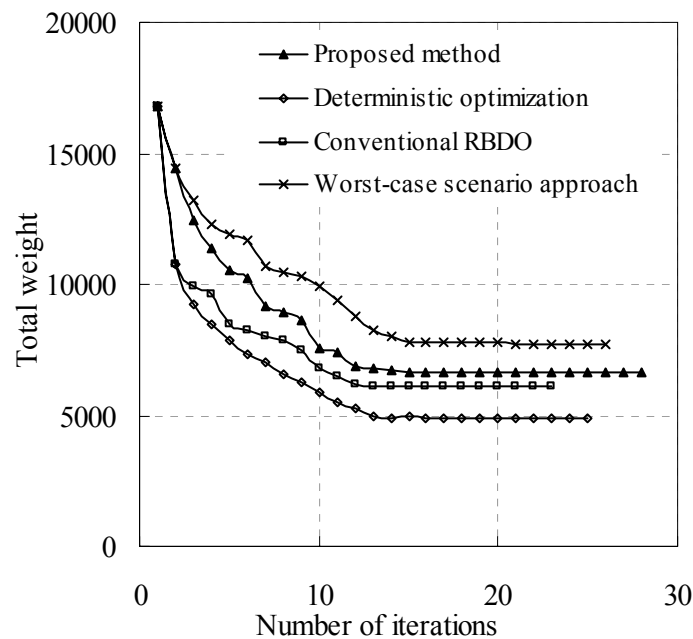


Fig. 5.6 Iteration histories of the optimization

5.3 OPTIMIZATION OF THE BONDED COMPOSITE BEAM

In this section, we considered the reliability-based design optimization of a simply supported bonded steel and concrete composite beam. The span of the beam is $L = 3486\text{mm}$ and a concentrated load F is applied to the mid-span of the beam. The optimization parameter model is shown in Fig.5.7. The material properties for the composite beam are similar to the beam P1 in Chapter 2 (given in Table 2.3).

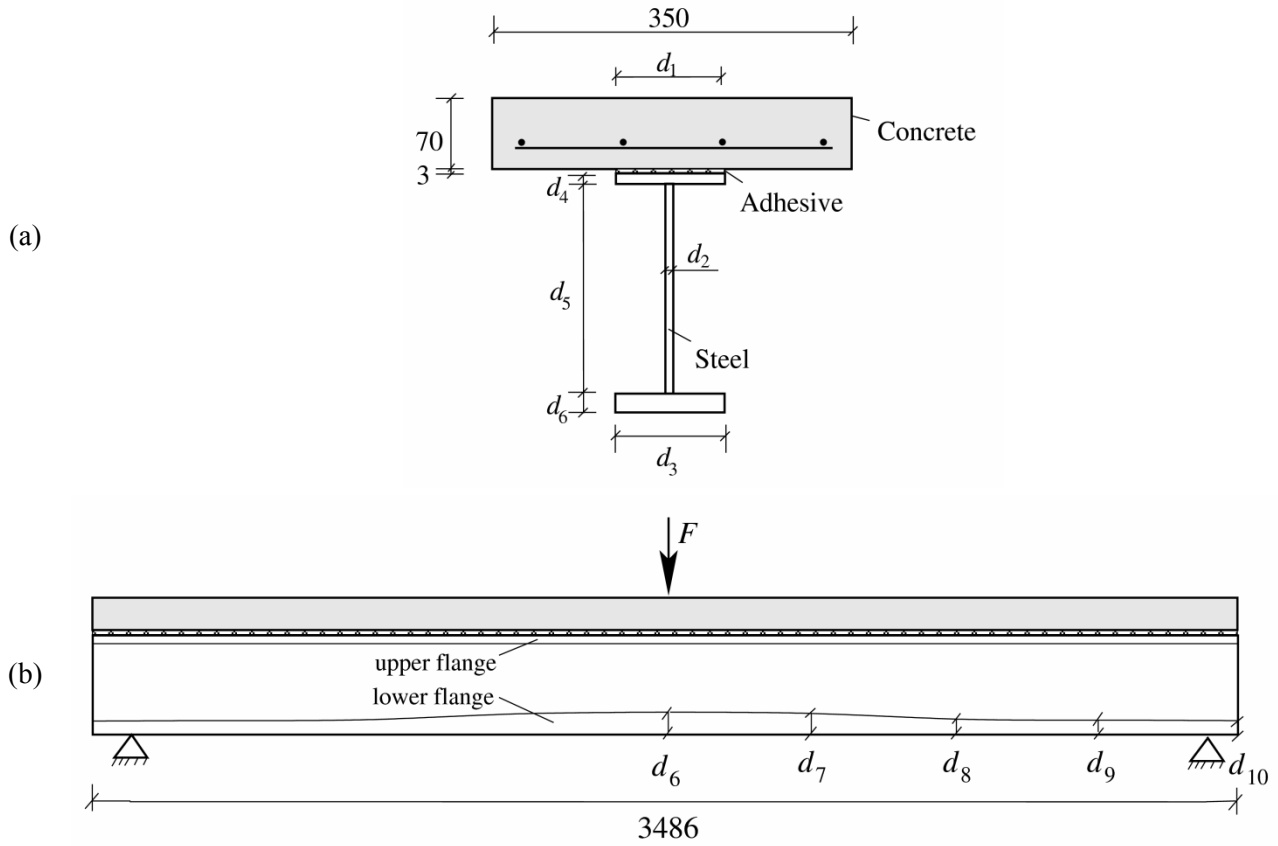


Fig. 5.7 Optimization parameter model of the bonded composite beam
(a) Middle cross-section; (b) Overall view (Unit: mm)

Table 5.4 Uncertainty properties for the bonded composite beam

Uncertainty	Young's modulus and yield stress of steel (E_s, f_s)	Young's modulus and ultimate stress of adhesive (E_a, f_a)	Young's modulus and compressive strength of concrete (E_c, f_c)	External load (F)
Distribution	Normal distribution	Normal distribution	Uncertain-but-bounded	Uncertain-but-bounded
Nominal value	(205GPa, 470MPa)	(12.3GPa, 19.5MPa)	(36.6GPa, 68MPa)	(200kN)
Probability model (COV)	0.08	0.08	--	--
Convex model	--	--	$\begin{bmatrix} \delta_{E_c} & \delta_{f_c} \end{bmatrix} \begin{bmatrix} 1 & 0 \\ 0 & 1 \end{bmatrix} \begin{bmatrix} \delta_{E_c} \\ \delta_{f_c} \end{bmatrix} \leq 0.1^2$	[180kN, 220kN]

The Young's modulus, the permissible stress and the applied load are considered as uncertain variables. This aggregately resulted in four probabilistic variables, including the Young's modulus and the permissible stresses of adhesive and steel girder. However, the Young's modulus and the permissible stress of concrete are assumed to be two non-probabilistic uncertain variables and bounded by an ellipsoid model. In addition, the load magnitude F is also a non-probabilistic uncertain variable and bounded by an interval. The uncertainty properties are given in Table 5.4.

5.3.1 Optimization modeling

(1) Design variables

The parameters shown in Fig.5.7 are taken as 10 design variables

$$\mathbf{d} = \{d_1 \ d_2 \ d_3 \ d_4 \ d_5 \ d_6 \ d_7 \ d_8 \ d_9 \ d_{10}\}^T \quad (5.26)$$

The lower bounds \mathbf{d}_{\min} , the upper bounds \mathbf{d}_{\max} and the initial values \mathbf{d}_0 of design variables are listed as follows.

$$\begin{aligned} \mathbf{d}_{\min} &= \{50 \quad 4.1 \quad 50 \quad 5.7 \quad 100 \quad 5.7 \quad 5.7 \quad 5.7 \quad 5.7 \quad 5.7\}^T \\ \mathbf{d}_{\max} &= \{200 \quad 12 \quad 200 \quad 16 \quad 500 \quad 16 \quad 16 \quad 16 \quad 16 \quad 16\}^T \\ \mathbf{d}_0 &= \{110 \quad 5.9 \quad 110 \quad 9.2 \quad 201.6 \quad 9.2 \quad 9.2 \quad 9.2 \quad 9.2 \quad 9.2\}^T \end{aligned} \quad (5.27)$$

where the unit is mm.

(2) Objective function

The design objective is to minimize the total structural price with satisfying the performance constraints. Herein, we only considered the price of steel girder which is controlled by the design variables. The objective function $C(\mathbf{d})$ is defined as

$$\begin{aligned} C(\mathbf{d}) &= P_s \cdot V_s \\ &= P_s \cdot L \cdot [d_1 d_4 + d_2 (d_5 + d_6) + (d_3 - d_2)(d_6 + d_7 + d_8 + d_9 + d_{10})/5] \end{aligned} \quad (5.28)$$

where P_s is the unit price of steel, V_s is the total volume of steel. In this paper, for simplification purpose, we set $P_s \cdot L = 1/\text{mm}^2$ and thus $C(\mathbf{d})$ is non-dimensional.

(3) *Constraint condition*

The considered constraints include displacement constraint, stress constraints, local stability constraints and geometrically constraints.

① Displacement constraint:

$U_{\text{mid}} \leq 12\text{mm}$, where U_{mid} is the vertical deformation of the mid-span.

② Stress constraints:

$\sigma_{s,\text{max}} \leq \bar{f}_s$, where $\sigma_{s,\text{max}}$ is the maximum normal stress of steel girder, \bar{f}_s is the design value of flexural strength of steel;

$\tau_{s,\text{max}} \leq \bar{f}_{s,v}$, where $\tau_{s,\text{max}}$ is the maximum shear stress of steel girder, $\bar{f}_{s,v}$ is the design value of shear strength of steel;

$\sigma_{c,\text{max}} \leq \bar{f}_c$, where $\sigma_{c,\text{max}}$ is the maximum compressive stress of concrete slab, \bar{f}_c is the design value of compressive strength of concrete;

$\sigma_{t,\text{max}} \leq \bar{f}_t$, where $\sigma_{t,\text{max}}$ is the maximum tensile stress in 3/4 height of concrete slab, \bar{f}_t is the limit value of concrete tensile strength. This constraint is applied for controlling the range of cracks in concrete slab.

③ Local stability constraints:

$\xi_{uf} = \frac{d_1 - d_2}{2d_4} \leq 15 \sqrt{\frac{235}{f_s^c}}$, in which ξ_{uf} is the width-thickness ratio of upper flange of the steel girder;

$\xi_{lf} = \frac{d_3 - d_2}{2d_6} \leq 15 \sqrt{\frac{235}{f_s^c}}$, in which ξ_{lf} is the width-thickness ratio of lower flange of the steel girder;

$\xi_w = \frac{d_5}{2d_2} \leq 80 \sqrt{\frac{235}{f_s^c}}$, in which ξ_w is the width-thickness ratio of web of the steel girder.

where f_s^c is the nominal value of the steel yield strength and the unit is MPa.

④ Geometry constraints:

$$\frac{h_{\text{beam}}}{L} \leq \frac{1}{15};$$

$$h_{\text{beam}} \leq 1.5(d_4 + d_5 + d_6).$$

where h_{beam} is the total height of the composite beam, namely $h_{\text{beam}} = 73 + d_4 + d_5 + d_6$.

(4) Reliability-based optimization mathematic model

Based on the nonlinear finite element model proposed in Chapter 2, the reliability-based optimization under mixed uncertain variables was carried out. The design objective is to minimize the total price of steel. The target reliability indices of displacement and stress constraints is required to be $\underline{\beta}_m = 3.0$. The reliability-based optimization problem is expressed as

$$\begin{aligned}
 & \min_{\mathbf{d}} \quad C(\mathbf{d}) \\
 & \text{s.t.} \quad \beta_m [g_1 = 12 - U_{\text{mid}} \geq 0] \geq \underline{\beta}_m, \\
 & \quad \beta_m [g_2 = \bar{f}_s - \sigma_{s,\text{max}} \geq 0] \geq \underline{\beta}_m, \\
 & \quad \beta_m [g_3 = \bar{f}_{s,v} - \tau_{s,\text{max}} \geq 0] \geq \underline{\beta}_m, \\
 & \quad \beta_m [g_4 = \bar{f}_c - \sigma_{c,\text{max}} \geq 0] \geq \underline{\beta}_m, \\
 & \quad \beta_m [g_5 = \bar{f}_t - \sigma_{t,\text{max}} \geq 0] \geq \underline{\beta}_m, \\
 & \quad \frac{d_1 - d_2}{2d_4} \leq 15\sqrt{235/f_s^c}, \\
 & \quad \frac{d_3 - d_2}{2d_6} \leq 15\sqrt{235/f_s^c}, \\
 & \quad \frac{d_5}{2d_2} \leq 80\sqrt{235/f_s^c}, \\
 & \quad h_{\text{beam}} \leq L/15, \\
 & \quad h_{\text{beam}} \leq 1.5(d_4 + d_5 + d_6), \\
 & \quad \mathbf{d}_{\min} \leq \mathbf{d} \leq \mathbf{d}_{\max}
 \end{aligned} \tag{5.29}$$

It should be noted that, for simplicity of expression, the uncertain variables and design variables enter the reliability index constraints in the optimization problem (5.29) as intrinsic variables rather than explicit ones.

5.3.2 Solutions and comparisons

The iteration history of the structural design problem plotted in Fig.5.8 show a steady convergence process in the structural design optimization problem. The achieved optimal solutions are summarized in Table 5.5. For comparison purpose, the deterministic optimization results are also presented, which are obtained using nominal values of the uncertain variables. As can be seen from the table, remarkable economic benefit is gained from the optimization approaches. The optimal solution obtained by the reliability-based optimization uses more material or price, which leads to more reliable design than the deterministic one. When the uncertainties are considered, the initial design and the deterministic optimal design result in a severe violation of the reliability constraints. In the final reliability-based design obtained by the present optimization method, the reliability requirements of the performance constraints are all met.

Table 5.5 Optimal solutions for the bonded composite beam

Design variables (mm)	Initial design	Optimal solutions	
		Deterministic optimization	Reliability-based optimization using mixed model
d_1	110	89.06	107.12
d_2	5.9	4.10	4.18
d_3	110	94.82	117.47
d_4	9.2	6.97	5.7
d_5	201.6	221.08	223.47
d_6	9.2	12.14	16.00
d_7	9.2	12.33	16.00
d_8	9.2	8.60	13.07
d_9	9.2	5.70	5.70
d_{10}	9.2	5.70	7.00
Objective function	3467	2384	2919
Reliability index β_m (for constraint $U_{mid} \leq 12\text{mm}$)	-7.73	-4.14	2.98

A comparison of the shapes of the initial design, the deterministic optimization design and the reliability-based optimization design is presented in Fig.5.10 and Fig.5.11. Based on the three different designs, nonlinear finite element analyses are carried out using the nominal values of uncertain inputs. The load versus mid-span deflection curves of the three designs are compared in Fig.5.9. The ultimate loads are 271.2kN for the deterministic optimization design and 340.3kN for the reliability-based optimization design. It showed a better mechanical performance of optimization designs, especially the reliability-based optimization design, than the initial design (in which the ultimate load is 230.5 kN). Therefore, from comparisons, it can be concluded that it is meaningful to accounting for the uncertainties in the optimization design of the bonded composite beam by a reliability-based approach.

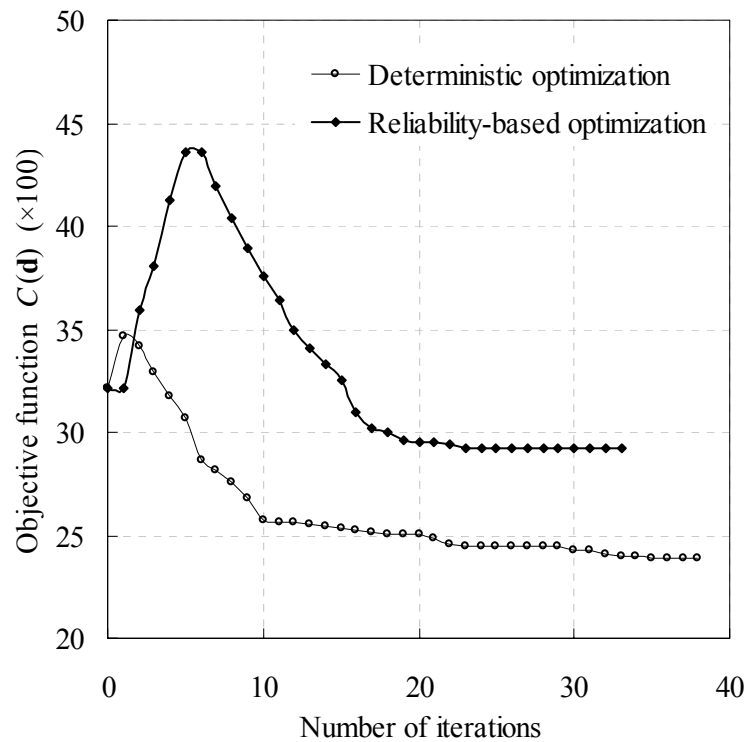


Fig. 5.8 Iteration histories of the optimization

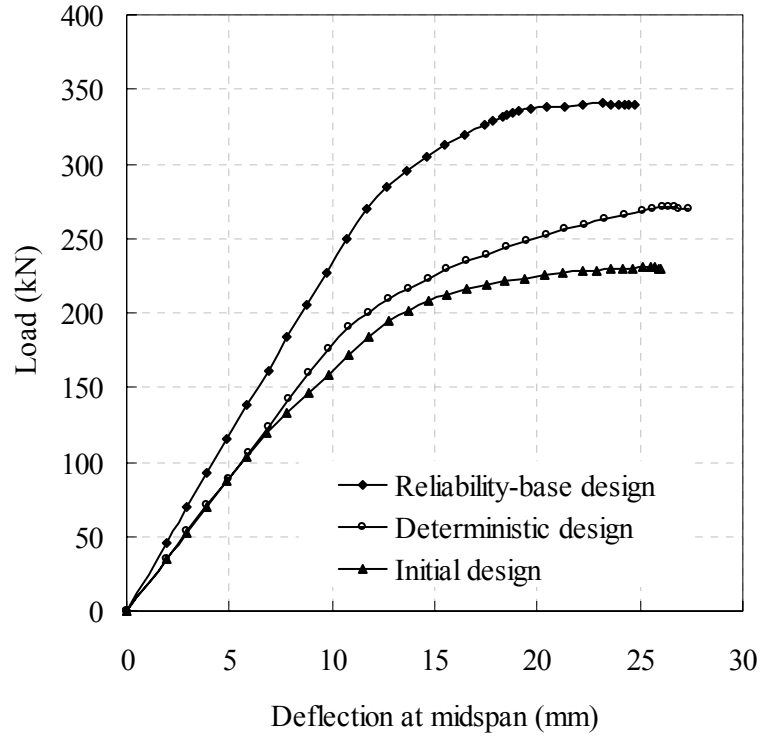


Fig. 5.9 Load-deflection curves at nominal values of uncertain inputs for three different designs

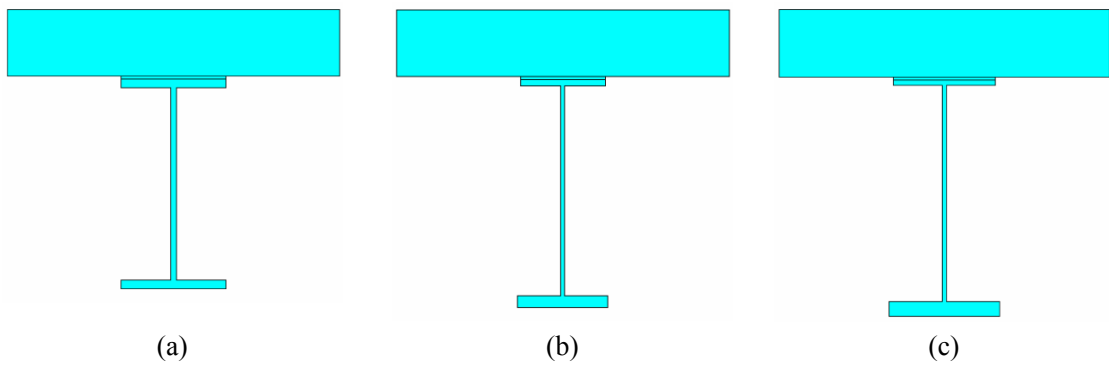


Fig. 5.10 A comparison of the middle cross-section

(a) Initial design; (b) Deterministic optimization design; (c) Reliability-based optimization design

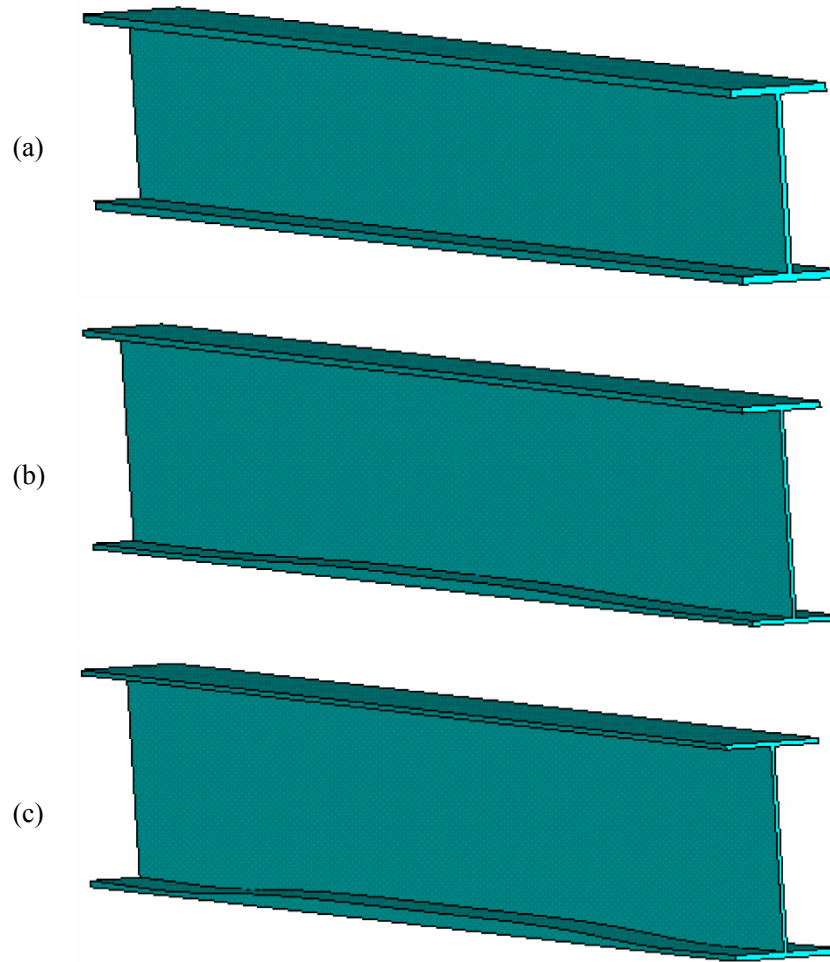


Fig. 5.11 A comparison of the steel girder

(a) Initial design; (b) Deterministic optimization design; (c) Reliability-based optimization design

5.4 SUMMARY

While the probabilistic randomness is a natural model for the stochastic parameter scatters exhibited by a structure, the multi-ellipsoid convex model provides an appealing non-probabilistic description method for the uncertain-but-bounded system variations. This chapter explores the reliability-based optimization design of non-deterministic structures with randomness and uncertain-but-bounded uncertainties. Based on the defined reliability index

under probability and convex set mixed model, the reliability-based optimization with constraints on such mixed reliability indices is formulated as a nested optimization problem. By employing the performance measure approach, the original optimization problem is reformulated into an inherently robust and superior one, in which the outer-loop aims to minimize the cost function while the inner-loop evaluates the target performance value. Two approaches, namely the nested double-loop approach and the linearization-based approach, are employed to solve the optimization problem. Two numerical examples confirm that both approaches are applicable but the linearization-based approach is more efficient since it avoids expensive iterations for inner-loop solution. The proposed optimization method is proven to be effective in ensuring the structural reliability requirements in presence of probabilistic and bounded uncertainties. In addition, the comparison of numerical examples also reveals that it may be dangerous to treat the inherently probabilistic variations with non-probabilistic models, and vice versa. This again implies the importance of the present study.

The proposed reliability-based optimization approach is then applied for the design of the bonded steel and concrete composite beam. Based on the optimal topology layout in Chapter 3, a sizing optimization model of the bonded composite beam with reliability constraints is presented. The comparisons of results revealed it is meaningful to accounting for the uncertainties in the optimization design of the bonded composite beam by a reliability-based approach.

CHAPTER 6: CONCLUSIONS

6.1 SUMMARY

The steel and concrete composite beam was widely used in practical engineering. However, the traditional mechanical fasten method has its weaknesses which may substantially reduce the durability of the composite beam. In particular, the steel and concrete composite beam bonded by adhesive has its particular advantages over the traditional composite beam. Therefore, adhesive bonding method has been developed as an alternative technique and the bonded steel and concrete composite beam is attracting increasing attentions recently.

In this dissertation, the previous work on the steel and concrete composite beams is first reviewed. The steel and concrete composite beam using the adhesive bonding technique makes it possible to decrease the appearance of stress concentration, to obtain a continuous transfer of the force and to use a prefabricated concrete slab. Experimental studies have testified the efficiency of the bonded composite beam. Then, the current state of research on structural optimization, structural topology optimization and structural optimization considering uncertainty is revealed.

In the second part of the dissertation, as a prerequisite, an experimental push-out test is carried out to study the debonding failure mode and determine the bonding strength. The debonding failure takes place within the first 2-5 mm of the concrete from the adhesive/concrete interface and the epoxy adhesive bonding connection can provide a bonding strength of 6.36MPa. Then, a validated three-dimensional nonlinear finite element model was proposed to predict the parametric effects of bonded steel and concrete composite beams. From the simulating results, it is shown that the response of the bonded composites is influenced significantly by elastic modulus of adhesive, the bonding strength and the bonding area, rather than the adhesive layer thickness.

For determining a more reasonable initial topology configuration, a three-dimensional topology optimization methodology of the bonded composite beam is presented. Following the SIMP approach, an artificial material model with penalization for elastic constants is assumed and elemental density variables are used for describing the structural layout. The

considered problem is thus formulated as to find the optimal structural topology that minimizes the structural cost (material volume) under specified displacement constraints. By using the adjoint variable method for the sensitivity analysis, the optimization problem is efficiently solved by the gradient-based optimization algorithm (MMA). The proposed topology approach presented a new structural topology of bonded steel and concrete composite beam.

In a practical bonded composite beam, the structural performance may exhibit some degree of degradation due to inherent uncertainties in material properties, geometrical dimensions and loading conditions. As the fourth part of the dissertation, we proposed a reliability assessment strategy of structures exhibiting both stochastic and bounded uncertainties by using a probability and convex set mixed model. The safety measure of a structure is quantified by a reliability index defined by a nested minimization problem. An iterative procedure is developed for seeking the worst-case point and the most probable failure point in the standard uncertainty space. Numerical examples demonstrated the validity and effectiveness of the proposed method. The proposed mixed model is then employed to assess the reliability of a bonded steel and concrete composite beam.

In the last part of the dissertation, the method for the reliability-based optimization design of the bonded composite beam is developed. The optimization problem incorporating constraints of mixed reliability indices is mathematically formulated. By using the performance measure approach, the optimization problem is converted into more tractable one. Moreover, the double-loop optimization problem is transformed into an approximate single-loop minimization problem using the linearization technique, which further facilitates efficient solution of the design problem. Two examples regarding design optimization of a mathematical function and a truss structure demonstrated the validity of the proposed formulation as well as the efficiency of the presented numerical techniques. Finally, the comparisons of optimization results for the bonded composite beam showed the significant meaning of accounting for the uncertainties in the composite beam optimization design by a reliability-based approach.

Though the reliability-based optimization design is meaningful in the design of bonded

steel and concrete composite beams, it is worth noting that the importance of the conventional deterministic design optimization should not be underestimated. The deterministic design of the bonded composite beam is also more economical and better in the mechanical performance than the initial design. In fact, the reliability-based optimization was developed to extend the applicability of the techniques used in conventional deterministic optimization by incorporating uncertainties.

6.2 OUTLOOK

In the present stage of this work, we have studied the numerical simulation and the reliability-based optimization design of the bonded steel and concrete composite beam. To better understand and validate the optimization design, the following remarks are considered for the continuation of our work.

- The present reliability-based optimization design cannot guarantee solving the target performance problem to global optimum if the limit-state function is non-convex. Difficulties also arise when the limit-state function is not smooth. Nevertheless, it can be expected that the convergence behaviour and the chance of finding the global optimum could be greatly improved by enhancing the standard mathematical programming algorithms with techniques such as multiple initial guesses and sequential linearization or other convex approximations of the limit-state function.
- In order to effectively validate the optimization results, it is necessary to carry out further experimental tests on a bonded composite beam with the optimal design dimensions. A comparison of the mechanical behaviour by experimental results may be particularly important and convictive.
- It may be very useful to analyze and design the bonded composite beams under other loading types and constraint conditions.
- For applying the bonded composite beams in the practical engineering, it is necessary to test and simulate the durability and the fatigue life of this type of structures.

BIBLIOGRAPHY

- [1] Brozzetti J. Design development of steel-concrete composite bridges in France. *Journal of Constructional Steel Research*, 2000, 55(1-3): 229-243.
- [2] Viest I M, Colaco J P, Furlong R W et al. *Composite construction design for buildings*. New York: ASCE McGraw-Hill, 1997, 460 pp.
- [3] Newmark N M, Siess C P, Viest I M. Tests and analysis of composite beams with incomplete interaction. *Proceeding of Society for Experimental Stress Analysis*, 1951, 9(1): 75-92.
- [4] Trouillet P. Comportement local de connecteurs acier/béton sollicités au cisaillement étude bibliographique. *Rapport des Laboratoires des Ponts et Chaussées, série Ouvrages d'art OA-3*. 1987.
- [5] Eurocode 4. *Design of composite steel and concrete structures*: European Committee for Standardisation, 1994.
- [6] Rabih M. *Comportement et modélisation de connecteurs de types cornière et goujon utilisés en construction mixte acier-béton*. Vandoeuvre-lès-Nancy, France: Institut National Polytechnique de Lorraine, 1994.
- [7] Jones H, Boxler A. Test on a simplified shear connector for steel-concrete composite construction commentary on experimental investigations. *Australian Welding Research Awra report*, 1979: 63-78.
- [8] Clarke J L. *The fatigue behaviour of stud shear connectors under rotating shear*. Cambridge: Cambridge University Engineering Department. 1972.
- [9] Davies C. Small-scale push-out tests on welded stud shear connectors. *Journal Concrete*, 1967, Sept: 311-316.
- [10] Chapman J C, Balakrishnan S. Experiments on composite beams. *The Structural Engineer*, 1964, 42(11): 369-383.
- [11] Slutter R G, Driscoll G C. Flexural strength of steel-concrete composite beams. *Journal of the Structural Division, ASCE*, 1965, 91(2): 71-99.
- [12] Reddy V M, Hendry A W. An experimental study of the ultimate load behaviour of composite steel-concrete bridge deck structures. *Building Science*, 1969, 4(3): 119-132.
- [13] Johnson R P, Willmington R T. Vertical shear in continuous composite beams. *ICE Proceedings*, 1972, 53(2): 189-205.
- [14] Roberts T M, Al-Amery R I M. Shear strength of composite plate girders with web cutouts. *Journal of Structural Engineering*, 1991, 117(7): 1897-1910.
- [15] Nie J, Xiao Y, Chen L. Experimental studies on shear strength of steel-concrete composite beams. *Journal of Structural Engineering*, 2004, 130(8): 1206-1213.
- [16] Allison R W, Johnson R P, May I M. Tension-field action in composite plate girders. *Proceeding of ICE*, 1982, 73(2): 255-276.

- [17] Clawson W C, Darwin D. Tests of composite beams with web openings. *Journal of the Structural Division*, 1982, 108(1): 145-162.
- [18] Lebet J P, Ducret J M. Experimental and theoretical study of the behaviour of composite bridges during construction. *Journal of Constructional Steel Research*, 1998, 46(1): 69-70.
- [19] Jurkiewicz B, Braymand S. Experimental study of a pre-cracked steel-concrete composite beam. *Journal of Constructional Steel Research*, 2007, 63(1): 135-144.
- [20] Chen S. Experimental study of prestressed steel-concrete composite beams with external tendons for negative moments. *Journal of Constructional Steel Research*, 2005, 61(12): 1613-1630.
- [21] Jurkiewicz B, Hottier J M. Static behaviour of a steel-concrete composite beam with an innovative horizontal connection. *Journal of Constructional Steel Research*, 2005, 61(9): 1286-1300.
- [22] Al-Saidy A H, Klaiber F W, Wipf T J. Strengthening of steel-concrete composite girders using carbon fiber reinforced polymer plates. *Construction and Building Materials*, 2007, 21(2): 295-302.
- [23] Batoz J L, Dhatt G. *Modélisation des structures par éléments finis*. Québec: Les Presses de l'Université Laval, 1992.
- [24] Wang C Q, Zheng C L. Semi-analytical finite element method for fictitious crack model in fracture mechanics of concrete. *Applied Mathematics and Mechanics*, 2004, 25(11): 1265-1270.
- [25] Zienkiewicz O C, Taylor R L. *The finite element method*, 4/E Vol II: Solid and fluid mechanics dynamics and non-linearity: McGraw-Hill International Editions, 1991.
- [26] Wegmuller A W, Amer H N. Nonlinear response of composite steel-concrete bridges. *Computers and Structures*, 1977, 7(2): 161-169.
- [27] Razaqpur A G, Nofal M. A finite element for modelling the nonlinear behavior of shear connectors in composite structures. *Computers and Structures*, 1989, 32(1): 169-174.
- [28] Salari M R, Spacone E, Shing P B et al. Nonlinear analysis of composite beams with deformable shear connectors. *Journal of Structural Engineering*, 1998, 124(10): 1148-1158.
- [29] Fabbrocino G, Manfredi G, Cosenza E. Non-linear analysis of composite beams under positive bending. *Computers and Structures*, 1999, 70(1): 77-89.
- [30] Faella C, Martinelli E, Nigro E. Steel and concrete composite beams with flexible shear connection: "exact" analytical expression of the stiffness matrix and applications. *Computers and Structures*, 2002, 80(11): 1001-1009.
- [31] Sebastian W M, McConnel R E. Nonlinear FE analysis of steel-concrete composite structures. *Journal of Structural Engineering*, 2000, 126(6): 662-674.
- [32] Sapountzakis E J, Katsikadelis J T. A new model for the analysis of composite steel-concrete slab and beam structures with deformable connection. *Computational Mechanics*, 2003, 31(3): 340-349.
- [33] Sapountzakis E J. Dynamic analysis of composite steel-concrete structures with deformable connection. *Computers and Structures*, 2004, 82(9-10): 717-729.

- [34] Dall'Asta A, Zona A. Comparison and validation of displacement and mixed elements for the non-linear analysis of continuous composite beams. *Computers and Structures*, 2004, 82(23-26): 2117-2130.
- [35] Hirst M J S, Yeo M F. The analysis of composite beams using standard finite element programs. *Computers and Structures*, 1980, 11: 233-237.
- [36] Thevendran V, Chen S, Shanmugam N E et al. Nonlinear analysis of steel-concrete composite beams curved in plan. *Finite Elements in Analysis and Design*, 1999, 32(3): 125-139.
- [37] Baskar K, Shanmugam N E, Thevendran V. Finite-element analysis of steel-concrete composite plate girder. *Journal of Structural Engineering*, 2002, 128(9): 1158-1168.
- [38] Liang Q Q, Uy B, Bradford M A et al. Ultimate strength of continuous composite beams in combined bending and shear. *Journal of Constructional Steel Research*, 2004, 60(8): 1109-1128.
- [39] Queiroz F D, Vellasco P C G S, Nethercot D A. Finite element modelling of composite beams with full and partial shear connection. *Journal of Constructional Steel Research*, 2007, 63(4): 505-521.
- [40] Sedlacek G, Bild S. A simplified method for the determination of the effective width due to shear lag effects. *Journal of Constructional Steel Research*, 1993, 24: 155-182.
- [41] BS5400: Part 5. Design of composite bridges. London: British Standards Institution, 1979.
- [42] LRFD. Bridge design specifications. Washington, DC: American Association of State Highway and Transportation Officials, 1998.
- [43] GB50017-2003. Code for design of steel structures. Beijing: China Planning Press, 2003.
- [44] Ahn I-S, Chiewanichakorn M, Chen S S et al. Effective flange width provisions for composite steel bridges. *Engineering Structures*, 2004, 26(12): 1843-1851.
- [45] Amadio C, Fragiaco M. Effective width evaluation for steel-concrete composite beams. *Journal of Constructional Steel Research*, 2002, 58(3): 373-388.
- [46] Amadio C, Fedrigo C, Fragiaco M et al. Experimental evaluation of effective width in steel-concrete composite beams. *Journal of Constructional Steel Research*, 2004, 60(2): 199-220.
- [47] Chen S, Zhang Z. Effective width of a concrete slab in steel-concrete composite beams prestressed with external tendons. *Journal of Constructional Steel Research*, 2006, 62(5): 493-500.
- [48] Raithby K D. External strengthening of concrete bridges with bonded steel plates, Rep. No. 612. Crowthorne, Berkshire: Transport and Road Research Laboratory. 1980.
- [49] Adhikary B B, Mutsuyoshi H. Numerical simulation of steel-plate strengthened concrete beam by a non-linear finite element method model. *Construction and Building Materials*, 2002, 16(5): 291-301.
- [50] Barnes R A, Mays G C. The transfer of stress through a steel to concrete adhesive bond. *International Journal of Adhesion and Adhesives*, 2001, 21(6): 495-502.
- [51] Swamy R N, Jones R, Bloxham J W. Structural behaviour of reinforced concrete beams strengthened by epoxy-bonded steel plates. *Structural Engineer, Part A*, 1987, 65(2): 59-68.

- [52] Casas J R, Pascual J. Debonding of FRP in bending: Simplified model and experimental validation. *Construction and Building Materials*, 2007, 21(10): 1940-1949.
- [53] Chen J F, Pan W K. Three dimensional stress distribution in FRP-to-concrete bond test specimens. *Construction and Building Materials*, 2006, 20(1-2): 46-58.
- [54] Lau K T, Dutta P K, Zhou L M et al. Mechanics of bonds in an FRP bonded concrete beam. *Composites Part B: Engineering*, 2001, 32(6): 491-502.
- [55] Li A, Assih J, Delmas Y. Shear strengthening of RC beams with externally bonded CFRP Sheets. *Journal of Structural Engineering*, 2001, 127(4): 374-380.
- [56] Lu X Z, Teng J G, Ye L P et al. Bond-slip models for FRP sheets/plates bonded to concrete. *Engineering Structures*, 2005, 27(6): 920-937.
- [57] Wang J. Debonding of FRP-plated reinforced concrete beam, a bond-slip analysis. I: Theoretical formulation. *International Journal of Solids and Structures*, 2006, 43(21): 6649-6664.
- [58] Miklofsky H A, Brpown M R, Gonsior M J. Epoxy bonding compounds as shear connectors in composite beams. *Engineering Research Series*, RR.62-2. New York: Department of Public Works. 1962.
- [59] Kriegh J D, Endebrock E G. The use of epoxy resins in reinforced concrete: Static load tests, Part II: *Engineering Research Laboratories*, the University of Arizona, 1963.
- [60] Burkhardt P, Hertig P, Aeschlimann H U. Expériences sur les poutres mixtes en acier-béton liées à l'aide d'adhésifs époxydes. *Materials and Structures*, 1975, 8(4): 261-277.
- [61] Carputi U, Noto A, Ermolli E R. Assemblages collés dans les structures composites acier-béton. *Materials and Structures*, 1981, 14(1): 3-11.
- [62] Hick F, Baar S. Structures métalliques collées. *Station d'Essais et de Recherches de la Construction Métallique*, SERCOM. Liège, Belgique. 1972.
- [63] Nordin H, Täljsten B. Testing of hybrid FRP composite beams in bending. *Composites Part B: Engineering*, 2004, 35(1): 27-33.
- [64] Si Larbi A, Ferrier E, Jurkiewicz B et al. Static behaviour of steel concrete beam connected by bonding. *Engineering Structures*, 2007, 29(6): 1034-1042.
- [65] Bouazaoui L, Perrenot G, Delmas Y et al. Experimental study of bonded steel concrete composite structures. *Journal of Constructional Steel Research*, 2007, 63: 1268-1278.
- [66] Zhao G, Li A. Numerical study of a bonded steel and concrete composite beam. *Computers and Structures*, 2008, 86: 1830-1838.
- [67] Kirsch U. Optimum structural design: Concepts, methods, and applications. New York: McGraw-Hill, 1981.
- [68] Naceur H, Guo Y Q, Batoz J L. Blank optimization in sheet metal forming using an evolutionary algorithm. *Journal of Materials Processing Technology*, 2004, 151(1-3): 183-191.

- [69] Sui Y, Du J, Guo Y Q. A method based on dual-quadratic programming for frame structural optimization with large scale. *Applied Mathematics and Mechanics*, 2006, 27(3): 383-391.
- [70] Olhoff N, Bendsøe M P, Rasmussen J. On CAD-integrated structural topology and design optimization. *Computer Methods in Applied Mechanics and Engineering*, 1991, 89: 259-279.
- [71] Michell A G M. The limits of economy of material in frame structure. *Philosophical Magazine*, 1904, 8(6): 589-597.
- [72] Ringertz U T. On topology optimization of trusses. *Engineering Optimization*, 1985, 9(3): 209-217.
- [73] Kirsch U. Optimal topologies of truss structures. *Computer Methods in Applied Mechanics and Engineering*, 1989, 72(1): 15-28.
- [74] Rozvany G I N, Bendsøe M P, Kirsch U. Layout optimization of structures. *Applied Mechanics Reviews*, 1995, 48: 41-119.
- [75] Bendsøe M P, Kikuchi N. Generating optimal topologies in structural design using a homogenization method. *Computer Methods in Applied Mechanics and Engineering*, 1988, 71(2): 197-224.
- [76] Eschenauer H A, Olhoff N. Topology optimization of continuum structures: A review. *Applied Mechanics Reviews*, 2001, 54(4): 331-389.
- [77] Olhoff N. On optimum design of structures and materials. *Meccanica*, 1996, 31(2): 143-161.
- [78] Nishiwaki S, Frecker M I, Min S et al. Topology optimization of compliant mechanisms using the homogenization method. *International Journal for Numerical Methods in Engineering*, 1998, 42(3): 535-559.
- [79] Suzuki K, Kikuchi N. A homogenization method for shape and topology optimization. *Computer Methods in Applied Mechanics and Engineering*, 1991, 93(3): 291-318.
- [80] Mlejnek H P, Schirmacher R. An engineer's approach to optimal material distribution and shape finding. *Computer methods in applied mechanics and engineering*, 1993, 106(1-2): 1-26.
- [81] Yang R J, Chuang C H. Optimal topology design using linear programming. *Computers and Structures*, 1994, 52(2): 265-275.
- [82] Rozvany G I N, Zhou M, Birker T. Generalized shape optimization without homogenization. *Structural and Multidisciplinary Optimization*, 1992, 4(3): 250-252.
- [83] Bendsøe M P. Optimal shape design as a material distribution problem. *Structural and Multidisciplinary Optimization*, 1989, 1(4): 193-202.
- [84] Zhou M, Rozvany G I N. The COC algorithm. II: Topological, geometrical and generalized shape optimization. *Computer Methods in Applied Mechanics and Engineering*, 1991, 89(1-3): 309-336.
- [85] Stolpe M, Svanberg K. An alternative interpolation scheme for minimum compliance topology optimization. *Structural and Multidisciplinary Optimization*, 2001, 22(2): 116-124.

- [86] Xie Y M, Steven G P. A simple evolutionary procedure for structural optimization. *Computers and Structures*, 1993, 49(5): 885-896.
- [87] Querin O M, Steven G P, Xie Y M. Evolutionary structural optimization (ESO) using a bidirectional algorithm. *Engineering computations*, 1998, 15: 1031-1048.
- [88] Young V, Querin O M, Steven G P et al. 3D and multiple load case bi-directional evolutionary structural optimization (BESO). *Structural and Multidisciplinary Optimization*, 1999, 18(2): 183-192.
- [89] Mattheck C, Burkhardt S. A new method of structural shape optimization based on biological growth. *International Journal of Fatigue*, 1990, 12(3): 185-190.
- [90] Baumgartner A, Harzheim L, Mattheck C. SKO(soft kill option): the biological way to find an optimum structure topology. *International Journal of Fatigue*, 1992, 14(6): 387-393.
- [91] Osher S, Sethian J A. Fronts propagating with curvature-dependent speed - algorithms based on Hamilton-Jacobi formulations. *Journal of Computational Physics*, 1988, 79(1): 12-49.
- [92] Sethian J A, Wiegmann A. Structural boundary design via level set and immersed interface methods. *Journal of Computational Physics*, 2000, 163(2): 489-528.
- [93] Wang M Y, Wang X, Guo D. A level set method for structural topology optimization. *Computer Methods in Applied Mechanics and Engineering*, 2003, 192(1-2): 227-246.
- [94] Allaire G, Jouve F, Toader A M. Structural optimization using sensitivity analysis and a level-set method. *Journal of Computational Physics*, 2004, 194(1): 363-393.
- [95] Eschenauer H A, Kobelev V V, Schumacher A. Bubble method for topology and shape optimization of structures. *Structural and Multidisciplinary Optimization*, 1994, 8(1): 42-51.
- [96] Ohsaki M. Genetic algorithm for topology optimization of trusses. *Computers and Structures*, 1995, 57(2): 219-225.
- [97] Papadrakakis M, Lagaros N D, Tsompanakis Y. Structural optimization using evolution strategies and neural networks. *Computer Methods in Applied Mechanics and Engineering*, 1998, 156(1): 309-333.
- [98] Cai K, Chen B S, Zhang H W. Topology optimization of continuum structures based on a new bionics method. *International Journal for Computational Methods in Engineering Science and Mech*, 2007, 8(4): 233-242.
- [99] Sui Y, Du J, Guo Y Q. Independent continuous mapping for topological optimization of frame structures. *Acta Mechanica Sinica*, 2006, 22(6): 611-619.
- [100] Li G. Statistical properties of the maximum elastoplastic story drift of steel frames subjected to earthquake load. *Steel and Composite Structures*, 2003, 3(3): 185-198.
- [101] Li G, Chen G. The performance-based seismic design - Theory, method and application. Beijing: Science Press, 2004.

- [102] Ditlevsen O D, Madsen H O. Structural reliability method. New York: John Wiley & Sons, 1996.
- [103] Hasofer A M, Lind N C. Exact and invariant second-moment code format. Journal of the Engineering Mechanics Division, 1974, 100(1): 111-121.
- [104] Rackwitz R, Fiessler B. Structural reliability under combined random load sequences. Computers and Structures, 1978, 9(5): 489-494.
- [105] Der Kiureghian A, Lin H, Hwang S. Second-order reliability approximations. Journal of Engineering Mechanics, 1987, 113(8): 1208-1225.
- [106] Fiessler B, Rackwitz R, Neumann H. Quadratic limit states in structural reliability. Journal of the Engineering Mechanics Division, 1979, 105(4): 661-676.
- [107] Köylüoğlu H U, Nielsen S R K. New approximations for SORM integrals. Structural Safety, 1994, 13: 235-246.
- [108] Faravelli L. Response-surface approach for reliability analysis. Journal of Engineering Mechanics, 1989, 115(12): 2763-2781.
- [109] Wong F S. Slope reliability and response surface method. Journal of Geotechnical Engineering, 1985, 111(1): 32-53.
- [110] Bucher C G, Bourgund U. A fast and efficient response surface approach for structural reliability problems. Structural Safety, 1990, 7(1): 57-66.
- [111] Kaymaz I, McMahon C A. A response surface method based on weighted regression for structural reliability analysis. Probabilistic Engineering Mechanics, 2005, 20(1): 11-17.
- [112] Kim S H, Na S W. Response surface method using vector projected sampling points. Structural Safety, 1997, 19(1): 3-19.
- [113] Rajashekhar M R, Ellingwood B R. A new look at the response surface approach for reliability analysis. Structural Safety, 1993, 12(3): 205-220.
- [114] Frangopol D M, Corotis R B. Reliability-based structural system optimization: State-of-the-art versus state-of-the-practice. Proceeding of the 12th conference on analysis and computation, Chicago, Cheng FY (Ed.) Analysis and Computation, ASCE. New York. 1996.
- [115] Papadrakakis M, Lagaros N D. Reliability-based structural optimization using neural networks and Monte Carlo simulation. Computer Methods in Applied Mechanics and Engineering, 2002, 191(32): 3491-3507.
- [116] Doltsinis I, Kang Z. Robust design of structures using optimization methods. Computer Methods in Applied Mechanics and Engineering, 2004, 193(23-26): 2221-2237.
- [117] Park G J, Lee T H, Lee K H et al. Robust design: An overview. AIAA Journal, 2006, 44(1): 181-191.
- [118] Beyer H G, Sendhoff B. Robust optimization - A comprehensive survey. Computer Methods in Applied Mechanics and Engineering, 2007, 196(33-34): 3190-3218.

- [119] Chandu S V L, Grandhi R V. General purpose procedure for reliability based structural optimization under parametric uncertainties. *Advances in Engineering Software*, 1995, 23(1): 7-14.
- [120] Enevoldsen I, Sørensen J D. Reliability-based optimization in structural engineering. *Structural safety*, 1994, 15(3): 169-196.
- [121] Tu J, Choi K K, Park Y H. A new study on reliability-based design optimization. *Journal of Mechanical Design*, 1999, 121(4): 557-564.
- [122] Lee J O, Yang Y S, Ruy W S. A comparative study on reliability-index and target-performance-based probabilistic structural design optimization. *Computers and Structures*, 2002, 80(3): 257-269.
- [123] Du X, Chen W. Sequential optimization and reliability assessment method for efficient probabilistic design. *ASME, Journal of Mechanical Design*, 2004, 126(2): 225-233.
- [124] Youn B D, Choi K K, Du L. Enriched performance measure approach for reliability-based design optimization. *AIAA Journal*, 2005, 43(4): 874-884.
- [125] Kharmanda G, Olhoff N. Reliability-based topology optimization. *Structural and Multidisciplinary Optimization*, Report 110. Denmark: Institute of Mechanical Engineering, Aalborg University. December 2001.
- [126] Liszka T, Ostoja-Starzewski M. Effects of microscale material randomness on the attainment of optimal structural shapes. *Structural and Multidisciplinary Optimization*, 2004, 26: 67-76.
- [127] Jung H S, Cho S. Reliability-based topology optimization of geometrically nonlinear structures with loading and material uncertainties. *Finite Elements in Analysis and Design*, 2004, 41(3): 311-331.
- [128] Allen M, Raulli M, Maute K et al. Reliability-based analysis and design optimization of electrostatically actuated MEMS. *Computers and Structures*, 2004, 82(13-14): 1007-1020.
- [129] Kim C, Wang S, Hwang I et al. Application of reliability-based topology optimization for microelectromechanical systems. *AIAA Journal*, 2007, 45(12): 2926-2934.
- [130] Liu M, Maute K, Frangopol D M. Multi-objective design optimization of electrostatically actuated microbeam resonators with and without parameter uncertainty. *Reliability Engineering and System Safety*, 2007, 92(10): 1333-1343.
- [131] Maute K, Frangopol D M. Reliability-based design of MEMS mechanisms by topology optimization. *Computers and Structures*, 2003, 81(8-11): 813-824.
- [132] Moon H, Kim C, Wang S. Reliability-based topology optimization of thermal systems considering convection heat transfer. 10 th AIAA/ISSMO Multidisciplinary Analysis and Optimization Conference. Albany, New York. 2004.
- [133] Wang S, Moon H, Kim C et al. Reliability-based topology optimization (RBTO). IUTAM Symposium on Topological Design Optimization of Structures, Machines and Materials: Solid Mechanics and Its Applications: Springer. 2006.

- [134] Gzyl H. The method of maximum entropy. Series on Advances in Mathematics for Applied Sciences, Edited by Bellomo N, Brezzi F. Vol. 29. 1995.
- [135] Jaynes E T. Information theory and statistical mechanics. *Physical Review*, 1957, 106(4): 620-630.
- [136] Elishakoff I. Essay on uncertainties in elastic and viscoelastic structures: From AM Freudenthal's criticisms to modern convex modeling. *Computers and Structures*, 1995, 56(6): 871-895.
- [137] Oberkampf W L, Helton J C, Joslyn C A et al. Challenge problems: uncertainty in system response given uncertain parameters. *Reliability Engineering and System Safety*, 2004, 85(1-3): 11-19.
- [138] Möller B, Beer M. Fuzzy randomness: uncertainty in civil engineering and computational mechanics: Springer, 2004.
- [139] Möller B, Beer M. Engineering computation under uncertainty - Capabilities of non-traditional models. *Computers and Structures*, 2008, 86(10): 1024-1041.
- [140] Ben-Haim Y. A non-probabilistic concept of reliability. *Structural Safety*, 1994, 14(4): 227-245.
- [141] Ben-Haim Y. A non-probabilistic measure of reliability of linear systems based on expansion of convex models. *Structural Safety*, 1995, 17(2): 91-109.
- [142] Elishakoff I. Discussion on: A non-probabilistic concept of reliability. *Structural Safety*, 1995, 17(3): 195-199.
- [143] Qiu Z, Elishakoff I. Antioptimization of structures with large uncertain-but-non-random parameters via interval analysis. *Computer Methods in Applied Mechanics and Engineering*, 1998, 152(3-4): 361-372.
- [144] Qiu Z, Elishakoff I. Anti-optimization technique - a generalization of interval analysis for nonprobabilistic treatment of uncertainty. *Chaos, Solitons and Fractals*, 2001, 12(9): 1747-1759.
- [145] Eilishakoff I, Haftka R T, Fang J. Structural design under bounded uncertainty-optimization with anti-optimization. *Computers and Structures*, 1994, 53(6): 1401-1405.
- [146] Tabakov P Y, Walker M. A technique for optimally designing engineering structures with manufacturing tolerances accounted for. *Engineering Optimization*, 2007, 39(1): 1-15.
- [147] Lombardi M, Haftka R T. Anti-optimization technique for structural design under load uncertainties. *Computer Methods in Applied Mechanics and Engineering*, 1998, 157(1): 19-31.
- [148] Pantelides C P, Ganzerli S. Design of trusses under uncertain loads using convex models. *Journal of Structural Engineering*, 1998, 124(3): 318-329.
- [149] Ganzerli S, Pantelides C P. Optimum structural design via convex model superposition. *Computers and Structures*, 2000, 74(6): 639-647.
- [150] Ben-Tal A, Nemirovski A. Robust optimization - Methodology and applications. *Mathematical Programming*, 2002, 92(3): 453-480.

- [151] Luo Y, Kang Z, Luo Z, Li A. Continuum topology optimization with non-probabilistic reliability constraints based on multi-ellipsoid convex model. *Structural and Multidiscipline Optimization*, 2008, DOI:10.1007/s00158-008-0329-1.
- [152] Elishakoff I, Colombi P. Combination of probabilistic and convex models of uncertainty when scarce knowledge is present on acoustic excitation parameters. *Computer Methods in Applied Mechanics and Engineering*, 1993, 104(2): 187-209.
- [153] Penmetsa R C, Grandhi R V. Efficient estimation of structural reliability for problems with uncertain intervals. *Computers and Structures*, 2002, 80(12): 1103-1112.
- [154] Kreinovich V, Xiang G, Starks S A et al. Towards combining probabilistic and interval uncertainty in engineering calculations: Algorithms for computing statistics under interval uncertainty, and their computational complexity. *Reliable Computing*, 2006, 12(6): 471-501.
- [155] Qiu Z, Yang D, Elishakoff I. Probabilistic interval reliability of structural systems. *International Journal of Solids and Structures*, 2008, 45: 2850-2860.
- [156] Du X, Sudjianto A, President S V et al. Reliability-based design with the mixture of random and interval variables. *Journal of Mechanical Design*, 2005, 127: 1068-1076.
- [157] Adduri P R, Penmetsa R C. Confidence bounds on component reliability in the presence of mixed uncertain variables. *International Journal of Mechanical Sciences*, 2008, 50(3): 481-489.
- [158] Du L, Choi K K. An inverse analysis method for design optimization with both statistical and fuzzy uncertainties. *Structural and Multidisciplinary Optimization*, 2008, 37(2): 107-119.
- [159] Lodwick W A, Jamison K D. Interval-valued probability in the analysis of problems containing a mixture of fuzzy, possibilistic and interval uncertainty. *Fuzzy Sets and Systems*, 2008, 159(21): 2845-2858.
- [160] ANSYS Inc. ANSYS theory reference, release 6.1, 2004.
- [161] Carreira D J, Chu K H. Stress-strain relationship for plain concrete in compression. *ACI Journal Proceedings*, 1985, 82(6): 797-804.
- [162] Svanberg K. The method of moving asymptotes - A new method for structural optimization. *International Journal for Numerical Methods in Engineering*, 1987, 24(2): 359-373.
- [163] Bendsoe M P, Sigmund O. *Topology optimization: Theory, methods, and applications*. Berlin Heidelberg: Springer, 2003.
- [164] Haber R B, Jog C S, Bendsoe M P. A new approach to variable-topology shape design using a constraint on perimeter. *Structural Optimization*, 1996, 11(1-12).
- [165] Petersson J, Sigmund O. Slope constrained topology optimization. *International Journal for Numerical Methods in Engineering*, 1998, 41(14): 1417-1434.
- [166] Diaz A, Sigmund O. Checkerboard patterns in layout optimization. *Structural Optimization*, 1995, 10: 40-45.

- [167] Sigmund O, Petersson J. Numerical instabilities in topology optimization: A survey on procedures dealing with checkerboards, mesh-dependencies and local minima. *Structural Optimization*, 1998, 16: 68-75.
- [168] Sigmund O. A 99 line topology optimization code written in Matlab. *Structural and Multidisciplinary Optimization*, 2001, 21: 120-127.
- [169] Du J, Olhoff N. Topological optimization of continuum structures with design-dependent surface loading—part I: new computational approach for 2D problems. *Structural and Multidisciplinary Optimization*, 2004, 27(2): 151-165.
- [170] Ben-Haim Y, Elishakoff I. *Convex models of uncertainty in applied mechanics*. Amsterdam: Elsevier, 1990.
- [171] Rosenblatt M. Remarks on a multivariate transformation. *Annals of Mathematical Statistics*, 1952, 23(3): 470-472.
- [172] Lawrence C, Zhou J L, Tits A L. User's guide for CFSQP version 2.5. <http://www.aemdesign.com>.
- [173] Liu P L, Kiureghian A D. Optimization algorithms for structural reliability. *Structural Safety*, 1991, 9(3): 161-177.
- [174] Wang L P, Grandhi R V. Efficient safety index calculation for structural reliability analysis. *Computers and Structures*, 1994, 52(1): 103-111.
- [175] Royset J O, Der Kiureghian A, Polak E. Reliability-based optimal structural design by the decoupling approach. *Reliability Engineering and System Safety*, 2001, 73(3): 213-221.
- [176] Cheng G, Xu L, Jiang L. A sequential approximate programming strategy for reliability-based structural optimization. *Computers and Structures*, 2006, 84(21): 1353-1367.
- [177] Chen X, Hasselman T K, Neill D J. Reliability based structural design optimization for practical applications. In: *Proceedings, 38th AIAA/ASME/ASCE/AHS/ASC Structures, structural dynamics, and materials conference and exhibit*. Orlando, FL. 1997.
- [178] Kuschel N, Rackwitz R. A new approach for structural optimization of series systems. *Applications of Statistics and Probability*, 2000, 2(8): 987-994.
- [179] Liang J, Mourelatos Z P, Nikolaidis E. A single-loop approach for system reliability-based design optimization. *Journal of Mechanical Design*, 2007, 129(12): 1215-1225.

Curriculum Vitae

Name: Yangjun LUO

Sex: male

Nationality: Chinese

Date of Birth: 25/10/1979

Education

2006-2009

Laboratoire de Génie Civil, Groupe de Mécanique Matériaux et Structures,
Université de Reims Champagne-Ardenne, France

2004-2009

The State Key Laboratory of Structural Analysis for Industrial Equipment,
Dalian University of Technology, China

2001-2003

College of Hydraulic and Architecture Engineering,
Northwest Sci-Tech University of Agriculture and Forestry, China

1997-2001

College of Hydraulic and Architecture Engineering,
Northwest Sci-Tech University of Agriculture and Forestry, China